การจำลองคานระดับนาโนภายใต้แรงกระทำทั่วไป

นางสาวจินตหรา ลาวงศ์เกิด

วิทยานิพนธ์นี้เป็นส่วนหนึ่งของการศึกษาตามหลักสูตรปริญญาวิศวกรรมศาสตรมหาบัณฑิต
สาขาวิชาวิศวกรรมโยธา ภาควิชาวิศวกรรมโยธา
คณะวิศวกรรมศาสตร์ จุฬาลงกรณ์มหาวิทยาลัย
ปีการศึกษา 2558

MODELING OF NANO-BEAMS UNDER GENERAL LOADING CONDITIONS

Miss Jintara Lawongkerd

A Thesis Submitted in Partial Fulfillment of the Requirements
for the Degree of Master of Engineering Program in Civil Engineering
Department of Civil Engineering
Faculty of Engineering
Chulalongkorn University
Academic Year 2015

Thesis Title	MODELING OF NANO-BEAMS UNDER GENERAL LOADING CONDITIONS
By	Miss Jintara Lawongkerd
Field of Study	Civil Engineering
Thesis Advisor	Associate Professor Jaroon Rungamornrat, Ph.D.

Accepted by the Faculty of Engineering, Chulalongkorn University in Partial Fulfillment of the Requirements for the Master's Degree

.....Dean of the Faculty of Engineering
(Associate Professor Supot Teachavorasinskun, D.Eng.)

THESIS COMMITTEE

.....Chairman
(Professor Teerapong Senjuntichai, Ph.D.)
.....Thesis Advisor
(Associate Professor Jaroon Rungamornrat, Ph.D.)
.....Examiner
(Assistant Professor Watanachai Smittakorn, Ph.D.)
.....External Examiner
(Punchet Thammarak, Ph.D.)

จินตหรา ลาวงศ์เกิด : การจำลองคานระดับนาโนภายใต้แรงกระทำทั่วไป (MODELING OF NANO-BEAMS UNDER GENERAL LOADING CONDITIONS) อ .ที่ปรึกษาวิทยานิพนธ์หลัก: รศ. ดร. จรูญ รุ่งอมรรัตน์, 107 หน้า.

วิทยานิพนธ์นี้นำเสนอการวิเคราะห์ผลตอบสนองการดัด การโก่งเดาะ และหลังการโก่งเดาะของคานนาโนภายใต้เงื่อนไขที่ปลายแบบต่างๆ แบบจำลองพื้นผิวยืดหยุ่นของเกอร์ดิน-เมอร์ดอคและแบบจำลองการยืดหยุ่นไม่เฉพาะที่ของอีริงเกนถูกนำไปรวมกับทฤษฎีคานของออยเลอร์-เบอนูลลีย์เพื่อสร้างแบบจำลองทางคณิตศาสตร์ที่สามารถจำลองอิทธิพลในระดับนาโนและการขึ้นอยู่กับขนาดของปรากกฏการณ์ทางกายภาพที่สังเกตได้ในระดับนาโน สมการกำกับหลักของการโก่งตัวของคานถูกพัฒนาขึ้นภายใต้สมมติฐานการขจัดและการหมุนมากโดยอาศัยระเบียบวิธีเชิงปริพันธ์วงรี และรูปแบบเชิงเส้นของสมการดังกล่าวสามารถเขียนอยู่ในรูปของปัญหาค่าไอเกนซึ่งกำกับค่าแรงโก่งเดาะ ขั้นตอนการวิเคราะห์พื้นฐานเพื่อหาค่าไอเกนถูกนำมาใช้หาค่าแรงโก่งเดาะแบบแม่นตรงและวิธีการของนิวตัน-ราฟสันถูกนำมาใช้ในการหาผลเฉลยเชิงตัวเลขของระบบสมการพิชคณิตไม่เชิงเส้นเพื่อหาการโก่งตัวของคานและปริมาณอื่นๆที่เกี่ยวข้อง ผลที่ได้จากศึกษาแสดงให้เห็นว่าทั้งผลของผิวและความไม่เฉพาะที่มีอิทธิพลเป็นอย่างมากต่อค่าแรงโก่งเดาะและผลตอบสนองด้านการดัดและพฤติกรรมหลังการโก่งเดาะของคานนาโน โดยฉพาะอย่างยิ่งผลของผิวและความไม่เฉพาะที่มีแนวโน้มที่จะลดค่าสติฟเนสรวมของคานและส่งผลให้แรงโก่งเดาะมี่ค่าลดลงในทุกกรณีที่ศึกษา นอกจากนี้ผลเฉลยที่ทำนายได้ยังขึ้นอยู่กับขนาดและมีอิทธิพลจากตัวแปรที่เกี่ยวข้องกับผลของผิวและความไม่เฉพาะที่อย่างมีนัยสำคัญ (อาทิเช่น โมดูลัสยืดหยุนที่ผิวและแรงตึงผิวคงค้าง) เมื่อขนาดเชิงเรขาคณิตของคานมีค่าใกล้เคียงกับขนาดที่แสดงคุณลักษณะของผิววัสดุ

ภาควิชา วิศวกรรมโยธา ลายมือชื่อนิสิต .....

สาขาวิชา วิศวกรรมโยธา ลายมือชื่อ อ.ที่ปรึกษาหลัก .....

ปีการศึกษา 2558

5670139021 : MAJOR CIVIL ENGINEERING

KEYWORDS: BENDING / BUCKLING / GURTIN-MURDOCH MODEL / NANO-BEAMS / NON-LOCAL EFFECT / POST-BUCKLING / SURFACE STRESSES

JINTARA LAWONGKERD: MODELING OF NANO-BEAMS UNDER GENERAL LOADING CONDITIONS. ADVISOR: ASSOC. PROF. JAROON RUNGAMORNRAT, Ph.D., 107 pp.

This thesis presents the analysis of bending, buckling, and post-buckling responses of a nano-beam under different end conditions. Both surface and non-local effects via Gurtin-Murdoch surface elasticity and Eringen non-local elasticity models are integrated into the classical Euler-Bernoulli beam theory to obtain a mathematical model capable of simulating the nano-scale influence and size-dependency of observed physical phenomena. The key governing equations for a deflected shape are formulated first within the context of large displacements and rotations using a classical elliptic integral technique and their linearized version is then established to form the eigen-value problem governing the buckling load. A conventional analytical procedure for eigen-hunt is employed to determine the exact buckling load whereas Newton-Raphson iterative scheme is adopted to solve a final system of nonlinear algebraic equations to obtain the deflected shape and other related quantities. Obtained results demonstrate that both the surface and non-local effects significantly influence the buckling load and bending and post-buckling responses of nano-beams. In particular, presence of those effects tends to reduce the overall stiffness of the beam and, as a result, decrease the buckling load for all cases considered. In addition, the predicted solutions exhibit strongly size-dependent and are significantly influenced by both the surface and non-local parameters (e.g., surface modulus of elasticity and residual surface tension) when the characteristic length of the beam is comparable to the intrinsic length of the material surface.

Department:	Civil Engineering	Student's Signature	.....
Field of Study:	Civil Engineering	Advisor's Signature	.....
Academic Year:	2015		

ACKNOWLEDGEMENTS

I would like to express my sincerest gratitude to my advisor, Associate Professor Dr. Jaroon Rungamornrat, who have supported me throughout my thesis. This thesis would not have been able to finish without your guidance, patience and knowledge. I would also like to thank my committee members, Professor Dr. Teerapong Senjuntichai, Assistant Professor Dr.Watanachai Smitthakorn, and Dr.Punchet Thammarak for serving as my committee members and for your brilliant comments and suggestions. I would also like to thank all of my good friends for help and support. I would also like to thank my parents for consult and Encouragement. Finally, I would also like to thank myself in patience and try to work it out successfully.

CONTENTS

Page

Page

LIST OF FIGURES

CHAPTER I

INTRODUCTION

The first chapter provides the key motivation and importance of the current research. Then, the research objectives, scope of work, and the methodology and procedure are clearly addressed. Finally, findings and contribution of the current investigation are summarized.

1.1 General

Nano-technology will play an essential role in the industrial development because the current technology (micro-based technology) may reach an impasse. In the near future, there may be something that we have never seen before, such as ultra-fast computers, products which create itself, unspoiled food innovation, fully solar energy consumption, and new creative inventions and devices from imagination. Human can design and invent various materials, devices, tools and parts resulting directly from the progress in nano-science and nano-technology. Measuring instruments with a very tiny scale, not only in a millimeter (one thousand meters) or a micrometer (one million meters) scale but also in a nanometer scale (one billionth of a meters, the average human hair is about 25,000 nanometers wide), have been increasingly found. Nano-technology has rapidly grown and become influential in various disciplines including physics, chemistry, biology, electronics, engineering, and material sciences. For instance, in the field of biology, the evolution of nano-biosensors, biological probes, chemical diagnosis using bio-molecules to change the structure of drugs in order to destroy contiguous cells, and applications in cosmetics for passing nutrients to the human skin have been emerged in the past two decades. Nano-electronics is an example of nano-products operating with high quality and efficiency; for examples, nano-electromechanical solar cells, nano-chips for significantly enhancing the computer speed, and evolution of high density probe storage devices. Significant breakthrough in nano-materials has been also observed; for instance, a catalyst for plastic film industry of nano-composites which has the ability to block the passage of certain gas and steam for packaging to prolong the freshness of fruits and vegetables and production of nano-particles production used for sterilizing bacteria or viruses.

Owing to the continuous development of nano-scale components, tools and devices, e.g., transistors, sensors, actuators and resonators used in the nano-electro-mechanical systems (i.e., NEMSs) and parts of nano-chips, studies towards the characterization of mechanical properties at such a tiny-scale level has rapidly gained interest from many investigators in past several decades. Understanding the mechanical behavior and other properties (e.g., bending, buckling, and post-buckling) of slender nano-components which are commonly found as parts of nano-devices and nano-systems (see Figure 1.1) is obviously essential and generally required in the design procedure to ensure the integrity and safety throughout their usage.

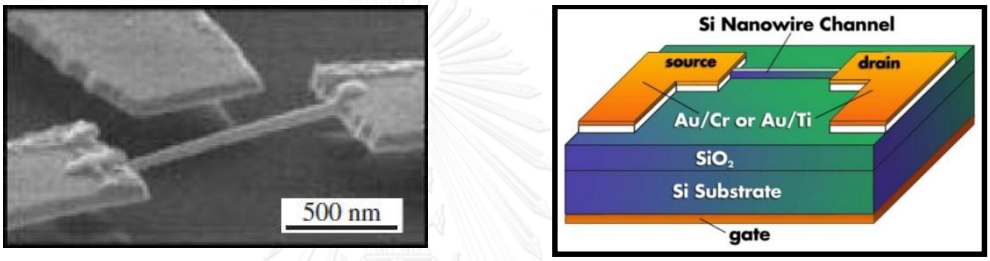

(a) **(b)**

Figure 1.1 Schematics of **(a)** SEM image of suspended nanowire device of 1.3 μm in length and 43 nm in diameter (image is taken from Husain et al. (2003)) and **(b)** silicon nanowire FET (image is taken from Koo et al. (2005)).

1.2 Background and Review

In the past two decades, researches have been extensively conducted to understand the fundamental behavior of nano-scale, slender structures such as nano-scale wires, rods, and beams. Most of existing studies can be separated into three categories based on the underlying methodology and procedure employed, one associated with experimental investigations and the other two concerning the discrete-based and continuum-based mathematical modeling.

Several experimental techniques have been proposed to study the real bending and buckling behavior of slender nano-elements. For instance, Jing et al. (2006) performed a three-point flexural test of nano-wires by a contact atomic force microscopy to obtain the their elastic modulus for various diameters. It was found from their study that the measured modulus depends primarily on the specimen size resulting

directly from the surface energy effects. Riaz et al. (2008) investigated the kinking, flexural and buckling responses of nano-rods/nano-wires using the nano-indentation technique. Results from the test were used to calculate the buckling energies, identify the critical buckling point, and described loading and unloading characteristics of bending behavior of tested nano-wires. Hsin et al. (2008) used atomic force microscopy cantilever technique along with a scanning electron microscope to examine mechanical properties of a single silicon nano-wire via a buckling test. Experimental data indicated that the nano-wire can resist a much larger strain and possesses much higher elastic modulus in comparison with the bulk material. Later, Ryu et al. (2009) conducted an experiment together with a mathematical simulations to describe both in-plane and lateral buckling behavior of silicon nano-wires by using scanning electron microscope and atomic force microscopy. Jahed et al. (2012) applied uniaxial nano-compression techniques to study the buckling behavior of polycrystalline nano-pillars. The critical buckling was recorded and used to extract the tangent modulus. While the experimental methods have been commonly used by various researchers to characterize the mechanical properties in the nano-scale level, the testing procedure generally requires high precision machines and well-equipped laboratories.

Alternative approaches using mathematical models integrating proper governing physics, postulates, and assumptions have increasingly gained attention from many investigators in the study of nano-scale structures due to their capabilities and cost effectiveness. Discrete-based techniques via sophisticated atomistic or molecular dynamics are ones of those theoretical simulations commonly used to investigate bending, buckling and post-buckling responses of nano-beams. Examples of those recent studies are briefly summarized below. Wang et al. (2008b) used atomistic calculations to examine the buckling responses of axially loaded GaN nano-wires. It was pointed out that the buckling strain and stress decrease as the wire length and the temperature increase. In the same year, Wang et al. (2008c) applied Stillinger-Weber-potential molecular dynamics simulations to explore the buckling characteristics of axially loaded GaN nano-tubes. The length of nano-tubes, strain rate, and the temperature used in the simulation were found significantly influenced the buckling behavior. Later, Jing et al. (2009) employed the same technique as that used by Wang et al. (2008c) to study buckling of single crystalline silicon nano-wires. Similar findings

and conclusions about parameters affecting the buckling responses were reported. Wen et al. (2010) examined the effect of size and slenderness ratio on mechanical properties and failure mechanism of Au nano-wires using molecular dynamics calculations. Results from their study indicated that elastic properties, yield strain and stress depend mainly on the slenderness ratios and diameters of the wires. The effect of the axial and surface orientation on the buckling responses of gold-nano-wires was later examined by Olsson and Park (2011) using atomistic simulations. While predicted results from various studies using atomistic or molecular dynamics simulations have shown the good agreement with testing results, the involved analysis generally consumes significant computational resources to handle a large number of unknowns and complicated governing physics.

In the past decade, classical continuum-based techniques have been increasingly proposed, as an alternative to atomistic and molecular dynamics simulations, and extensively used to study nano-beam problems. The positive features are based principally on the simplicity of the governing physics and low requirement of computational resources, in comparison with atomistic and molecular-based simulations. In general, existing classical Timoshenko and Euler-Bernoulli beam models (e.g., Timoshenko and Gere (1961)) have been enhanced by integrating Eringen nonlocal constitutive law (e.g., Eringen (1976); Eringen (1983); Eringen (2002)) and Gurtin-Murdoch surface elasticity model (e.g., Gurtin and Ian Murdoch (1975); Gurtin and Murdoch (1978); Gurtin et al. (1998)) to be capable of handling nano-scale phenomena, such as nonlocal and size-dependent behavior, observed from experimental investigations and atomistic calculations. Recent relevant literatures are reviewed and key features of those existing studies are briefly summarized in chronological order below.

Wang et al. (2006) developed an exact expression of the buckling load for micro- and nano-rods/tubes by including the influence of both non-locality and shear deformation. In their formulation, the linearized Timoshenko beam theory and Eringen constitutive model were employed along with the principle of virtual work to derive the key governing equation. Guo and Zhao (2007) explored the size-dependent bending behavior of nano-beams by considering the effect of both surface tension and surface relaxation of a layer on the surface of the beam into account. The linearized Euler-

Bernoulli beam model along with the apparent flexural rigidity and elastic modulus resulting from the surface effects was employed to derive an exact expression of the beam deflection. Wang and Liew (2007) derived closed form deflections of micro- and nano-rods/tubes by employing linearized Timoshenko and Euler-Bernoulli beam models and Eringen nonlocal elasticity. Results from their parametric study indicated that the size dependent characteristics of predicted solutions are evident for nano-elements not micro-structures. Wang et al. (2008a) applied linearized Timoshenko beam theory along with Eringen nonlocal constitutive law to obtain analytical responses of short and stubby micro- and nano-beams. They also pointed out the significant contribution of the shear deformation and the small-scale effects on obtained results. He and Lilley (2008) developed a closed-form solution of the deflected shape of cantilever, simply-supported, and fixed-fixed nano-beams using an enhanced linear Euler-Bernoulli beam model with Gurtin-Murdoch surface elasticity model. The latter was utilized to derive the effective flexural rigidity and fictitious transverse force along the beam. Their simulated results were found in agreement with existing testing data.

In 2009, Pradhan and Phadikar (2009) explored the buckling, bending and vibration of single-wall and double-wall nano-tubes under various end conditions by using a nonlocal theory of linear elasticity and classical beam theory. In their study, both material and geometric data were assumed spatially dependent and a numerical technique based on the general differential-quadrature was implemented to solve the governing differential equations. Aydogdu (2009a) presented a general formulation of a linear beam theory incorporating Eringen nonlocal constitutive law for the analysis of buckling, bending and vibration of nano-elements. The obtained governing equations can recover those associated with various existing beam models such as Timoshenko, Euler-Bernoulli, Reddy, Levinson, and Aydogdu models (e.g., Levinson (1981); Reddy (1984); Aydogdu (2009b)). Wang and Feng (2009) derived a closed form formula for the buckling load of axially loaded nano-wires by considering the effect of surface energy via Gurtin-Murdoch surface elasticity theory. The incremental-deformation theory along with Timoshenko beam model was employed by Song and Huang (2009) to investigate both vibration and bending of nano-wires. The geometric nonlinearity was considered in terms of Lagrangian strain and Gurtin-Murdoch surface stress model was integrated via the Hamilton's principle. Later, Jiang and Yan (2010) combined

linearized Timoshenko beam theory and surface stress effects to investigate the contribution of surface elastic modulus, residual surface tension, and shear deformation on the transverse displacement, modulus and stiffness of nano-wires under different end conditions. Results from their study were in agreement with available testing data from Jing et al. (2006) and also confirmed the size-dependency characteristics. Zeng and Zheng (2010) formulated the governing differential equations of nano-beams undergoing large deflection by taking the surface stress effects into account. Explicit results for fixed-fixed and fixed-free nano-beams under a concentrated force were also reported and used to demonstrate the contribution of the surface stresses. It is remarked that while the geometric nonlinearity was taken into account in their formulation, its applicability is still limited due to discarding contribution of higher order terms in kinematical relations. Fu et al. (2010) developed a numerical technique based on Galerkin procedure to simulate free vibration, buckling load, and post-buckling responses of nano-beams with consideration of surface energy effects. Nonlinear kinematics was formulated in terms of strain-displacement relations of the von Karman type. The influence of surface energy on the size-dependency of obtained results were fully investigated and discussed. It is remarked however that similar to most of previous studies, the contribution of the residual stress within the bulk is discarded.

Later, Ansari and Sahmani (2011) integrated Gurtin-Murdoch surface elasticity model to enhance various classical linearized beam theories such as Timoshenko, Euler-Bernoulli, Levinson and Reddy models to predict both buckling and flexural responses of nano-beams. Exact expressions for both the buckling load and deflected shape of a simply-supported beam were derived and then used to investigate the size-dependency behavior and significant contribution on the beam stiffness. Li et al. (2011) applied the classical linear strain gradient elasticity theory to formulate linear high-order differential equations governing the transverse deflection of nano-beams. Free-vibration, buckling and flexural responses of nano-beams were then obtained by solving such governing equations. It was indicated that results were in good agreement with testing results and the beam stiffness, buckling load and natural frequency were found size dependent. Wang and Yang (2011) applied the classical beam theory together with Gurtin-Murdoch model to compute the buckling load and post-buckling shape of a fixed-pinned nano-wire. In their study, the shooting method was utilized to construct

the post-buckling configuration and predicted results indicated the significant contribution of surface material parameters. Roque et al. (2011) developed a meshless technique with both global and local collocation schemes to investigate free vibration, buckling and flexural behavior of nano-beams. The linearized Timoshenko beam theory is utilized along with Eringen nonlocal linear elasticity to formulate the governing differential equations. Their numerical solutions were found in excellent agreement with exact results generated by Reddy (2007). Chiu and Chen (2011a), Chiu and Chen (2011b) examined the buckling and bending behavior of nano-beams under various end conditions. In their formulation, the linearized Euler-Bernoulli beam theory was utilized along with the high-order surface stress effects via Young-Laplace equation. By validating with existing experimental data, the higher-order surface stress model was found yielding more accurate results than the conventional one. Later, Juntarasaid et al. (2012) applied both Eringen nonlocal constitutive relation and Gurtin-Murdoch surface theory together with the linearized Euler-Bernoulli beam model to derive analytical solutions of both buckling load and small deflection of nano-beams subjected to different end conditions. It is important to point out that while their mathematical model can characterize the nano-scale influence but the contribution of the residual stress within the bulk material due to the non-zero residual surface tension was not considered. Samaei et al. (2012) investigated the buckling of nano-wires by taking the piezoelectric effect, surface stresses and transverse shear deformation into account. The linearized Timoshenko beam theory was utilized as a basis of their formulation and the critical electric potential was derived analytically in terms of surface parameters, elastic and piezoelectric constants, and geometry of nano-wires. The contribution of the transverse shear deformation was clearly demonstrated by comparing predicted results with those obtained from Euler-Bernoulli beam model. Janghorban (2012) developed the differential quadrature method to obtain the bending response of tapered nano-wires under fixed-fixed and simply-supported end conditions. The Eringen nonlocal constitutive relation was integrated into linearized Euler-Bernoulli beam theory to simulate the nano-scale influence. Mahmoud et al. (2013) applied both the surface and nonlocal elasticity models along with the linearized Euler-Bernoulli beam theory to derive a key differential equation governing the deflected shape of nano-beams under transverse loadings. A standard finite element procedure was adopted to construct

approximate solutions and an extensive parametric study was performed to examine the important role of both surface and nonlocal parameters on the size dependency of computed results. Yao and Yun (2012) explored the effect of non-uniform surface elasticity on the buckling load of ZnO nano-wires under fixed-fixed and fixed-pinned conditions. The exponential variation of the surface parameters was assumed and the analytical expression of the buckling load was derived for both cases. Thai (2012) derived the closed-form solutions of the buckling load, transverse deflection and natural frequency of nonlocal nano-beams. In the formulation, the linear shear deformation beam theory with a parabolic shear strain over the cross section was utilized together with the nonlocal constitutive law. Computed results were compared with solutions generated by Timoshenko, Euler-Bernoulli and Reddy beam models and also found strongly dependent on nonlocal parameters. Thai and Vo (2012) reinvestigated the same problem as that carried out by Thai (2012) except that the sinusoidal shear-deformation beam model was employed in their study. Exact solutions of a simply-supported beam were obtained and compared with results obtained by Timoshenko beam model integrated by nonlocal effects. Xu et al. (2012) applied Timoshenko beam theory and Eringen nonlocal elasticity to estimate the buckling load and post-buckling shape of a cantilever nano-rod. A semi-analytical technique based on the homotopy perturbation scheme was utilized to determine the solution of the nonlinear differential equation. Results from their study indicated that the shear deformation and the nonlocal parameters play a crucial role on the value of the buckling load and the post-buckling deflection. Liu et al. (2012) studied nano-wires subjected to transverse loads and undergoing large displacement and rotation. The residual surface tension and surface elasticity were incorporated in the derivation of the governing equation and the numerical solutions were obtained via a shooting method. Again, in this study, the initial residual stress within the bulk was discarded.

Recently, Şimşek and Yurtcu (2013) developed closed-form results associated with flexural response and buckling load of a simply-supported nano-beam made from a functionally graded material with power-law effective properties. The nonlocal elasticity model and linearized Timoshenko and Euler-Bernoulli beam theories were utilized in the formulation to simulate effects of the transverse shear deformation and small-scale influence. Li and Zhang (2013) utilized a classical Euler-Bernoulli beam

model to estimate the critical load and length of nano-wires rested on the elastic substrate due to the self-weight and tip force. The supporting elastic substrate was replaced by a rotational spring at the base of the wire in the modeling and an integral equation method was proposed to derive a simplified approximate expression for the buckling load. Emam (2013) proposed a general formulation to model buckling and post-buckling of nano-beams by incorporating Eringen nonlocal elasticity and a generalized kinematics suitable for handling Timoshenko, Euler-Bernoulli and higher-order shear-deformation beam theories. Closed-form solutions of both the critical load and the amplitude of the post-buckling shape were reported for both simply-supported and fixed-fixed end conditions. Chiu and Chen (2013) derived analytical expressions for transverse displacement and resonance frequency of nano-wires by using high-order surface stresses and a linearized Timoshenko beam model. Predicted solutions were compared extensively with existing experimental results and those generated by Euler-Bernoulli beam theory including simple surface stresses. It was pointed out from their study that the high-order surface stresses show strong influence on the response of nano-wires with relatively small cross section. Ghannadpour et al. (2013) examined the buckling, flexural and free-vibration problems by utilizing the linearized Euler-Bernoulli beam model along with the nonlocal linear elasticity. The Ritz method was adopted to construct approximate solution of beams under general loading and boundary conditions. Ansari et al. (2013) integrated Gurtin-Murdoch surface elasticity into the classical Euler-Bernoulli beam model to investigate the post-buckling behavior and size-dependency of predicted responses of nano-beams. In their study, the virtual work principle along with the generalized differential quadrature technique and Newton-Raphson scheme was utilized to obtain numerical solutions. Eltaher et al. (2013) studied the size-dependent behavior and the influence of end conditions and material property profile on the buckling load of a nano-element made from a functionally graded material. The Eringen nonlocal elasticity was integrated into a classical linear Euler-Bernoulli beam theory to formulate the governing equation and a standard finite element procedure was adopted to obtain numerical solutions. Later, Ansari et al. (2014) revisited the post-buckling of nano-beams reported by Ansari et al. (2013) by replacing Euler-Bernoulli beam model by Timoshenko beam theory. The same surface elasticity model and similar numerical procedure were adopted in their

work. Hu et al. (2014) applied both the nonlocal constitutive model and the surface stresses to enhance the classical linearized beam theory in the study of the buckling load and vibration of nano-wires. Analytical solutions for both cases were derived using a fundamental approach in a theory of differential equations. It should be remarked that in their formulation, the initial residual stress within the bulk was fully ignored and the effect of the residual surface tension was lumped to the fictitious longitudinal force. Li et al. (2014) presented analytical solutions of linearized Timoshenko nano-beams subjected to concentrated transverse force. The nano-scale influence was incorporated in their formulation via Gurtin-Murdoch model with the contribution of both surface elasticity and residual surface tension. Results from their study confirm the significant effect of surface stresses on the overall stiffness of the beam and size-dependency characteristic of computed solutions. Eltaher et al. (2014b) combined the linearized Timoshenko beam theory and Eringen nonlocal linear elasticity to study both bending and buckling of functionally graded nano-beams for various end conditions. In their work, a standard finite element method is adopted to construct the numerical solutions and the influence of nonlocal parameters, boundary conditions and material properties on the predicted results was fully investigated. Eltaher et al. (2014a) developed a finite element technique based upon Eringen nonlocal elasticity with higher-order strain gradient and linearized Euler-Bernoulli theory to investigate bending, buckling and free vibration of a single nano-beam subjected to different end conditions. The ability of the higher order strain gradient model to predict the size-dependent behavior of nano-beams was concluded. Most recently, Wu et al. (2015) presented a continuum-based mathematical model by integrating small-rotation Euler-Bernoulli beam theory, surface elasticity theory, and nonlocal linear elasticity effects to examine the bending response of nanowires for various boundary conditions.

As clearly demonstrated, results from an extensive review of existing studies indicate the vast applications of nonlocal constitutive models and surface elasticity theory to investigate the size-dependent characteristic and nano-scale influence of bending, buckling, and post-buckling of nano-beams. It is crucial to point out however that integration of both nonlocal and surface stresses effects to investigate bending and post-buckling behavior of nano-elements within the context of large displacement and rotation is not well established. In addition, most of existing investigations fully

neglected the contribution of the residual stress within the bulk material when Gurtin-Murdoch model was utilized. The contribution of the non-zero residual surface tension was integrated mainly through the fictitious longitudinal force. This ignorance can lead to either inaccurate or erroneous predicted solutions as pointed out by Wang et al. (2010).

1.3 Research Objectives

The main objectives of the present study are to

(i) develop a theoretical model capable of simulating the nano-scale influence on responses of nano-beams,

(ii) develop a semi-analytical technique to obtain bending, buckling, and post-buckling responses of nano-beams under various end conditions, and

(iii) fully investigate the nano-scale influence and size-dependency of predicted solutions.

1.4 Scope of Research

The present study is carried out within following context:

(i) a single nano-element of a rectangular cross section is treated;

(ii) a bulk material is assumed linear, homogeneous, and isotropic with its behavior governed by Eringen's nonlocal linear elasticity model;

(iii) the effect of surface stresses is fully described by a complete Gurtin-Murdoch surface model;

(iv) external excitations are modeled in terms of loads applied only at the end of the beam and their direction remains unchanged for the entire loading history;

(v) solution procedure and results are presented only for fixed-free and fixed-pinned beams; and

(vi) axial and shear deformations are fully ignored.

1.5 Research Methodology

Fundamental theories and key assumptions, methodology and research procedures essential for the present study are summarized below.

(i) A classical Euler-Bernoulli beam theory within the context of the large displacement and rotation is used to formulate equilibrium equations and geometric relations of the beam. The well-known assumptions of the cross-section kinematics, such as "*plane section remains plane*" and "*axial and shear deformations are negligible*", are also employed.

(ii) The theory of linear nonlocal elasticity and Gurtin-Murdoch surface elasticity are employed to integrate the influence of nonlocal and surface stresses into the moment-curvature relationship.

(iii) The technique analogous to the elliptic integral method is applied to transform governing nonlinear differential equations to a set of nonlinear algebraic equations governing nano-elements under general end boundary conditions.

(iv) A small-rotation-based approximation is applied to derive a linear, fourth-order, ordinary differential equation governing the buckled shape of the beam.

(v) A standard analytical procedure for determining eigen values and eigen functions is adopted to determine the buckling load and corresponding buckled shape of axially loaded nano-elements.

(vi) A nonlinear solver based on Newton-Raphson iteration is employed to solve a system of nonlinear algebraic equations.

(vii) A selected variable transformation along with standard Gaussian quadrature is adopted to accurately and efficiently integrate all weakly singular integrals.

(viii) A verified in-house computer code is then utilized in the parametric study for investigating the nano-scale influence and size-dependency on predicted solutions.

1.6 Research Significance

The present study offers a continuum-based mathematical model along with an efficient and accurate solution procedure for simulating bending, buckling, and post-buckling responses of nano-beams with consideration of the nano-scale influence. Due to the vast capability of the proposed technique, it should provide an attractive alternative tool, in addition to experimental methods and atomistic and molecular dynamic simulations, to explore the mechanical behavior of slender nano-scale elements. In addition, results and findings from the current parametric study should also enhance the fundamental understanding of the nano-scale influence on the size-dependent characteristics of predicted results.

CHAPTER II

PROBLEM FORMULATION

In this chapter, a clear problem description is presented along with the integration of three basic field equations including constitutive relations, equilibrium equations and kinematics to form a complete set of nonlinear differential equations governing an element of nano-beams undergoing large displacements and rotations.

2.1 Problem Description

Consider a perfectly straight, prismatic, nano-element with length l and rectangular cross-section of width b and depth h. The bulk material of the nano-element is made from an isotropic, homogeneous, linear elastic material governed by a non-local constitutive model with fully prescribed material constants. The surface of the element is made from a linearly elastic material with its behavior fully described by a complete version of Gurtin-Murdoch model with both the residual surface tension and in-plane elastic constants fully prescribed. An element with four different end conditions (see Figure 2.1) are considered; (i) a fixed-free element under a transverse concentrated force at the free end, (ii) a fixed-free element under a longitudinal concentrated force at the free end, (iii) a fixed-rollered element under a concentrated moment at the rollered end, and (iv) a fixed-rollered element under a longitudinal concentrated load at the rollered end.

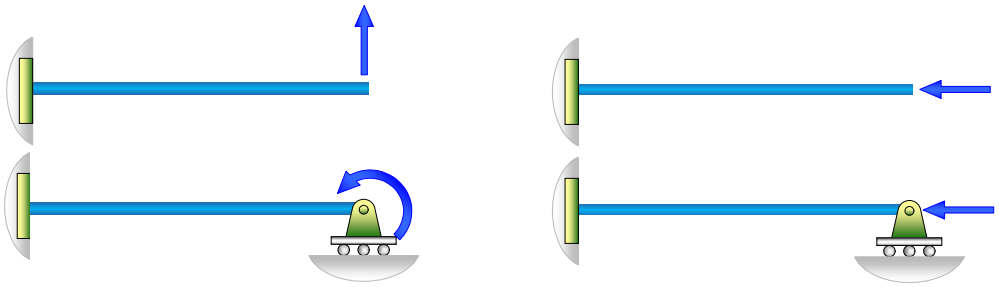

Figure 2.1 Schematics of perfectly straight nano-beams subjected to various types of end loads and restraints considered in the present study

The problem statement is to establish a solution procedure to obtain responses of the nano-beam such as the deformed shape, internal forces, buckling load, and post-buckling behavior with the integration of the nano-scale influence via the surface and nonlocal effects. In addition, the size-dependency and the nano-scale influence of predicted solutions is also investigated.

2.2 Basic Equations

The classical theory of Euler-Bernoulli beam (e.g., Lowe (1971); Altenbach et al. (2004)), the non-local linear elasticity theory (e.g., Eringen (1983)), and the Gurtin-Murdoch surface-elasticity model (e.g., Gurtin and Ian Murdoch (1975); Gurtin and Murdoch (1978); and Gurtin et al. (1998)) are employed to derive basic field equations governing responses of the nano-beam undergoing large displacements and rotations. Details of such formulation are presented below.

The centroidal axis of a nano-element in its undeformed state is represented by a straight line connecting points $(0,0)$ and $(l,0)$ as indicated in Figure 2.2(a). This one-dimensional representation together with the information of the cross section completely describes the three-dimensional aspect of the initial beam geometry. Under the action of external loads, the beam displaces and deforms to a new configuration with the deformed centroidal axis defined by a locus of points $(x(S), y(S))$ where $S \in [0,l]$ denotes the initial length coordinate measured from the left end to any cross section in its undeformed state. The deformed arc-length coordinate measured from the left end to any cross section in its deformed state is denoted by $s \in [0,l']$ where l' denotes the arc length of the deformed element. It is noted that the information of the deformed centroidal axis and the assumed cross-section kinematics provide the complete description of the deformation of the entire element.

The displacements of any cross section located at point $(S,0)$ in the $x-$ and $y-$directions are denoted by $u = u(S)$ and $v = v(S)$, respectively, and they are related to the coordinates $x(S)$ and $y(S)$ by

$$u(S) = x(S) - S \tag{2.1}$$

$$v(S) = y(S) \tag{2.2}$$

Due to the slenderness of typical nano-beams, it is common to ignore the contribution of the axial deformation in the response prediction and the centroidal axis of the element is assumed inextensible in the current investigation. Based on such assumption along with the consideration of the deformed centroidal axis of the element, it leads to the following relationship among the displacements u and v, the rotation θ at any cross section, and the initial and deformed arc length S and s:

$$\frac{ds}{dS} = 1 \tag{2.3}$$

$$\sin\theta = \frac{dy}{ds} = \frac{dv}{dS} \tag{2.4}$$

$$\cos\theta = \frac{dx}{ds} = 1 + \frac{du}{dS} \tag{2.5}$$

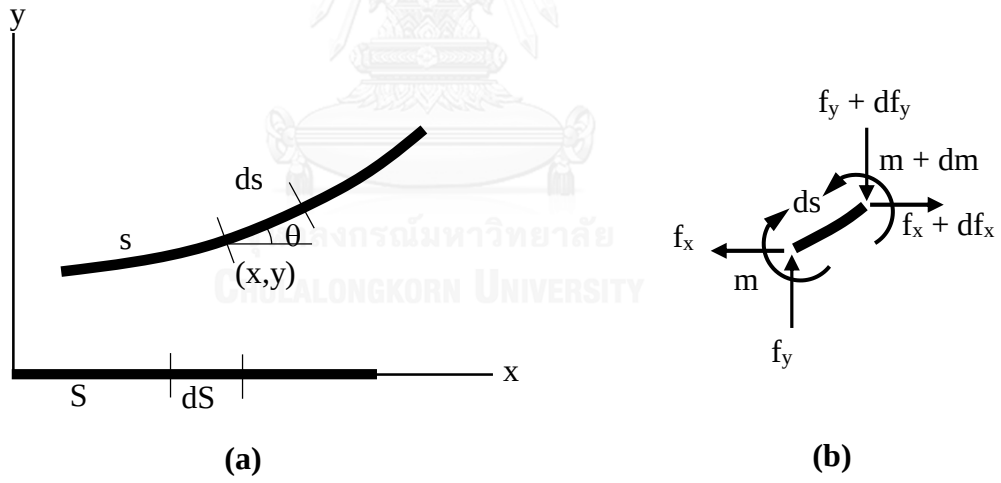

Figure 2.2 (a) Schematic indicating undeformed and deformed states of centroidal axis of nano-element and **(b)** free body diagram of infinitesimal deformed element ds

The relation (2.3) indicates that there is no difference of using the initial or deformed arc length S and s as the reference coordinate. From equilibrium of the deformed state of an infinitesimal element with the length ds in the absence of interior loadings (see Figure 2.2(b)), the force resultant in the $x-$direction denoted by f_x, the force resultant

in the $y-$direction denoted by f_y, and the bending moment denoted by m at any cross section must satisfy following partial differential equations:

$$\frac{df_x}{dS} = 0 \tag{2.6}$$

$$\frac{df_y}{dS} = 0 \tag{2.7}$$

$$\frac{dm}{dS} = f_x \sin\theta + f_y \cos\theta \tag{2.8}$$

It can be seen from (2.4) and (2.5) that the member free of the interior load possesses constant resultant forces f_x and f_y for its entire length. In addition, the resultant axial force (measured perpendicular to deformed cross section) and resultant shear force (measured parallel to the deformed cross section), denoted respectively by F and V, can be related to the force resultants f_x and f_y by

$$F = f_x \cos\theta - f_y \sin\theta \tag{2.9}$$

$$V = f_x \sin\theta + f_y \cos\theta \tag{2.10}$$

From a well-known "*plane section remains plane*" assumption along with discarding the shear deformation, the engineering normal strain within the cross section, denoted by ε, depends primarily on the distance from the centroidal axis of the cross section, denoted by z, via the following linear relation:

$$\varepsilon = -\frac{d\theta}{dS} z \tag{2.11}$$

By applying the theory of nonlocal linear elasticity to treat the nonlocal phenomena (e.g., Eringen (1983); Peddieson et al. (2003)) and the surface elasticity theory developed by Gurtin and Ian Murdoch (1975) to capture the effect of the surface free energy along with the kinematics of the cross section (2.10), the final nonlocal

relationship between the gradient of the rotation $d\theta/dS$ (i.e., the curvature of the deformed centroid axis) and the bending moment m is given by

$$m = \left(e_0 a\right)^2 \frac{d^2 m}{dS^2} + EI^* \frac{d\theta}{dS} \tag{2.12}$$

where a denotes the internal intrinsic length, e_0 denotes a dimensionless constant, and EI^* represent the apparent flexural rigidity of the cross section taking the surface stresses into account.

To determine EI^*, Gurtin-Murdoch model (e.g., Gurtin and Ian Murdoch (1975); Gurtin and Murdoch (1978); and Gurtin et al. (1998)) is utilized. In this model, the surface or boundary of the body is treated as an infinitesimally thin layer of material adhering perfectly to the bulk with its own properties. For an isotropic case, a linear constitutive relation is completely described by

$$\sigma^s_{\alpha\beta} = \tau^s \delta_{\alpha\beta} + 2(\mu^s - \tau^s)\varepsilon^s_{\alpha\beta} + (\lambda^s + \tau^s)\varepsilon^s_{\gamma\gamma}\delta_{\alpha\beta} + \tau^s u^s_{\alpha,\beta} \;\; ; \;\; \sigma^s_{3\alpha} = \tau^s u^s_{3,\alpha} \tag{2.13}$$

where the superscript "s" is employed to designate quantities associated with the surface; $\sigma^s_{3\alpha}$ and $\sigma^s_{\alpha\beta}$ denote components of the out-of-plane and in-plane surface stresses, respectively; $\varepsilon^s_{\alpha\beta}$ denotes components of the in-plane surface strain; u^s_3 and u^s_α denote components of the out-of-plane and in-plane surface displacement, respectively; μ^s and λ^s denote Lamé constants of the surface; τ^s denotes the residual surface tension; $\delta_{\alpha\beta}$ is a two-dimensional Kronecker symbol; and standard indicial notations apply. By specializing the constitutive relation (2.13) to the nano-beam along with the use of assumed cross-section kinematics, the explicit expression of EI^* can be derived. For instance, Wang et al. (2010) exploited the virtual work principle along with the constitutive relation of the bulk material with the presence of initial residual stress to derive the formula of EI^* due to the contribution of the residual surface tension τ^s and

the in-plane surface parameters. For a member with the length l and the rectangular cross-section of depth h and width b, the normalized EI^* can be obtained as

$$\eta = \frac{EI^*}{EI} = 1 + \frac{6}{\bar{h}} + \frac{2}{\bar{b}} + \frac{2\bar{\tau}^s}{\Lambda \bar{b}} \left(2\nu^2 \frac{\bar{b}^2}{\bar{h}^2} - \frac{\bar{l}^2}{\bar{h}^2} \right) \tag{2.14}$$

Where ν and E denote Poisson' ratio and Young's modulus of the bulk material; I is the cross-section moment of inertia; and $\bar{\tau}^s = \tau^s / E$, $\bar{h} = h/\Lambda$, $\bar{b} = b/\Lambda$, $\bar{l} = l/\Lambda$, $\Lambda = E^s/E$, and $E^s = \mu^s(2\mu^s + 3\lambda^s)/(\mu^s + 3\lambda^s)$. It is apparent from (2.14) that in the absence of the residual surface tension (i.e., $\bar{\tau}^s = 0$), the apparent flexural rigidity is always higher than that of the classical case and such discrepancy becomes more significant when the cross section is relatively small in comparison with the intrinsic length parameter Λ. On the contrary, presence of the positive residual surface tension can reverse the effect due to the residual compressive stress generated within the bulk material and such influence is substantially magnified when the slenderness ratio of the member increases. A different expression of the modified flexural rigidity due to the presence of surface effects was utilized by He and Lilley (2008), Wang and Feng (2009), Jiang and Yan (2010), and Juntarasaid et al. (2012) in the study of bending and buckling of nano-elements. The normalized EI^* for a rectangular cross section is proposed as

$$\eta = \frac{EI^*}{EI} = 1 + \frac{6}{\bar{h}} + \frac{2}{\bar{b}} \tag{2.15}$$

Clearly, this expression is independent of the residual surface tension and identical to that of (2.14) when $\bar{\tau}^s = 0$. The independence of $\bar{\tau}$ results directly from that the equilibrium of the entire body in its unstrained state is maintained using a set of fictitious forces at the boundary of the surface instead of considering the initial residual stress within the bulk. As a direct consequence of this unrealistic assumption, the effect of the surface residual surface tension was integrated into the governing equation in terms of such fictitious forces.

It can be remarked further that the nonlocal effect simulated through the linear theory of nonlocal elasticity influences the constitutive relationship via the appearance of the first term on the right-hand side of (2.12). From the study of Yang and Lim (2011), an extensive parametric study was carried out by calibrating results predicted by nonlocal Timoshenko beam model with solutions generated by molecular dynamic simulations and they finally suggested the suitable range of the non-local parameters as follows: $\mu = (e_0 a)^2 / l^2 \le 0.04$ and $e_0 < 14$. In the present investigation, values of both parameters e_0 and a used in numerical simulations are chosen to satisfy this range.

By substituting the equilibrium equation (2.8) into the constitutive relation (2.12), it yields the moment/curvature relationship:

$$\bar{m} = \left\{ \eta + \mu \left(\bar{f}_x \cos\theta - \bar{f}_y \sin\theta \right) \right\} \frac{d\theta}{d\bar{S}} \tag{2.16}$$

where $\bar{m} = ml/EI$, $\mu = (e_0 a)^2 / l^2$, $\bar{f}_x = f_x l^2 / EI$, $\bar{f}_y = f_y l^2 / EI$ and $\bar{S} = S/l$. By substituting (2.16) back into (2.8), an alternative form of the moment equilibrium equation is obtained as

$$\frac{d}{d\bar{S}} \left[\left\{ \eta + \mu \left(\bar{f}_x \cos\theta - \bar{f}_y \sin\theta \right) \right\} \frac{d\theta}{d\bar{S}} \right] = \bar{f}_x \sin\theta + \bar{f}_y \cos\theta \tag{2.17}$$

To suit the direct integration of the differential equation (2.12) with respect to the rotation θ, the left hand side of (2.17) is first re-expressed by using the chain rule as

$$\frac{d}{d\bar{S}} \left[\left\{ \eta + \mu \left(\bar{f}_x \cos\theta - \bar{f}_y \sin\theta \right) \right\} \frac{d\theta}{d\bar{S}} \right] = \frac{d\theta}{d\bar{S}} \cdot \frac{d}{d\theta} \left[\left\{ \eta + \mu \left(\bar{f}_x \cos\theta - \bar{f}_y \sin\theta \right) \right\} \frac{d\theta}{d\bar{S}} \right] \tag{2.18}$$

By substituting the relation (2.18) into the equilibrium equation (2.17) and then multiplying both sides of by a function $\eta + \mu \left(\bar{f}_x \cos\theta - \bar{f}_y \sin\theta \right)$, the resulting differential equation can subsequently be integrated to obtain

$$\left[\left\{\eta+\mu\left(\bar{f}_x\cos\theta-\bar{f}_y\sin\theta\right)\right\}\frac{d\theta}{d\bar{S}}\right]^2=C-2\eta\left(\bar{f}_x\cos\theta-\bar{f}_y\sin\theta\right)-\mu\left(\bar{f}_x\cos\theta-\bar{f}_y\sin\theta\right)^2 \quad (2.19)$$

where C denote a constant arising from the integration process and it can be obtained from prescribed end conditions. As apparent from (2.12), both the normalized bending moment $\bar{m}$ and the term $\left\{\eta+\mu\left(\bar{f}_x\cos\theta-\bar{f}_y\sin\theta\right)\right\}d\theta/d\bar{S}$ must have the same sign; as a result, only one of the two solutions of $d\theta/d\bar{S}$ obtained from (2.19) is physically acceptable. The unique solution can therefore be expressed in the form

$$\frac{d\bar{S}}{d\theta}=\frac{sign(\bar{m})\left\{\eta+\mu\left(\bar{f}_x\cos\theta-\bar{f}_y\sin\theta\right)\right\}}{\sqrt{C-2\eta\left(\bar{f}_x\cos\theta-\bar{f}_y\sin\theta\right)-\mu\left(\bar{f}_x\cos\theta-\bar{f}_y\sin\theta\right)^2}} \quad (2.20)$$

where $sign(\bar{m})$ is a moment-dependence function defined by

$$sign(\bar{m})=\begin{cases}1, & \bar{m}>0\\ -1, & \bar{m}<0\\ 0, & \bar{m}=0\end{cases} \quad (2.21)$$

Combining (2.20) and the geometric relations (2.4) and (2.5) yields two differential equations governing the displacements u and v:

$$\frac{d\bar{u}}{d\theta}=\frac{sign(\bar{m})\left(\cos\theta-1\right)\left\{\eta+\mu\left(\bar{f}_x\cos\theta-\bar{f}_y\sin\theta\right)\right\}}{\sqrt{C-2\eta\left(\bar{f}_x\cos\theta-\bar{f}_y\sin\theta\right)-\mu\left(\bar{f}_x\cos\theta-\bar{f}_y\sin\theta\right)^2}} \quad (2.22)$$

$$\frac{d\bar{v}}{d\theta}=\frac{sign(\bar{m})\sin\theta\left\{\eta+\mu\left(\bar{f}_x\cos\theta-\bar{f}_y\sin\theta\right)\right\}}{\sqrt{C-2\eta\left(\bar{f}_x\cos\theta-\bar{f}_y\sin\theta\right)-\mu\left(\bar{f}_x\cos\theta-\bar{f}_y\sin\theta\right)^2}} \quad (2.23)$$

where $\bar{u}=u/l$ and $\bar{v}=v/l$. A set of three generic differential equations (2.20), (2.22) and (2.23) is sufficient for formulating the key governing equations of nano-beams under various end conditions. It is worth noting that both η and μ appearing in above equations are essential parameters concerning the surface stresses and the nonlocal

linear elasticity, respectively, and are used to simulate the nano-scale influence on the responses of the nano-beams. By setting $\eta = 1$ and $\mu = 0$, the above equations reduces directly to those obtained by Rungamornrat and Tangnovarad (2011) for a classical beam (i.e., without the influence of nonlocal elasticity and surface stresses). By performing the direct integration of (2.20), (2.22) and (2.23) with respect to the independent variable θ from $\bar{S} = 0$ to $\bar{S} = \xi \in [0,1]$, it leads to

$$\xi = \int_{\theta_1}^{\theta(\xi)} \frac{sign(\bar{m})\left\{\eta + \mu\left(\bar{f}_x \cos\theta - \bar{f}_y \sin\theta\right)\right\}}{\sqrt{C - 2\eta\left(\bar{f}_x \cos\theta - \bar{f}_y \sin\theta\right) - \mu\left(\bar{f}_x \cos\theta - \bar{f}_y \sin\theta\right)^2}} d\theta \tag{2.24}$$

$$\bar{u}(\xi) - \bar{u}_1 = \int_{\theta_1}^{\theta(\xi)} \frac{sign(\bar{m})(\cos\theta - 1)\left\{\eta + \mu\left(\bar{f}_x \cos\theta - \bar{f}_y \sin\theta\right)\right\}}{\sqrt{C - 2\eta\left(\bar{f}_x \cos\theta - \bar{f}_y \sin\theta\right) - \mu\left(\bar{f}_x \cos\theta - \bar{f}_y \sin\theta\right)^2}} d\theta \tag{2.25}$$

$$\bar{v}(\xi) - \bar{v}_1 = \int_{\theta_1}^{\theta(\xi)} \frac{sign(\bar{m})\sin\theta\left\{\eta + \mu\left(\bar{f}_x \cos\theta - \bar{f}_y \sin\theta\right)\right\}}{\sqrt{C - 2\eta\left(\bar{f}_x \cos\theta - \bar{f}_y \sin\theta\right) - \mu\left(\bar{f}_x \cos\theta - \bar{f}_y \sin\theta\right)^2}} d\theta \tag{2.26}$$

where $\bar{u}_1 = \bar{u}(\bar{S} = 0)$, $\bar{v}_1 = \bar{v}(\bar{S} = 0)$ and $\theta_1 = \theta(\bar{S} = 0)$. By setting $\xi = 1$, above relations (2.24)-(2.26) become

$$1 = \int_{\theta_1}^{\theta_2} \frac{sign(\bar{m})\left\{\eta + \mu\left(\bar{f}_x \cos\theta - \bar{f}_y \sin\theta\right)\right\}}{\sqrt{C - 2\eta\left(\bar{f}_x \cos\theta - \bar{f}_y \sin\theta\right) - \mu\left(\bar{f}_x \cos\theta - \bar{f}_y \sin\theta\right)^2}} d\theta \tag{2.27}$$

$$\bar{u}_2 - \bar{u}_1 = \int_{\theta_1}^{\theta_2} \frac{sign(\bar{m})(\cos\theta - 1)\left\{\eta + \mu\left(\bar{f}_x \cos\theta - \bar{f}_y \sin\theta\right)\right\}}{\sqrt{C - 2\eta\left(\bar{f}_x \cos\theta - \bar{f}_y \sin\theta\right) - \mu\left(\bar{f}_x \cos\theta - \bar{f}_y \sin\theta\right)^2}} d\theta \tag{2.28}$$

$$\bar{v}_2 - \bar{v}_1 = \int_{\theta_1}^{\theta_2} \frac{sign(\bar{m})\sin\theta\left\{\eta + \mu\left(\bar{f}_x \cos\theta - \bar{f}_y \sin\theta\right)\right\}}{\sqrt{C - 2\eta\left(\bar{f}_x \cos\theta - \bar{f}_y \sin\theta\right) - \mu\left(\bar{f}_x \cos\theta - \bar{f}_y \sin\theta\right)^2}} d\theta \tag{2.29}$$

where $\bar{u}_2 = \bar{u}(\bar{S} = 1)$, $\bar{v}_2 = \bar{v}(\bar{S} = 1)$ and $\theta_2 = \theta(\bar{S} = 1)$. A system of nonlinear algebraic equations (2.27)-(2.29) along with the well-posed natural and essential end conditions

of an element is sufficient for determining the unknown constant C and kinematical unknowns from a set $\{\bar{u}_1, \bar{u}_2, \bar{v}_1, \bar{v}_2, \theta_1, \theta_2\}$. Once all primary unknowns at both ends of the member are solved, the displacement and rotation of any cross section can readily be obtained from the relations (2.24)-(2.26). The support reactions can also be determined from static equilibrium of the whole beam in its deformed state whereas the internal forces at any cross section such as the shear force V, axial force F and the bending moment m are obtained from the method of sections and static equilibrium of a portion of the beam.

2.3 Linearized Equations for Buckling Load Analysis

For a perfectly straight nano-beam with proper end restraints and subjected only to the action of a pure axial compression force P, it is apparent that the straight configuration (i.e., $u = v = \theta = 0$) and the pure axial state (i.e., $f_x = -P, f_y = m = 0$) is always an equilibrium state (i.e., equations (2.3)-(2.8) and (2.12) are automatically satisfied). Besides this trivial solution, it is more informative to determine the critical compression force P at the onset of the buckling, i.e., a state that the beam begins to admit a non-straight equilibrium configuration. At the onset of the buckling, the rotation θ is infinitesimally small and, as a result, the first-order approximations $\sin\theta \approx \theta, \cos\theta = 1$ are admissible. The kinematical relations (2.4)-(2.5), the equilibrium equations (2.6)-(2.8), and the moment-curvature relationship (2.16) for this particular case reduce to

$$\frac{d\bar{v}}{d\bar{S}} = \theta \tag{2.30}$$

$$\frac{d\bar{u}}{d\bar{S}} = 0 \tag{2.31}$$

$$\frac{d\bar{f}_x}{d\bar{S}} = 0 \tag{2.32}$$

$$\frac{d\bar{f}_y}{d\bar{S}} = 0 \tag{2.33}$$

$$\frac{d\bar{m}}{d\bar{S}} = \bar{f}_x\theta + \bar{f}_y \tag{2.34}$$

$$\bar{m} = \left\{ \eta + \mu \bar{f}_x \right\} \frac{d\theta}{d\bar{S}} \tag{2.35}$$

It is evident from the relation (2.31) along with the prescribed displacement in the longitudinal direction of the element to prevent the rigid body motion that $\bar{u}$ must vanish. Similarly, the equilibrium equation (2.32) and the prescribed compression force P at the end of the beam imply that $\bar{f}_x = -Pl^2/EI = -k$. By applying the result $\bar{f}_x = -k$ and the relation (2.30) to (2.34) and (2.35), it yields the normalized resultant force $\bar{f}_y$ and the normalized bending moment $\bar{m}$ in terms of the normalized displacement $\bar{v}$

$$\bar{f}_y = \left(\eta - \mu k \right) \frac{d^3 \bar{v}}{d\bar{S}^3} + k \frac{d\bar{v}}{d\bar{S}} \tag{2.36}$$

$$\bar{m} = \left(\eta - \mu k \right) \frac{d^2 \bar{v}}{d\bar{S}^2} \tag{2.37}$$

Finally, the linearized governing equation for the normalized displacement $\bar{v}$ is obtained, by substituting (2.36) into the equilibrium equation (2.33), as

$$\left(\eta - \mu k \right) \frac{d^4 \bar{v}}{d\bar{S}^4} + k \frac{d^2 \bar{v}}{d\bar{S}^2} = 0 \tag{2.38}$$

The linear differential equation (2.38) along with the prescribed essential and natural boundary conditions forms the eigenvalue problem for determining the buckling load and buckled shape.

CHAPTER III

BENDING PROBLEMS

In this chapter, the basic governing equations established in the previous chapter are employed to formulate a set of nonlinear equations governing the bending responses both fixed-free and fixed-pinned nano-beams. The constant C resulting from the integration process and certain components of internal forces are obtained by properly enforcing the boundary conditions.

3.1 Fixed-free Nano-beam

Consider a fixed-free nano-beam clamped at the left end and subjected to a transverse concentrated force P at the right end as indicated in Figure 3.1. The corresponding natural and essential end conditions for this particular case can be summarized as follows:

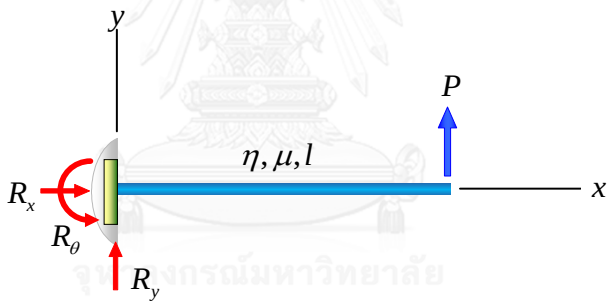

Figure 3.1 A fixed-free nano-beam clamped at left end and subjected to a transverse concentrated force P at free end

$$\bar{u}(\bar{S}=0)=0 \tag{3.1}$$

$$\bar{v}(\bar{S}=0)=0 \tag{3.2}$$

$$\theta(\bar{S}=0)=0 \tag{3.3}$$

$$\bar{f}_x(\bar{S}=1)=0 \tag{3.4}$$

$$\bar{f}_y(\bar{S}=1)=-Pl^2/EI\equiv -k \tag{3.5}$$

$$\bar{m}(\bar{S}=1)=0 \tag{3.6}$$

By using (3.4) and (3.5) along with the fact that the resultant forces $\bar{f}_x$ and $\bar{f}_y$ are constant throughout the element, it can be concluded that

$$\bar{f}_x(\bar{S}) = 0, \quad \bar{f}_y(\bar{S}) = -k \quad \forall \bar{S} \in [0,1] \tag{3.7}$$

By using the relation (2.11) and the end condition (3.6), it implies that

$$\frac{d\theta}{d\bar{S}}(\bar{S} = 1) = 0 \tag{3.8}$$

Enforcing the conditions (3.7) and (3.8) along with the relation (2.19) leads to the unknown constant C, for this particular case, as

$$C = 2\eta k \sin\theta_2 + \mu k^2 \sin^2\theta_2 \tag{3.9}$$

By combining the results (3.7) and (3.9) along with the essential boundary conditions (3.1)-(3.3), a set of nonlinear algebraic equations (2.27)-(2.29) simply reduces to

$$1 = \int_0^{\theta_2} \frac{\eta + \mu k \sin\theta}{\sqrt{2\eta k\left(\sin\theta_2 - \sin\theta\right) + \mu k^2\left(\sin^2\theta_2 - \sin^2\theta\right)}} d\theta \tag{3.10}$$

$$\bar{u}_2 = \int_0^{\theta_2} \frac{\left(\eta + \mu k \sin\theta\right)\left(\cos\theta - 1\right)}{\sqrt{2\eta k\left(\sin\theta_2 - \sin\theta\right) + \mu k^2\left(\sin^2\theta_2 - \sin^2\theta\right)}} d\theta \tag{3.11}$$

$$\bar{v}_2 = \int_0^{\theta_2} \frac{\left(\eta + \mu k \sin\theta\right)\sin\theta}{\sqrt{2\eta k\left(\sin\theta_2 - \sin\theta\right) + \mu k^2\left(\sin^2\theta_2 - \sin^2\theta\right)}} d\theta \tag{3.12}$$

Note that the moment-dependent function $sign(\bar{m})$ takes the value 1 for the entire beam since the normalized bending moment is always positive except at the right end where $\bar{m}$ vanishes. A set of equations (3.10)-(3.12) is sufficient for determining the unknown rotation and displacements at the right end of the element (i.e., $\bar{u}_2$, $\bar{v}_2$ and θ_2).

Similarly, the post-processing equations (2.24)-(2.26) for computing the rotation and displacements at any point $\bar{S} = \xi \in (0,1)$ take the form

$$\xi = \int_0^{\theta(\xi)} \frac{\eta + \mu k \sin\theta}{\sqrt{2\eta k\left(\sin\theta_2 - \sin\theta\right) + \mu k^2\left(\sin^2\theta_2 - \sin^2\theta\right)}} d\theta \tag{3.13}$$

$$\bar{u}(\xi) = \int_0^{\theta(\xi)} \frac{\left(\eta + \mu k \sin\theta\right)\left(\cos\theta - 1\right)}{\sqrt{2\eta k\left(\sin\theta_2 - \sin\theta\right) + \mu k^2\left(\sin^2\theta_2 - \sin^2\theta\right)}} d\theta \tag{3.14}$$

$$\bar{v}(\xi) = \int_0^{\theta(\xi)} \frac{\left(\eta + \mu k \sin\theta\right)\sin\theta}{\sqrt{2\eta k\left(\sin\theta_2 - \sin\theta\right) + \mu k^2\left(\sin^2\theta_2 - \sin^2\theta\right)}} d\theta \tag{3.15}$$

Once the rotation and displacement for the whole element are determined, the support reactions at the clamped end and the internal forces at any cross section can be determined as described below. By enforcing static equilibrium of the whole beam in its deformed state, the support reactions $\{R_x, R_y, R_\theta\}$ are given explicitly by

$$\bar{R}_x = R_x l^2 / EI = 0 \tag{3.16}$$

$$\bar{R}_y = R_y l^2 / EI = -k \tag{3.17}$$

$$\bar{R}_\theta = R_\theta l / EI = -k(1 + \bar{u}_2) \tag{3.18}$$

The shear force, the axial force, and the bending moment at any cross section $\bar{S} = \xi \in (0,1)$ are obtained by first portioning the beam along that particular cross section and then enforcing static equilibrium of the right portion of the beam in its deformed state. The final results are given by

$$\bar{F} = Fl^2 / EI = k \sin\theta(\xi) \tag{3.19}$$

$$\bar{V} = Vl^2 / EI = -k \cos\theta(\xi) \tag{3.20}$$

$$\bar{m} = ml / EI = k(1 + \bar{u}_2 - \xi - \bar{u}(\xi)) \tag{3.21}$$

3.2 Fixed-rollered Nano-beam

Consider, next, a fixed-rollered nano-element clamped at the left end and subjected to a point moment M_0 at the right end (i.e., the roller support) as shown in Figure 3.2. The corresponding natural and essential end conditions for this particular case are given by

$$\bar{u}(\bar{S}=0)=0 \tag{3.22}$$

$$\bar{v}(\bar{S}=0)=0 \tag{3.23}$$

$$\theta(\bar{S}=0)=0 \tag{3.24}$$

$$\bar{v}(\bar{S}=1)=0 \tag{3.25}$$

$$\bar{f}_x(\bar{S}=1)=0 \tag{3.26}$$

$$\bar{m}(\bar{S}=1)=\bar{m}_0=M_0 l/EI \tag{3.27}$$

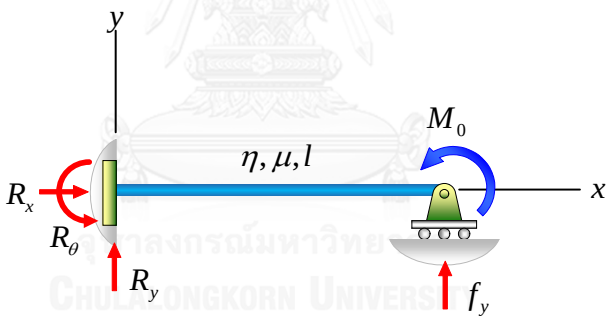

Figure 3.2 A perfectly straight nano-element clamped at left end, pinned at right end and subjected to point moment M_0 at left end

The constant C appearing in (2.27)-(2.29) can be obtained by enforcing the condition at an interior inflection point $\bar{S}=\xi_z$ (i.e., $\bar{m}(\bar{S}=\xi_z)=0$ and the result is given by

$$C=-2\eta\bar{f}_y\sin\theta_z+\mu\bar{f}_y^2\sin^2\theta_z \tag{3.28}$$

where θ_z is the rotation at the inflection point. By applying the two natural boundary conditions (3.26) and (3.27), it leads to

$$\bar{F}(\theta) = -\bar{f}_y \sin\theta \tag{3.29}$$

$$\bar{m}_0^2 = \mu \bar{f}_y^2 (\sin^2\theta_z - \sin^2\theta_2) + 2\eta \bar{f}_y (\sin\theta_2 - \sin\theta_z) \tag{3.30}$$

Finally, by employing essential boundary conditions (3.22)-(3.25), the two relations (3.29)-(3.30), and the governing equations (2.27)-(2.29), it yields a set of four nonlinear algebraic equations governing the four unknowns $\theta_2, \theta_z, \bar{u}_2, \bar{f}_y$:

$$\begin{aligned} 1 = &\int_0^{\theta_2} \frac{\eta - \mu \bar{f}_y \sin\theta}{\sqrt{\bar{m}_0^2 + \mu \bar{f}_y^2 (\sin^2\theta_2 - \sin^2\theta) + 2\eta \bar{f}_y (\sin\theta - \sin\theta_2)}} d\theta \\ &- 2\int_0^{\theta_z} \frac{\eta - \mu \bar{f}_y \sin\theta}{\sqrt{\mu \bar{f}_y^2 (\sin^2\theta_z - \sin^2\theta) + 2\eta \bar{f}_y (\sin\theta - \sin\theta_z)}} d\theta \end{aligned} \tag{3.31}$$

$$\begin{aligned} 0 = &\int_0^{\theta_2} \frac{\sin\theta(\eta - \mu \bar{f}_y \sin\theta)}{\sqrt{\bar{m}_0^2 + \mu \bar{f}_y^2 (\sin^2\theta_2 - \sin^2\theta) + 2\eta \bar{f}_y (\sin\theta - \sin\theta_2)}} d\theta \\ &- 2\int_0^{\theta_z} \frac{\sin\theta(\eta - \mu \bar{f}_y \sin\theta)}{\sqrt{\mu \bar{f}_y^2 (\sin^2\theta_z - \sin^2\theta) + 2\eta \bar{f}_y (\sin\theta - \sin\theta_z)}} d\theta \end{aligned} \tag{3.32}$$

$$\begin{aligned} \bar{u}_2 = &\int_0^{\theta_2} \frac{(\cos\theta - 1)(\eta - \mu \bar{f}_y \sin\theta)}{\sqrt{\bar{m}_0^2 + \mu \bar{f}_y^2 (\sin^2\theta_2 - \sin^2\theta) + 2\eta \bar{f}_y (\sin\theta - \sin\theta_2)}} d\theta \\ &- 2\int_0^{\theta_z} \frac{(\cos\theta - 1)(\eta - \mu \bar{f}_y \sin\theta)}{\sqrt{\mu \bar{f}_y^2 (\sin^2\theta_z - \sin^2\theta) + 2\eta \bar{f}_y (\sin\theta - \sin\theta_z)}} d\theta \end{aligned} \tag{3.33}$$

$$\bar{m}_0^2 = \mu \bar{f}_y^2 (\sin^2\theta_z - \sin^2\theta_2) + 2\eta \bar{f}_y (\sin\theta_2 - \sin\theta_z) \tag{3.34}$$

To obtain the displacement and rotation at any point $\bar{S} = \xi^* \in [0,1]$, the beam must be divided into three segments due to the variation of the rotation across the member: the first segment is taken from the fixed end to the interior inflection point with the rotation at any normalized coordinate ξ_1^* ranging from 0 to θ_z; the second segment is from the inflection point to the point of zero-rotation with the rotation at any normalized

coordinate ξ_2^* ranging from θ_z to 0; and the last segment is from the point of zero-rotation to the right end with the rotation at any normalized coordinate ξ_3^* ranging from 0 to θ_2. A final set of integral relations used for determining the interior displacement and interior rotation of the first, second and third segments are given by

$$\xi_1^* = -\int_0^{\theta(\xi_1^*)} \frac{\eta - \mu \bar{f}_y \sin\theta}{\sqrt{\mu \bar{f}_y^2(\sin^2\theta_z - \sin^2\theta) + 2\eta \bar{f}_y(\sin\theta - \sin\theta_z)}} d\theta \tag{3.35}$$

$$\bar{v}(\xi_1^*) = -\int_0^{\theta(\xi_1^*)} \frac{\sin\theta(\eta - \mu \bar{f}_y \sin\theta)}{\sqrt{\mu \bar{f}_y^2(\sin^2\theta_z - \sin^2\theta) + 2\eta \bar{f}_y(\sin\theta - \sin\theta_z)}} d\theta \tag{3.36}$$

$$\bar{u}(\xi_1^*) = -\int_0^{\theta(\xi_1^*)} \frac{(\cos\theta - 1)(\eta - \mu \bar{f}_y \sin\theta)}{\sqrt{\mu \bar{f}_y^2(\sin^2\theta_z - \sin^2\theta) + 2\eta \bar{f}_y(\sin\theta - \sin\theta_z)}} d\theta \tag{3.37}$$

$$\begin{aligned}\xi_2^* = &-\int_0^{\theta_z} \frac{\eta - \mu \bar{f}_y \sin\theta}{\sqrt{\mu \bar{f}_y^2(\sin^2\theta_z - \sin^2\theta) + 2\eta \bar{f}_y(\sin\theta - \sin\theta_z)}} d\theta \\ &+ \int_{\theta(\xi_2^*)}^{0} \frac{\eta - \mu \bar{f}_y \sin\theta}{\sqrt{\mu \bar{f}_y^2(\sin^2\theta_z - \sin^2\theta) + 2\eta \bar{f}_y(\sin\theta - \sin\theta_z)}} d\theta\end{aligned} \tag{3.38}$$

$$\begin{aligned}\bar{v}(\xi_2^*) = &-\int_0^{\theta_z} \frac{\sin\theta(\eta - \mu \bar{f}_y \sin\theta)}{\sqrt{\mu \bar{f}_y^2(\sin^2\theta_z - \sin^2\theta) + 2\eta \bar{f}_y(\sin\theta - \sin\theta_z)}} d\theta \\ &+ \int_{\theta(\xi_2^*)}^{0} \frac{\sin\theta(\eta - \mu \bar{f}_y \sin\theta)}{\sqrt{\mu \bar{f}_y^2(\sin^2\theta_z - \sin^2\theta) + 2\eta \bar{f}_y(\sin\theta - \sin\theta_z)}} d\theta\end{aligned} \tag{3.39}$$

$$\begin{aligned}\bar{u}(\xi_2^*) = &-\int_0^{\theta_z} \frac{(\cos\theta - 1)(\eta - \mu \bar{f}_y \sin\theta)}{\sqrt{\mu \bar{f}_y^2(\sin^2\theta_z - \sin^2\theta) + 2\eta \bar{f}_y(\sin\theta - \sin\theta_z)}} d\theta \\ &+ \int_{\theta(\xi_2^*)}^{0} \frac{(\cos\theta - 1)(\eta - \mu \bar{f}_y \sin\theta)}{\sqrt{\mu \bar{f}_y^2(\sin^2\theta_z - \sin^2\theta) + 2\eta \bar{f}_y(\sin\theta - \sin\theta_z)}} d\theta\end{aligned} \tag{3.40}$$

$$\xi_3^* = -\int_0^{\theta_z} \frac{\eta - \mu \bar{f}_y \sin\theta}{\sqrt{\mu \bar{f}_y^2(\sin^2\theta_z - \sin^2\theta) + 2\eta \bar{f}_y(\sin\theta - \sin\theta_z)}} d\theta + \int_{\theta_z}^{0} \frac{\eta - \mu \bar{f}_y \sin\theta}{\sqrt{\mu \bar{f}_y^2(\sin^2\theta_z - \sin^2\theta) + 2\eta \bar{f}_y(\sin\theta - \sin\theta_z)}} d\theta + \int_0^{\theta(\xi_3^*)} \frac{\eta - \mu \bar{f}_y \sin\theta}{\sqrt{\mu \bar{f}_y^2(\sin^2\theta_z - \sin^2\theta) + 2\eta \bar{f}_y(\sin\theta - \sin\theta_z)}} d\theta \tag{3.41}$$

$$\bar{v}(\xi_3^*) = -\int_0^{\theta_z} \frac{\sin\theta(\eta - \mu \bar{f}_y \sin\theta)}{\sqrt{\mu \bar{f}_y^2(\sin^2\theta_z - \sin^2\theta) + 2\eta \bar{f}_y(\sin\theta - \sin\theta_z)}} d\theta + \int_{\theta_z}^{0} \frac{\sin\theta(\eta - \mu \bar{f}_y \sin\theta)}{\sqrt{\mu \bar{f}_y^2(\sin^2\theta_z - \sin^2\theta) + 2\eta \bar{f}_y(\sin\theta - \sin\theta_z)}} d\theta + \int_0^{\theta(\xi_3^*)} \frac{\sin\theta(\eta - \mu \bar{f}_y \sin\theta)}{\sqrt{\mu \bar{f}_y^2(\sin^2\theta_z - \sin^2\theta) + 2\eta \bar{f}_y(\sin\theta - \sin\theta_z)}} d\theta \tag{3.42}$$

$$\bar{u}(\xi_3^*) = -\int_0^{\theta_z} \frac{(\cos\theta - 1)(\eta - \mu \bar{f}_y \sin\theta)}{\sqrt{\mu \bar{f}_y^2(\sin^2\theta_z - \sin^2\theta) + 2\eta \bar{f}_y(\sin\theta - \sin\theta_z)}} d\theta + \int_{\theta_z}^{0} \frac{(\cos\theta - 1)(\eta - \mu \bar{f}_y \sin\theta)}{\sqrt{\mu \bar{f}_y^2(\sin^2\theta_z - \sin^2\theta) + 2\eta \bar{f}_y(\sin\theta - \sin\theta_z)}} d\theta + \int_0^{\theta(\xi_3^*)} \frac{(\cos\theta - 1)(\eta - \mu \bar{f}_y \sin\theta)}{\sqrt{\mu \bar{f}_y^2(\sin^2\theta_z - \sin^2\theta) + 2\eta \bar{f}_y(\sin\theta - \sin\theta_z)}} d\theta \tag{3.43}$$

The support reactions at the clamped end $\{R_x, R_y, R_\theta\}$ can be readily determined from equilibrium of the whole element and final results are obtained as

$$\bar{R}_x = R_x l^2/EI = 0 \tag{3.44}$$

$$\bar{R}_y = R_y l^2/EI = -\bar{f}_y \tag{3.45}$$

$$\bar{R}_\theta = R_\theta l/EI = -\bar{f}_y(1+\bar{u}_2) - \bar{m}_0 \tag{3.46}$$

The internal forces (including axial and shear forces and bending moment) at any cross section $\bar{S} = \xi \in (0,1)$ are obtained by using the method of section together with

enforcing static equilibrium of the right portion of the beam in its deformed state. The final results are given explicitly by

$$\bar{F} = Fl^2/EI = \bar{f}_y \sin\theta(\xi) \tag{3.47}$$

$$\bar{V} = Vl^2/EI = -\bar{f}_y \cos\theta(\xi) \tag{3.48}$$

$$\bar{m} = ml/EI = \bar{f}_y(1+\bar{u}_2 - \xi - \bar{u}(\xi)) + \bar{m}_0 \tag{3.49}$$

CHAPTER IV

BUCKLING AND POST-BUCKLING PROBLEMS

This chapter demonstrates how to apply basic equations established in Chapter II to formulate the boundary value problem for buckling and post-buckling of nano-beams under prescribed end conditions. The enforcement of essential and natural boundary conditions to obtain both the unknown constant C and a final set of key governing equations and the determination of support reactions and internal forces for each particular problem are clearly described.

4.1 Fixed-free Nano-beam

Consider a perfectly straight nano-element clamped at the left end and subjected to a longitudinal concentrated force P at the right end as depicted in Figure 4.1. Natural and essential boundary conditions for this particular element can be described by

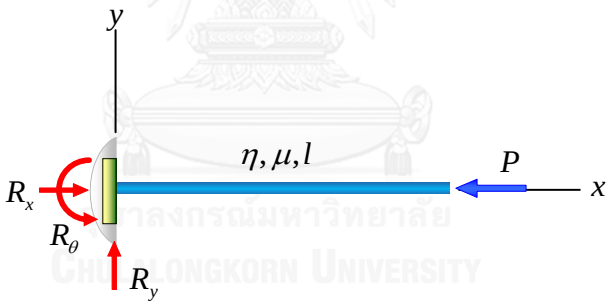

Figure 4.1 A perfectly straight nano-beam clamped at left end and subjected to longitudinal concentrated force P at the tip

$$\bar{u}(\bar{S}=0)=0 \tag{4.1}$$

$$\bar{v}(\bar{S}=0)=0 \tag{4.2}$$

$$\theta(\bar{S}=0)=0 \tag{4.3}$$

$$\bar{f}_x(\bar{S}=1)=-Pl^2/EI \equiv -k \tag{4.4}$$

$$\bar{f}_y(\bar{S}=1)=0 \tag{4.5}$$

$$\bar{m}(\bar{S}=1)=0 \tag{4.6}$$

By enforcing the boundary conditions (4.2), (4.3), (4.5) and (4.6) along with the relations (2.30), (2.36) and (2.37), an eigenvalue boundary value problem for determining the buckling load and buckled shape of this particular beam is given by

$$\left(\eta-\mu\bar{P}\right)\frac{d^4\bar{v}}{d\bar{S}^4}+\bar{P}\frac{d^2\bar{v}}{d\bar{S}^2}=0 \tag{4.7}$$

$$\bar{v}(0)=0 \tag{4.8}$$

$$\frac{d\bar{v}}{d\bar{S}}(0)=0 \tag{4.9}$$

$$\left(\eta-\mu k\right)\frac{d^3\bar{v}}{d\bar{S}^3}(1)+k\frac{d\bar{v}}{d\bar{S}}(1)=0 \tag{4.10}$$

$$\left(\eta-\mu k\right)\frac{d^2\bar{v}}{d\bar{S}^2}(1)=0 \tag{4.11}$$

To construct the key governing equations for post-buckling of this particular element, the same procedure as that described in the previous chapter is followed. From the natural boundary conditions (4.4) and (4.5) and the relations (2.6) and (2.7), the resultant forces $\bar{f}_x$ and $\bar{f}_y$ at any cross section of the beam are known as

$$\bar{f}_x(\bar{S})=-k,\quad \bar{f}_y(\bar{S})=0\quad \forall\bar{S}\in[0,1] \tag{4.12}$$

The relation (2.11) and the condition (4.6) imply that

$$\frac{d\theta}{d\bar{S}}(\bar{S}=1)=0 \tag{4.13}$$

By applying the relation (2.19) at $\bar{S}=1$ and then using the conditions (4.12)-(4.13), it leads to the unknown constant C:

$$C=-2\eta k\cos\theta_2+\mu k^2\cos^2\theta_2 \tag{4.14}$$

By substituting the constant C from (4.14), the conditions (4.12)-(4.13), and the essential boundary conditions (4.1)-(4.3) into (2.27)-(2.29), it yields a set of three nonlinear algebraic equations containing the unknown rotation and displacements at the right end of the element (i.e., $\bar{u}_2$, $\bar{v}_2$ and θ_2):

$$1 = \int_0^{\theta_2} \frac{\eta - \mu k \cos\theta}{\sqrt{2\eta k\left(\cos\theta - \cos\theta_2\right) + \mu k^2\left(\cos^2\theta_2 - \cos^2\theta\right)}} d\theta \tag{4.15}$$

$$\bar{u}_2 = \int_0^{\theta_2} \frac{\left(\eta - \mu k \cos\theta\right)\left(\cos\theta - 1\right)}{\sqrt{2\eta k\left(\cos\theta - \cos\theta_2\right) + \mu k^2\left(\cos^2\theta_2 - \cos^2\theta\right)}} d\theta \tag{4.16}$$

$$\bar{v}_2 = \int_0^{\theta_2} \frac{\left(\eta - \mu k \cos\theta\right)\sin\theta}{\sqrt{2\eta k\left(\cos\theta - \cos\theta_2\right) + \mu k^2\left(\cos^2\theta_2 - \cos^2\theta\right)}} d\theta \tag{4.17}$$

Note that the moment-dependent function $sign(\bar{m})$ is chosen equal to 1 without loss of generality since the post-buckling shape possesses a single-curvature and the normalized bending moment $\bar{m}$ at any point possesses the same sign. Once the end displacements and rotations are solved, the displacement and rotation at any interior point $\bar{S} = \xi \in (0,1)$ can be obtained from (by specializing (2.24)-(2.26) to this particular case)

$$\xi = \int_0^{\theta(\xi)} \frac{\eta - \mu k \cos\theta}{\sqrt{2\eta k\left(\cos\theta - \cos\theta_2\right) + \mu k^2\left(\cos^2\theta_2 - \cos^2\theta\right)}} d\theta \tag{4.18}$$

$$\bar{u}(\xi) = \int_0^{\theta(\xi)} \frac{\left(\eta - \mu k \cos\theta\right)\left(\cos\theta - 1\right)}{\sqrt{2\eta k\left(\cos\theta - \cos\theta_2\right) + \mu k^2\left(\cos^2\theta_2 - \cos^2\theta\right)}} d\theta \tag{4.19}$$

$$\bar{v}(\xi) = \int_0^{\theta(\xi)} \frac{\left(\eta - \mu k \cos\theta\right)\sin\theta}{\sqrt{2\eta k\left(\cos\theta - \cos\theta_2\right) + \mu k^2\left(\cos^2\theta_2 - \cos^2\theta\right)}} d\theta \tag{4.20}$$

Similarly, the support reactions at the clamped end can be obtained from static equilibrium of the whole beam in its deformed state and the final results are given by

$$\bar{R}_x = R_x l^2/EI = k \tag{4.21}$$

$$\bar{R}_y = R_y l^2/EI = 0 \tag{4.22}$$

$$\bar{R}_\theta = R_\theta l/EI = k\bar{v}_2 \tag{4.23}$$

The normalized internal forces (i.e., axial force F, shear force V, and bending moment m) at any point $\bar{S} = \xi \in (0,1)$ are obtained, by the method of sections, as

$$\bar{F} = Fl^2/EI = -k\cos\theta(\xi) \tag{4.24}$$

$$\bar{V} = Vl^2/EI = -k\sin\theta(\xi) \tag{4.25}$$

$$\bar{m} = ml/EI = k(\bar{v}_2 - \bar{v}(\xi)) \tag{4.26}$$

4.2 Fixed-roller Nano-beam

Next, consider a perfectly straight nano-beam clamped at the left end, rollered at the right end and subjected to a longitudinal concentrated force P at the right end as depicted in Figure 4.2. The corresponding natural and essential end conditions can be summarized below.

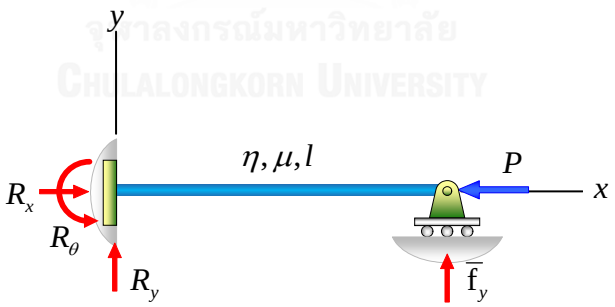

Figure 4.2 A perfectly straight nano-beam clamped at left end, rollered at right end and subjected to longitudinal concentrated force P at right end

$$\bar{u}(\bar{S} = 0) = 0 \tag{4.27}$$

$$\bar{v}(\bar{S} = 0) = 0 \tag{4.28}$$

$$\theta(\bar{S} = 0) = 0 \tag{4.29}$$

$$\bar{f}_x(\bar{S}=1) = -Pl^2/EI \equiv -k \tag{4.30}$$

$$\bar{v}(\bar{S}=1) = 0 \tag{4.31}$$

$$\bar{m}(\bar{S}=1) = 0 \tag{4.32}$$

By applying the boundary conditions (4.28), (4.29), (4.31) and (4.32) and the relations (2.30) and (2.37), a boundary value problem for the buckling of this particular beam is given by

$$\left(\eta - \mu\bar{P}\right)\frac{d^4\bar{v}}{d\bar{S}^4} + \bar{P}\frac{d^2\bar{v}}{d\bar{S}^2} = 0 \tag{4.33}$$

$$\bar{v}(0) = 0 \tag{4.34}$$

$$\left(\eta - \mu k\right)\frac{d^2\bar{v}}{d\bar{S}^2}(0) = 0 \tag{4.35}$$

$$\bar{v}(1) = 0 \tag{4.36}$$

$$\frac{d\bar{v}}{d\bar{S}}(1) = 0 \tag{4.37}$$

By using (4.30) along with the fact that the internal resultant forces $\bar{f}_x$ is constant throughout the member, it can be concluded that

$$\bar{f}_x(\bar{S}) = -k, \quad \forall \bar{S} \in [0,1] \tag{4.38}$$

Since the element possesses an interior inflection point, the internal moment at that particular point vanishes, or equivalently

$$\frac{d\theta}{d\bar{S}}(\theta = \theta_z) = 0 \tag{4.39}$$

where θ_z denote the rotation at the interior inflection point. By enforcing (4.39) along with (2.13), the constant C for this particular case is given by

$$C = -2\eta(k\cos\theta_z - \bar{f}_y\sin\theta_z) + \mu(k\cos\theta_z - \bar{f}_y\sin\theta_z)^2 \tag{4.40}$$

By combining the results (4.33) and (4.40) along with the essential boundary conditions (4.27)-(4.29), the key governing nonlinear algebraic equations (2.21)-(2.23) reduce to

$$1 = \int_0^{\theta_2} \frac{\vartheta(\bar{m})[\eta - \mu(k\cos\theta + \bar{f}_y\sin\theta)]}{\sqrt{2\eta f(\theta_z, \bar{f}_y) + \mu g(\theta_z, \bar{f}_y)}}\, d\theta \tag{4.41}$$

$$0 = \int_0^{\theta_2} \frac{\vartheta(\bar{m})(\sin\theta)[\eta - \mu(k\cos\theta + \bar{f}_y\sin\theta)]}{\sqrt{2\eta f(\theta_z, \bar{f}_y) + \mu g(\theta_z, \bar{f}_y)}}\, d\theta \tag{4.42}$$

$$\bar{u}_2 = \int_0^{\theta_2} \frac{\vartheta(\bar{m})(\cos\theta - 1)[\eta - \mu(k\cos\theta + \bar{f}_y\sin\theta)]}{\sqrt{2\eta f(\theta_z, \bar{f}_y) + \mu g(\theta_z, \bar{f}_y)}}\, d\theta \tag{4.43}$$

where the two-argument functions *f* and *g* are defined by

$$f(\theta_z, \bar{f}_y) = k(\cos\theta - \cos\theta_z) + \bar{f}_y(\sin\theta - \sin\theta_z) \tag{4.44}$$

$$g(\theta_z, \bar{f}_y) = k(\cos\theta_z - \cos\theta_z)^2 + \bar{f}_y(\sin\theta - \sin\theta)^2 \tag{4.45}$$

By using the relation (2.10) and the end condition (4.32), it results in

$$\frac{d\theta}{d\bar{S}}(\bar{S} = 1) = \frac{d\theta}{d\bar{S}}(\theta = \theta_2) = 0 \tag{4.46}$$

Enforcing (4.40) and (4.46) along with (2.13) leads to another essential nonlinear equation

$$\begin{aligned} &2\eta\left[k(\cos\theta_2 - \cos\theta_z) + \bar{f}_y(\sin\theta_2 - \sin\theta_z)\right] \\ &+\mu\left[(k\cos\theta_z + \bar{f}_y\sin\theta_z)^2 - (k\cos\theta_2 + \bar{f}_y\sin\theta_2)^2\right] = 0 \end{aligned} \tag{4.47}$$

After properly incorporating the moment-dependent function $\vartheta(\bar{m})$ to each part of the beam and then applying to the nonlinear equations (4.41)-(4.43), it yields a final set of governing equations

$$1=\int_0^{\theta_2}\frac{\eta-\mu(k\cos\theta+\bar{f}_y\sin\theta)}{\sqrt{2\eta f(\theta_2,\bar{f}_y)+\mu g(\theta_2,\bar{f}_y)}}d\theta-2\int_0^{\theta_z}\frac{\eta-\mu(k\cos\theta+\bar{f}_y\sin\theta)}{\sqrt{2\eta f(\theta_z,\bar{f}_y)+\mu g(\theta_z,\bar{f}_y)}}d\theta \tag{4.48}$$

$$\begin{aligned}0=&\int_0^{\theta_2}\frac{\sin\theta\left[\eta-\mu(k\cos\theta+\bar{f}_y\sin\theta)\right]}{\sqrt{2\eta f(\theta_2,\bar{f}_y)+\mu g(\theta_2,\bar{f}_y)}}d\theta\\&-2\int_0^{\theta_z}\frac{\sin\theta\left[\eta-\mu(k\cos\theta+\bar{f}_y\sin\theta)\right]}{\sqrt{2\eta f(\theta_z,\bar{f}_y)+\mu g(\theta_z,\bar{f}_y)}}d\theta\end{aligned} \tag{4.49}$$

$$\begin{aligned}\bar{u}_2=&\int_0^{\theta_2}\frac{(\cos\theta-1)\left[\eta-\mu(k\cos\theta+\bar{f}_y\sin\theta)\right]}{\sqrt{2\eta f(\theta_2,\bar{f}_y)+\mu g(\theta_2,\bar{f}_y)}}d\theta\\&-2\int_0^{\theta_z}\frac{(\cos\theta-1)\left[\eta-\mu(k\cos\theta+\bar{f}_y\sin\theta)\right]}{\sqrt{2\eta f(\theta_z,\bar{f}_y)+\mu g(\theta_z,\bar{f}_y)}}d\theta\end{aligned} \tag{4.50}$$

where the two-argument functions *f* and *g* are defined by

$$f(\theta_2,\bar{f}_y)=k(\cos\theta-\cos\theta_2)+\bar{f}_y(\sin\theta-\sin\theta_2) \tag{4.51}$$

$$g(\theta_2,\bar{f}_y)=k(\cos\theta_2-\cos\theta_2)^2+\bar{f}_y(\sin\theta-\sin\theta)^2 \tag{4.52}$$

To obtain the displacement and rotation at any interior point $\bar{S}=\xi^*\in[0,1]$, the nano-beam must be separated into three segments due to variation of the rotation across the member: the first segment is taken from the right end to the interior inflection point with the rotation at any normalized coordinate ξ_1^* ranging from 0 to θ_z; the second segment is from the inflection point to the point of zero-rotation with the rotation at any normalized coordinate ξ_2^* ranging from θ_z to 0; and the last segment is from the point of zero-rotation to the pinned-end with the rotation at any normalized coordinate ξ_3^*

ranging from 0 to θ_2. The final set of integral relations used for determining the interior displacement and interior rotation of the first segment is given by

$$\xi_1^* = -\int_0^{\theta(\xi_1^*)} \frac{\eta - \mu(k\cos\theta + \bar{f}_y \sin\theta)}{\sqrt{2\eta f(\theta_z, \bar{f}_y) + \mu g(\theta_z, \bar{f}_y)}} d\theta \tag{4.53}$$

$$\bar{v}(\xi_1^*) = -\int_0^{\theta(\xi_1^*)} \frac{(\sin\theta)\left[\eta - \mu(k\cos\theta + \bar{f}_y \sin\theta)\right]}{\sqrt{2\eta f(\theta_z, \bar{f}_y) + \mu g(\theta_z, \bar{f}_y)}} d\theta \tag{4.54}$$

$$\bar{u}(\xi_1^*) = -\int_0^{\theta(\xi_1^*)} \frac{(\cos\theta - 1)\left[\eta - \mu(k\cos\theta + \bar{f}_y \sin\theta)\right]}{\sqrt{2\eta f(\theta_z, \bar{f}_y) + \mu g(\theta_z, \bar{f}_y)}} d\theta \tag{4.55}$$

The interior displacement and rotation of the second segment can be computed from

$$\begin{aligned}\xi_2^* = &-\int_0^{\theta_z} \frac{\eta - \mu(k\cos\theta + \bar{f}_y \sin\theta)}{\sqrt{2\eta f(\theta_z, \bar{f}_y) + \mu g(\theta_z, \bar{f}_y)}} d\theta \\ &+ \int_{\theta(\xi_2^*)}^{0} \frac{\eta - \mu(k\cos\theta + \bar{f}_y \sin\theta)}{\sqrt{2\eta f(\theta_z, \bar{f}_y) + \mu g(\theta_z, \bar{f}_y)}} d\theta\end{aligned} \tag{4.56}$$

$$\begin{aligned}\bar{v}(\xi_2^*) = &-\int_0^{\theta_z} \frac{(\sin\theta)\left[\eta - \mu(k\cos\theta + \bar{f}_y \sin\theta)\right]}{\sqrt{2\eta f(\theta_z, \bar{f}_y) + \mu g(\theta_z, \bar{f}_y)}} d\theta \\ &+ \int_{\theta(\xi_2^*)}^{0} \frac{(\sin\theta)\left[\eta - \mu(k\cos\theta + \bar{f}_y \sin\theta)\right]}{\sqrt{2\eta f(\theta_z, \bar{f}_y) + \mu g(\theta_z, \bar{f}_y)}} d\theta\end{aligned} \tag{4.57}$$

$$\begin{aligned}\bar{u}(\xi_2^*) = &-\int_0^{\theta_z} \frac{(\cos\theta - 1)\left[\eta - \mu(k\cos\theta + \bar{f}_y \sin\theta)\right]}{\sqrt{2\eta f(\theta_z, \bar{f}_y) + \mu g(\theta_z, \bar{f}_y)}} d\theta \\ &+ \int_{\theta(\xi_2^*)}^{0} \frac{(\cos\theta - 1)\left[\eta - \mu(k\cos\theta + \bar{f}_y \sin\theta)\right]}{\sqrt{2\eta f(\theta_z, \bar{f}_y) + \mu g(\theta_z, \bar{f}_y)}} d\theta\end{aligned} \tag{4.58}$$

Finally, the displacement and rotation of the last segment can be computed from

$$\xi_3^* = -\int_0^{\theta_z} \frac{\eta - \mu(k\cos\theta + \bar{f}_y \sin\theta)}{\sqrt{2\eta f(\theta_z, \bar{f}_y) + \mu g(\theta_z, \bar{f}_y)}} d\theta + \int_{\theta_z}^{0} \frac{\eta - \mu(k\cos\theta + \bar{f}_y \sin\theta)}{\sqrt{2\eta f(\theta_z, \bar{f}_y) + \mu g(\theta_z, \bar{f}_y)}} d\theta + \int_0^{\theta(\xi_3^*)} \frac{\eta - \mu(k\cos\theta + \bar{f}_y \sin\theta)}{\sqrt{2\eta f(\theta_z, \bar{f}_y) + \mu g(\theta_z, \bar{f}_y)}} d\theta \tag{4.59}$$

$$\bar{v}(\xi_3^*) = -\int_0^{\theta_z} \frac{(\sin\theta)\left[\eta - \mu(k\cos\theta + \bar{f}_y \sin\theta)\right]}{\sqrt{2\eta f(\theta_z, \bar{f}_y) + \mu g(\theta_z, \bar{f}_y)}} d\theta + \int_{\theta_z}^{0} \frac{(\sin\theta)\left[\eta - \mu(k\cos\theta + \bar{f}_y \sin\theta)\right]}{\sqrt{2\eta f(\theta_z, \bar{f}_y) + \mu g(\theta_z, \bar{f}_y)}} d\theta + \int_{\theta_z}^{0} \frac{(\sin\theta)\left[\eta - \mu(k\cos\theta + \bar{f}_y \sin\theta)\right]}{\sqrt{2\eta f(\theta_z, \bar{f}_y) + \mu g(\theta_z, \bar{f}_y)}} d\theta \tag{4.60}$$

$$\bar{u}(\xi_3^*) = -\int_0^{\theta_z} \frac{(\cos\theta - 1)\left[\eta - \mu(k\cos\theta + \bar{f}_y \sin\theta)\right]}{\sqrt{2\eta f(\theta_z, \bar{f}_y) + \mu g(\theta_z, \bar{f}_y)}} d\theta + \int_{\theta_z}^{0} \frac{(\cos\theta - 1)\left[\eta - \mu(k\cos\theta + \bar{f}_y \sin\theta)\right]}{\sqrt{2\eta f(\theta_z, \bar{f}_y) + \mu g(\theta_z, \bar{f}_y)}} d\theta + \int_0^{\theta(\xi_3^*)} \frac{(\cos\theta - 1)\left[\eta - \mu(k\cos\theta + \bar{f}_y \sin\theta)\right]}{\sqrt{2\eta f(\theta_z, \bar{f}_y) + \mu g(\theta_z, \bar{f}_y)}} d\theta \tag{4.61}$$

The support reactions at the clamped end can be obtained from static equilibrium of the whole beam in its deformed state and the final results are given by

$$\bar{R}_x = R_x l^2 / EI = k \tag{4.62}$$

$$\bar{R}_y = R_y l^2 / EI = -\bar{f}_y \tag{4.63}$$

$$\bar{R}_\theta = R_\theta l / EI = -\bar{f}_y (1 + \bar{u}_2) \tag{4.64}$$

The internal forces (i.e., axial force F, shear force V, and bending moment m) at any point $\bar{S} = \xi \in (0,1)$ are obtained, by the method of sections, as

$$\bar{F} = Fl^2 / EI = \bar{f}_y \sin\theta(\xi) - k\cos\theta(\xi) \tag{4.65}$$

$$\bar{V} = Vl^2/EI = -\bar{f}_y \cos\theta(\xi) - k\sin\theta(\xi) \tag{4.66}$$

$$\bar{m} = ml/EI = \bar{f}_y(1+\bar{u}_2 - \xi - \bar{u}(\xi)) + k(\bar{v}_2 - \bar{v}(\xi)) \tag{4.67}$$

CHAPTER V

SOLUTION METHODOLOGY

In this chapter, a solution procedure for determining the bending behaviors, buckling load, and buckled shape of nano-beams, a selected numerical technique for obtaining a full set of nonlinear equations, and the quadrature rule adopted in the numerical evaluation of all involved integrals are briefly summarized.

5.1 Determination of Buckling Load and Buckled Shape

The buckling load and the corresponding buckled shape of a fixed-free nano-element clamped at the left end and subjected to the longitudinal force at the right end (shown in Figure 4.1) can be obtained using a standard procedure similar to that employed by Timoshenko and Gere (1961) in the determination of the buckling load of elastic columns. First, the general solution of the homogeneous, 4th-order, linear, ordinary differential equation (4.7) is obtained, from a fundamental theory of differential equations, as

$$\bar{v}(\bar{S}) = C_1 \cos\lambda\bar{S} + C_2 \sin\lambda\bar{S} + C_3\bar{S} + C_4 \tag{5.1}$$

where the unknowns C_1, C_2, C_3 and C_4 are constant and $\lambda = \sqrt{k/(\eta - \mu k)}$. By applying homogenous boundary conditions (4.8)-(4.11), it leads to the following homogeneous set of linear equations

$$\begin{bmatrix} 1 & 0 & 0 & 1 \\ 0 & \lambda & 1 & 0 \\ 0 & 0 & \lambda^2 & 0 \\ \lambda^2\cos\lambda & \lambda^2\sin\lambda & 0 & 0 \end{bmatrix} \begin{Bmatrix} C_1 \\ C_2 \\ C_3 \\ C_4 \end{Bmatrix} = \begin{Bmatrix} 0 \\ 0 \\ 0 \\ 0 \end{Bmatrix} \tag{5.2}$$

It is evident that $C_1 = C_2 = C_3 = C_4 = 0$ is always a solution of (5.2) for any value of λ or normalized load k, and this trivial solution corresponds directly to an equilibrium state of a straight configuration. The condition allowing the system (5.2) to admit a non-

zero solution (i.e., yielding an equilibrium state associated with a non-straight configuration) is that the determinant of the coefficient matrix is zero, i.e.,

$$\det\begin{bmatrix} 1 & 0 & 0 & 1 \\ 0 & \lambda & 1 & 0 \\ 0 & 0 & \lambda^2 & 0 \\ \lambda^2\cos\lambda & \lambda^2\sin\lambda & 0 & 0 \end{bmatrix} = 0 \tag{5.3}$$

The lowest value of λ satisfying the characteristic equation (5.3), denoted by $\lambda_{\min}$, can be readily determined using a selected nonlinear solver and the corresponding normalized buckling load k can then be computed from

$$k = \frac{\lambda_{\min}^2 \eta}{1+\lambda_{\min}^2 \mu} \tag{5.4}$$

The buckled shape corresponding to $\lambda = \lambda_{\min}$ can be obtained by solving the eigen vector from (5.2) and then substituting into the general solution (5.1). While the technique is demonstrated specifically for the fixed-free case, the same procedure applies equally to nano-beams under different end restraints. The only difference is the form of the coefficient matrix of (5.2) which results directly from the different prescribed end conditions. By noting that the normalized classical buckling load is $k^c = \lambda_{\min}^2$, the ratio k/k^c or P_{cr}/P_{cr}^c is given by

$$\frac{k}{k^c} = \frac{P_{cr}}{P_{cr}^c} = \frac{\eta}{1+\lambda_{\min}^2 \mu} \tag{5.5}$$

For the special cases of pinned-rollered, fixed-free, fixed-fixed, fixed-guided, and fixed-rollered beams, $\lambda_{\min}$ takes the value π, $\pi/2$, 2π, and 1.4303π, respectively.

5.2 Solution Procedure for System of Nonlinear Equations

To obtain the complete response of a nano-beam subjected to four types of boundary conditions indicated in Chapter III (for fixed-free and fixed-rollered beams under bending load) and Chapter IV (for fixed-free and fixed-rollered beams under axial

load), the four systems of nonlinear algebraic equations (3.10)-(3.12), (3.31)-(3.34), (4.15)-(4.17) and (4.47)-(4.50) must be solved. Due to the strong nonlinearity of those governing equations and their fully coupled feature, their solution can be obtained numerically using the well-known Newton-Raphson iterative scheme (e.g., Hamming (1987)). Once all primary unknowns at both ends of the beam and at the interior inflection point for the fixed-roller case are fully determined, the rotation and displacements at any location of the element can be obtained from the post-process equations (3.13)-(3.15), (3.35)-(3.43), (4.18)-(4.20), and (4.53)-(4.61) whereas all support reactions at the clamped end and internal resultant forces can be obtained from (3.16)-(3.21), (3.44)-(3.49), (4.21)-(4.26), (4.62)-(4.67).

5.2.1 Fixed-free Nano-beam

For the special case of a fixed-free nano-element shown in Figure 3.1, the nonlinear equation (3.10) is fully uncoupled from (3.11) and (3.12) and it involves only the unknown rotation at the right end θ_2 and the normalized load k. Such similar feature of the governing equations is also observed for the case of a fixed-rollered nano-element shown in Figure 4.1. As a result, for a prescribed normalized load k, the equation (3.10) or (4.15) is solved directly via Newton-Raphson iterative scheme to obtain θ_2. Once the end rotation θ_2 is determined, the normalized end displacements $\bar{u}_2$ and $\bar{v}_2$ can be obtained directly from (3.11)-(3.12) or from (4.16)-(4.17), respectively. Once $\{\bar{u}_2, \bar{v}_2, \theta_2\}$ are determined for a given normalized load k, the displacement and rotation at any interior point, support reactions and internal forces can be computed using the post-processing equations (3.13)-(3.21) for the nano-beam shown in Figure 3.1 and (4.18)-(4.26) for the nano-beam shown in Figure 4.1.

5.2.2 Fixed-rollered Nano-beams

On the contrary, the set of governing nonlinear equations for the fixed-rollered case is not fully-uncoupled; therefore, the technique used in the fixed-free case cannot be applied. For the fixed-rollered nano-beam under the end moment M_0, its response is governed by a set of four nonlinear algebraic equations (3.31)-(3.34) involving four unknowns $\theta_2, \theta_z, \bar{u}_2, \bar{f}_y$. Since equations (3.31), (3.32) and (3.34) are independent of the

unknown $\bar{u}_2$, they are solved simultaneously using Newton-Raphson algorithm to obtain $\theta_2, \theta_z, \bar{f}_y$ for a prescribed end moment $\bar{m}_0$. Once $\theta_2, \theta_z, \bar{f}_y$ are determined, the unknown $\bar{u}_2$ can be readily obtained from (3.33). Once all primary unknowns are solved, the relations (3.35)-(3.43) are utilized to post-process for the displacement and rotation at any interior point. Finally, the support reactions at the clamped end and all internal forces are calculated from (3.44)-(3.49).

For the fixed-rollered nano-beam under the tip axial force shown in Figure 4.2, the key governing equations (4.47)-(4.50) contains four unknowns $\{\theta_2, \theta_z, \bar{u}_2, \bar{f}_y\}$. Similar to the previous case, $\{\theta_2, \theta_z, \bar{f}_y\}$ are determined first by solving a set of three nonlinear algebraic equations (4.47)-(4.49) for a prescribed load k using Newton-Raphson iterative scheme. Then, the displacement $\bar{u}_2$ can be computed from the relation (4.50). Once the complete set of $\{\theta_2, \theta_z, \bar{u}_2, \bar{f}_y\}$ for the prescribed load k is determined, the interior displacement and rotation can be readily computed from the post-process relations (4.53)-(4.61) and the support reactions and internal forces are obtained from (4.62)-(4.67).

5.3 Numerical Integration of Weakly Singular Integrals

It is apparent that the integrand of all integrals in the governing nonlinear algebraic equations exhibit weakly singular behavior at points where the bending moment vanishes, e.g., the free end of beams shown in Figure 3.1 and Figure 4.1, the rollered end of a beam shown in Figure 3.2, and the interior inflection point of fixed-rollered beams shown in Figure 3.2 and Figure 4.2. While such singularity does not affect the convergence of those integrals in the sense of Riemann, it can render the numerical integration by standard Gaussian quadrature computationally inefficient. To overcome this difficulty, a technique based on the regularization of the integrand through a variable transformation is employed. While the procedure is demonstrated here only for the case that the singularity present at the free end of the element shown in Figure 3.1, it can be applied equally to other locations of the singularity. By introducing the following variable transformation

$$\phi = (\theta_2 - \theta)^{\gamma} \tag{5.16}$$

where γ is a selected constant. The differential form of (5.16) is given by

$$d\theta = (1/\gamma)(\theta_2 - \theta)^{1-\gamma} d\phi \tag{5.17}$$

By substituting (5.16) and (5.17) into (3.10)-(3.12), it leads to

$$1 = \frac{1}{\gamma}\int_0^{\theta_2^{\gamma}} \frac{(\eta + \mu k \sin\theta)(\theta_2 - \theta)^{1-\gamma}}{\sqrt{2\eta k(\sin\theta_2 - \sin\theta) + \mu k^2(\sin^2\theta_2 - \sin^2\theta)}} d\phi \tag{5.18}$$

$$\bar{u}_2 = \frac{1}{\gamma}\int_0^{\theta_2^{\gamma}} \frac{(\eta + \mu k \sin\theta)(\cos\theta - 1)(\theta_2 - \theta)^{1-\gamma}}{\sqrt{2\eta k(\sin\theta_2 - \sin\theta) + \mu k^2(\sin^2\theta_2 - \sin^2\theta)}} d\phi \tag{5.19}$$

$$\bar{v}_2 = \frac{1}{\gamma}\int_0^{\theta_2^{\gamma}} \frac{(\eta + \mu k \sin\theta)\sin\theta(\theta_2 - \theta)^{1-\gamma}}{\sqrt{2\eta k(\sin\theta_2 - \sin\theta) + \mu k^2(\sin^2\theta_2 - \sin^2\theta)}} d\phi \tag{5.20}$$

Since the term $\sqrt{2\eta k(\sin\theta_2 - \sin\theta) + \mu k^2(\sin^2\theta_2 - \sin^2\theta)}$ is of $\mathcal{O}(\sqrt{\theta_2 - \theta})$, the singularity of the integrand of (5.18)-(5.20) can be completely eliminated if $\gamma = 1/2$ is chosen. This regularization procedure can be equally applied to the equations (3.31)-(3.33), (4.15)-(4.17), and (4.48)-(4.50) for nano-beams under other end conditions. Once the integrand is completely regularized, the final integral can be integrated efficiently by standard Gaussian quadrature.

CHAPTER VI

NUMERICAL RESULTS AND DISCUSSION

In this chapter, numerical results obtained from the proposed model is reported and also compared with existing solutions for the classical case to verify the current formulation and implementations. The effect of surface stresses and nonlocal elasticity on the buckling load, bending and post-buckling responses for both fixed-free and fixed-rollered nano-beams is also discussed. In the numerical study, material parameters reported by Juntarasaid et al. (2012) are employed; in particular, the Poisson ratio and modulus of elasticity of the bulk material are chosen to be ν = 0.3 and E = 76 GPa and the surface modulus of elasticity and residual surface tension are taken as E^s = 1.22 N/m and τ^s = 0.89 N/m. For the nonlocal effect, Yang and Lim (2011) performed an extensive parametric study by calibrating results generated by a nonlocal Timoshenko beam model with solutions generated from molecular dynamic simulations and they finally suggested the suitable range of the non-local parameters as follows: $\mu = (e_0 a)^2 / l^2 \le 0.04$ and $e_0 < 14$.

It is seen from equation (2.14) that the normalized apparent flexural rigidity η is a function of the surface modulus of elasticity E^s, the residual surface tension τ^s and dimensions of the element. To demonstrate the influence of E^s and τ^s on the values of η, the aspect ratio of the cross section and the slenderness ratio of the nano-beam are taken as $b/h \in \{0.5, 1, 2\}$ and $l/h \in \{5, 10, 15\}$, respectively. The relationship between η and E^s is reported in Figure 6.1 for $\tau^s = 0$ and $\tau^s = 0.89$ N/m. It can be deduced that increase of the surface modulus of elasticity tends to enhance the apparent flexural rigidity for the fixed value of residual surface tension. Clearly, the apparent flexural rigidity is always greater than the classical flexural rigidity (i.e., $\eta \ge 1$) for $\tau^s = 0$ whereas the its value can be significant lower than that of the classical case when positive τ^s is present. In addition, the parameter η depends on both the aspect ratio of the cross section and the slenderness ratio of the beam for non-zero τ^s but is independent of the slenderness ratio for $\tau^s = 0$. In summary, increase of the surface

modulus of elasticity tends to stiffen the nano-beam and this influence is more significant when the slenderness ratio of the beam becomes smaller whereas the aspect ratio of the cross section becomes larger.

(a)

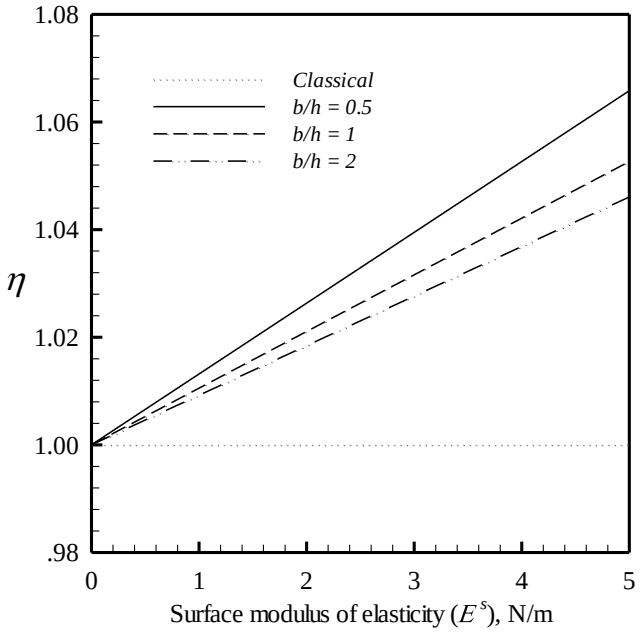

(b)

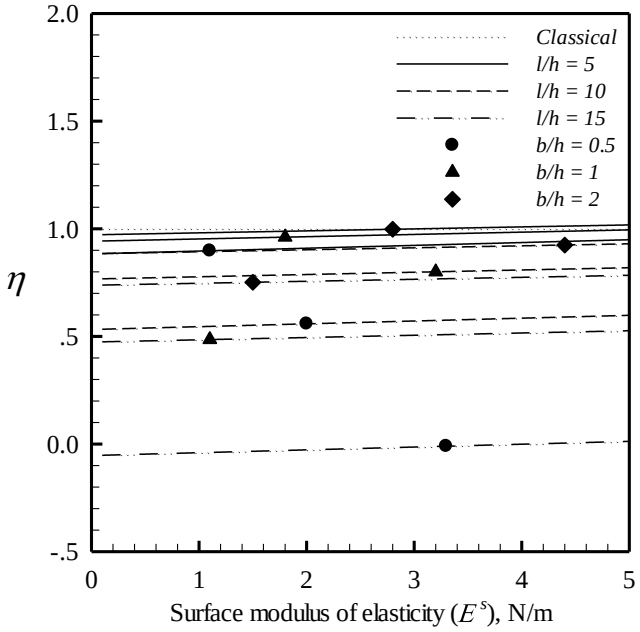

Figure 6.1 Relationship between η and **(a)** surface modulus of elasticity for $\tau^s = 0$ and **(b)** surface modulus of elasticity for $\tau^s = 0.89\,\text{N/m}$

The relationship between η and the residual surface tension τ^s for $E^s = 1.22$ is shown in Figure 6.2. Unlike the surface modulus of elasticity, the increment of the residual surface tension tends to soften the nano-beam and, clearly, this influence is more significant when the slenderness ratio of the beam becomes smaller whereas the aspect ratio of the cross section becomes larger. In addition, the relationship between the nonlocal parameter μ and the length of a nano-element is also shown in Figure 6.3 for different values of $(e_0 a)^2 = \alpha (e_0 a)^2_{ref}$ where $(e_0 a)^2_{ref} = 10^{-14}\,\mathrm{m}^2$ and $\alpha \in \{1, 0.1, 0.01\}$. As become clear from this set of results, the nonlocal parameter μ decreases as the length of the beam increases and, as a result, the nonlocal effect can be neglected for sufficiently large element length.

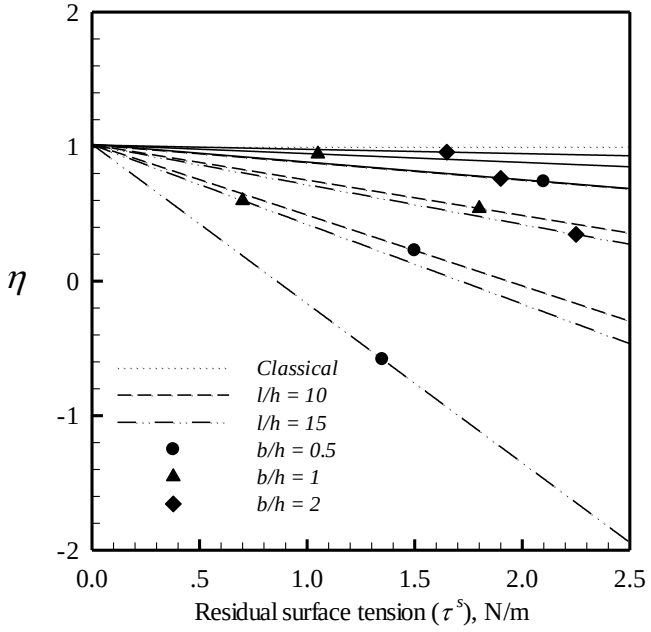

Figure 6.2 Relationship between residual surface tension and η of nano-beam with different slenderness ratio and different aspect ratio of cross section

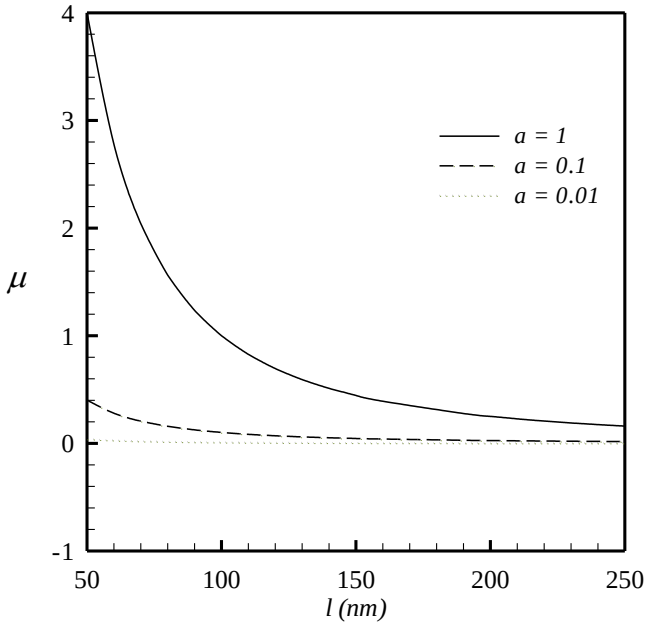

Figure 6.3 Relationship between nonlocal parameter and length of nano-beam

6.1 Bending of Nano-beams

A selected set of numerical results obtained from the proposed model are presented in various forms. To demonstrate the accuracy and efficiency of the current technique, results generated by a classical model (i.e., model without the influence of surface stresses and local effects, i.e. $\eta = 1$ and $\mu = 0$) are obtained and compared with existing benchmark cases. Once the formulation and implementation are fully checked, the technique is then applied to explore the effect of the surface stresses and nonlocal elasticity on the bending behaviors of both fixed-free and fixed-rollered nano-beams.

6.1.1 Verification

Consider the bending of fixed-free nano-beam without the the surface stresses and nonlocal linear elasticity (i.e., $\eta = 1$ and $\mu = 0$). Results of the bending shape of the fixed-free nano-beam subjected to a normalized transverse load $k = 2$ is reported and compared with those presented by Liu et al. (2012) in Figure 6.4. It is apparent that the developed numerical procedure yield very accurate numerical results for the classical case. In particular, the computed shape of the deflection tends to align with the analytical solution.

Next, the bending shape of fixed-rollered nano-beam without the surface stresses and nonlocal linear elasticity (i.e., $\eta = 1$ and $\mu = 0$) and subjected to the normalized end moment $\bar{m}_0 = 1/3$ is reported and compared with finite element model from ABAQUS as shown in Figure 6.5. Similar to the previous case, numerical results generated by the proposed technique and the reference solutions are almost indistinguishable for the entire beam.

6.1.2 Size Dependence Behavior

In order to explore the effect of surface stresses and nonlocality on the bending behavior of both fixed-free and fixed-rollered nano-beams, results are obtained for four different models, Model-1 without the surface and nonlocal effects (i.e., $\eta = 1, \mu = 0$), Model-2 considering only the surface effect (i.e., $\mu = 0$), Model-3 considering only the nonlocal effect (i.e., $\eta = 1$), and Model-4 considering both the surface and nonlocal effects. To show the size-dependent characteristic of the numerical solutions, results are obtained for various values of the normalized length $\bar{l} = l/\Lambda$ while maintaining the slenderness ratio $l/h = 10$ and the aspect ratio of the cross section $b/h = 1$.

The tip rotation (θ_2), the normalized longitudinal tip displacement ($\bar{u}_2$), and the normalized transverse tip displacement ($\bar{v}_2$) for the fixed-free nano-beam are reported in Figures 6.6-6.8, for all four model and two values of the normalized end load $k \in \{2, 4\}$. The deflected shapes of the fixed-free nano-beam for *l* = 50 nm and *l* = 200 nm are also shown in Figures 6.9 and 6.10 for $k = 2$ and $k = 4$, respectively. It can be deduced from those results that presence of the surface stresses with or without nonlocal effects (i.e., Model-2 and Model-4) tends to soften the nano-beam (i.e., reduce the apparent bending stiffness) and the predicted solutions are considerably different from results generated by the classical case (i.e., Model-1). It should be also evident by comparing results obtained from the Model-2 and the Model-3 that the surface stress effect is more prominent than the local effect. This, as a consequence, renders the solutions generated by the Model-2 and Model-4 only slightly different. Another crucial finding is that the bending response of the nano-beam is obviously size-dependent when the surface stresses and nonlocal effects are added into the mathematical model. This

observed behavior is in contrast to that of the classical solution which is size-independent upon the proper normalization.

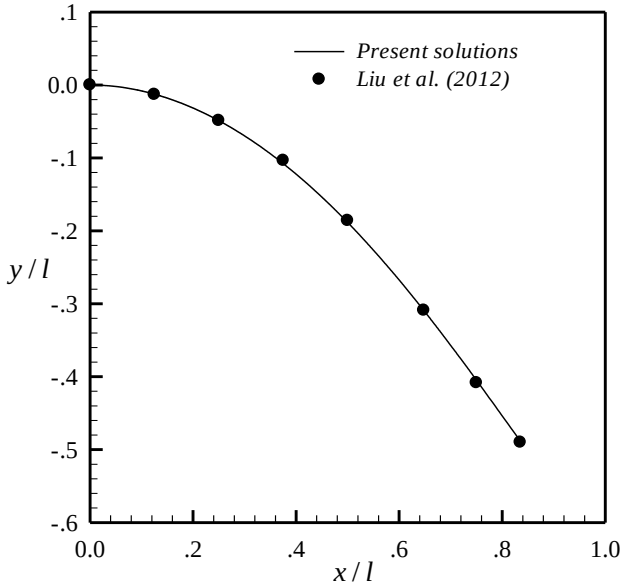

Figure 6.4 Deflected shape of fixed-free nano-beam subjected to normalized tip load $k = 2$. Results are reported for the present solutions and compared with those reported by Liu et al. (2012)

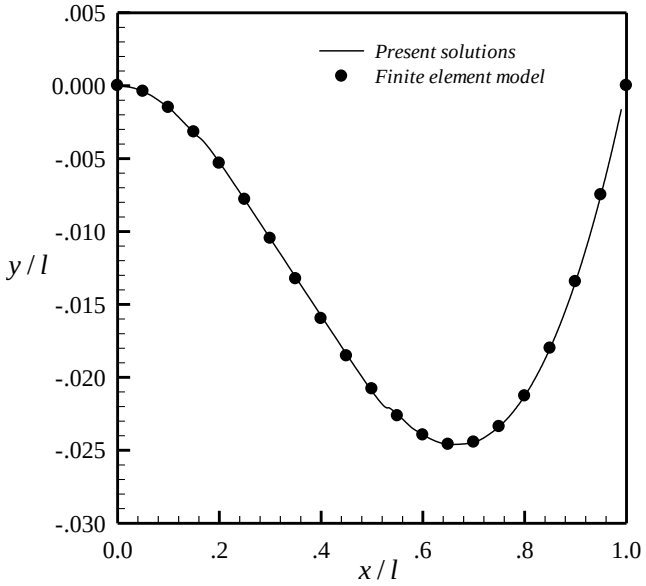

Figure 6.5 Deflected shape of fixed-rollered nano-beam subjected to normalized end moment $\bar{m}_0 = 0.67$. Results are reported for the classical case and compared with those generated by ABAQUS

It is obviously seen from Figures 6.6-6.8 that, when the length of the nano-beam becomes smaller, results obtained from the Model-2 and Model-4 are distinctly different from the classical solutions and, as the length is relatively large in comparison with the intrinsic length Λ, the solutions tend to converge to results for the classical case. It is important to point out that the observed discrepancy for a particular length l is more noticeable for results generated by the models incorporating the surface stresses (i.e., Model-2 and Model-4). Based on the characteristic of the displacements and deflected shapes observed in the numerical study, the reduction of the apparent bending stiffness can become substantial when the dimension of the beam decreases to a nano level (i.e., comparable to the material intrinsic length scale Λ), and this implies the necessity to properly incorporate the surface stresses and the nonlocal effects in the theoretical model to physically capture the nano-scale influence.

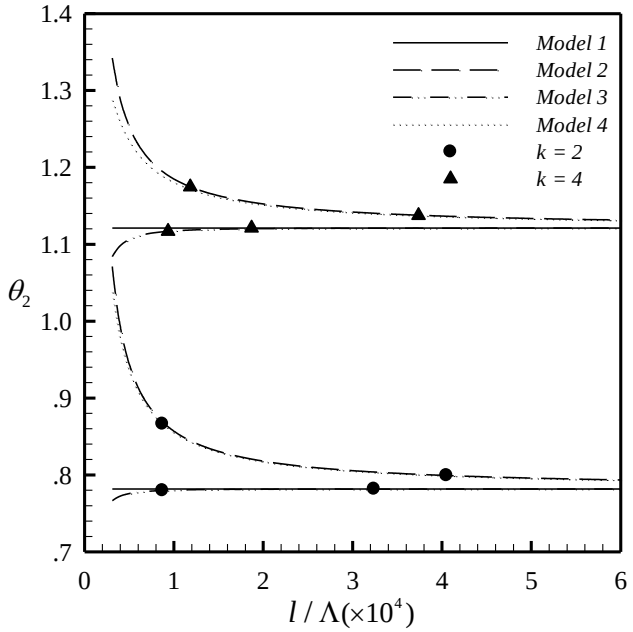

Figure 6.6 Relationship between normalized length and tip rotation of fixed-free nano-beam subjected to normalized tip load $k \in \{2, 4\}$

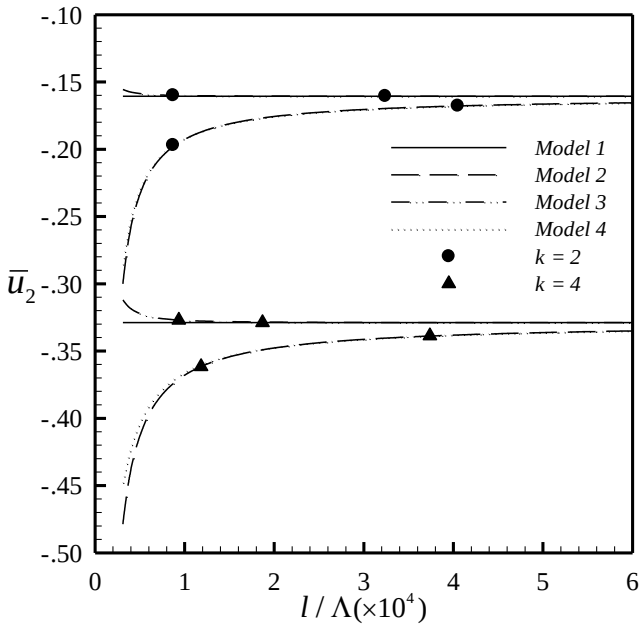

Figure 6.7 Relationship between normalized length and normalized longitudinal tip displacement of fixed-free nano-beam subjected to normalized tip load $k \in \{2, 4\}$

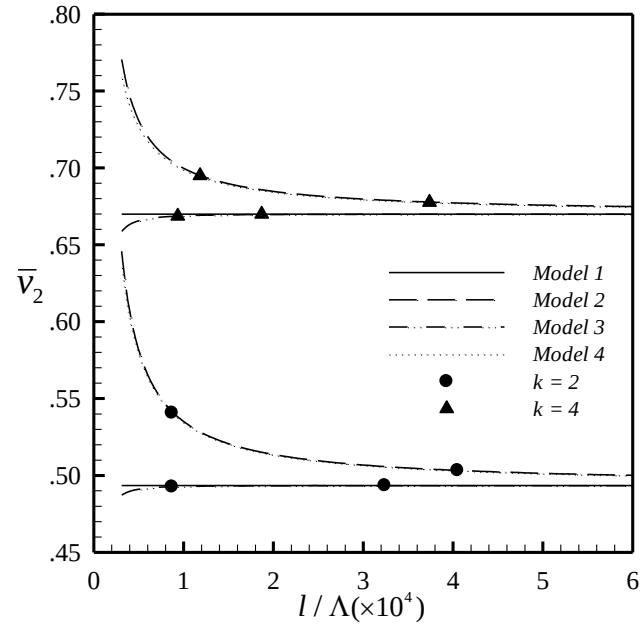

Figure 6.8 Relationship between normalized length and normalized transverse tip displacement of fixed-free nano-beam subjected to normalized tip load $k \in \{2, 4\}$

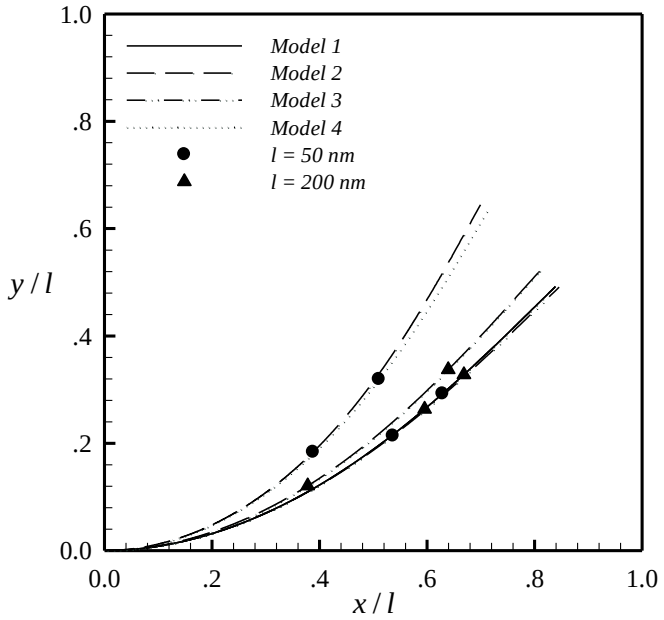

Figure 6.9 Deflected shape of fixed-free nano-beam under normalized transverse force $k = 2$ for l = 50, 200 nm

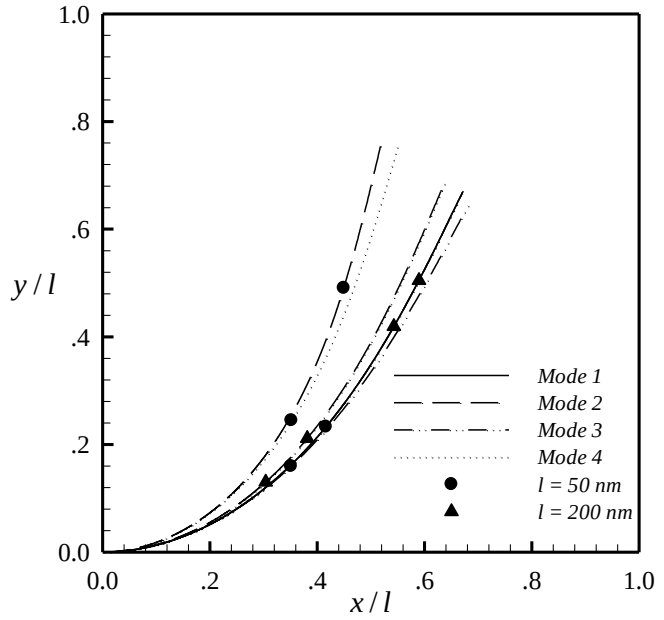

Figure 6.10 Deflected shape of fixed-free nano-beam under normalized transverse force $k = 4$ for l = 50, 200 nm

A similar set of numerical experiments has also been conducted to examine the influence of surface stresses and nonlocal effect on the bending behavior of the fixed-rollered nano-beam. Results are obtained for many values of the normalized length $\bar{l} = l/\Lambda$ while maintaining the slenderness ratio $l/h = 10$ and the cross-section aspect ratio $b/h = 1$ to shown the size-dependent behavior of the solution. The tip rotation (θ_2), the rotation at the interior inflection point (θ_z), the normalized maximum longitudinal displacement ($\bar{u}_{\max} = u_{\max}/l$), and the normalized maximum transverse displacement ($\bar{v}_{\max} = v_{\max}/l$) as a function of the normalized length l/Λ are reported in Figures 6.8-6.14 for all four models and two values of the normalized moment $\bar{m}_0 \in \{5.5, 6\}$.

The deflected shape of the beam for $l = 75$ nm and $l = 450$ nm are also shown in Figure 6.15 and Figure 6.16 for $\bar{m}_0 = 5.5$ and $\bar{m}_0 = 6$, respectively. Similar to the fixed-free case, results predicted by the model including the surface stresses significantly deviate from those of the classical case and presence of the surface effect considerably lower the apparent bending stiffness of the beam if its length l is close to the material intrinsic length scale Λ.Likewise, the role of the nonlocal elasticity effect depends mainly on the characteristic length scale of the problem relative to the parameter μ; in particular, if the length of the beam decreases to a nano-scale, the effect in reducing the member stiffness is prominent. It is also apparent from these results that the discrepancy between responses obtained by the model incorporating only the surface stresses (Model-2) and the classical solution is much larger than that predicted by the model considering only the nonlocal effect (Model-3). In addition, the Model-4 (incorporating both the surface stresses and nonlocal effects) yields results nearly identical to those obtained from the Model-2. Similar to the fixed-free case, all models incorporating the nano-scale influence (i.e., Model-2, Model-3 and Model-4) exhibit strong size-dependent behavior. Specifically, as the element size reduces to that comparable to the intrinsic length of the material surface, the influence of both nonlocal elasticity and surface stresses are substantial and they must be properly considered in a mathematical model to reasonably capture the nano-scale phenomena.

6.1.3 Influence of Material Parameters

In order to investigate the contribution of material properties on the bending behavior of the fixed-free nano-beam, its responses for various values of the surface modulus of elasticity E^s and residual surface tension τ^s are obtained and compared. In the simulation, the beam length 500 nm, the slenderness ratios $l/h \in \{10,15,20\}$, the cross sectional aspect ratio $b/h = 1$, the nonlocal parameter $(e_0 a)^2 = 10^{-16}$ m^2, and the normalized tip load k = 2.5 are chosen. The relationship between the tip rotation (θ_2), the normalized longitudinal tip displacement ($\bar{u}_2$), and the normalized transverse tip displacement ($\bar{v}_2$) of the fixed-free nano-beam and the surface modulus of elasticity (E^s) is presented in Figures 6.17-6.19. It is deduced from obtained results that the increase of the surface modulus tends to stiffen the nano-beam. In addition, results obtained as a function of the residual surface tension (τ^s) are reported in Figures 6.20-6.22. Unlike the surface modulus of elasticity, the increment of τ^s tends to soften the nano-beam.

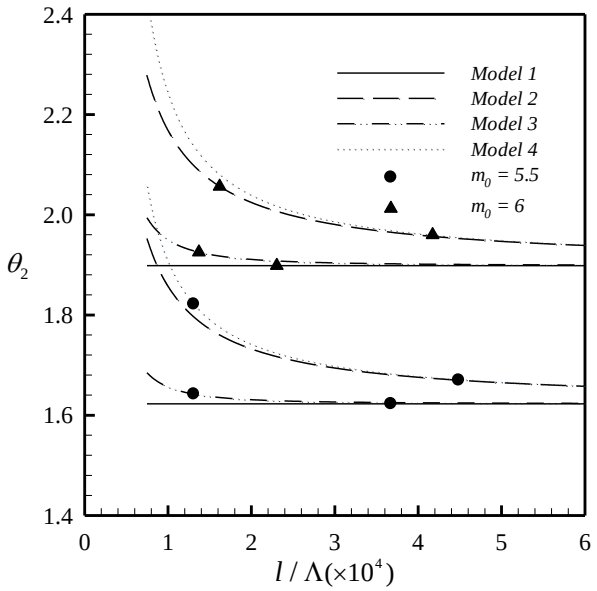

Figure 6.11 Relationship between normalized length and tip rotation of fixed-rollered nano-beam under normalized end moment $\bar{m}_0 \in \{5.5, 6\}$

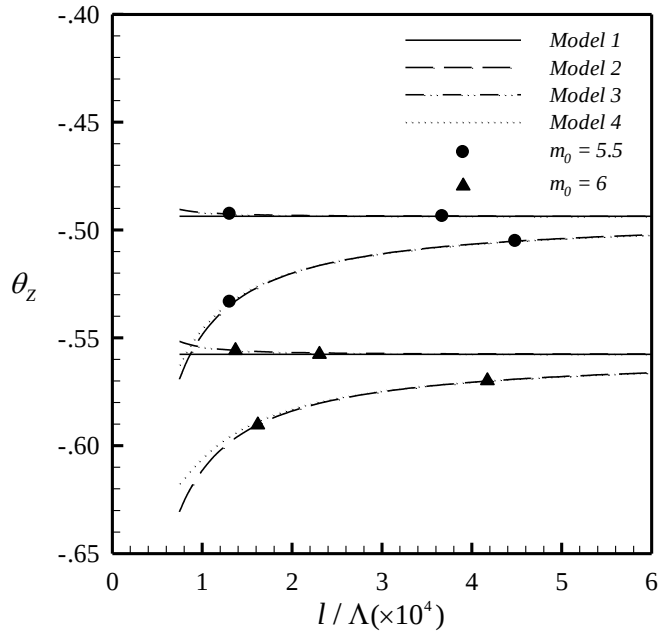

Figure 6.12 Relationship between normalized length and rotation at interior inflection point of fixed-rollered nano-beam under normalized end moment $\bar{m}_0 \in \{5.5, 6\}$

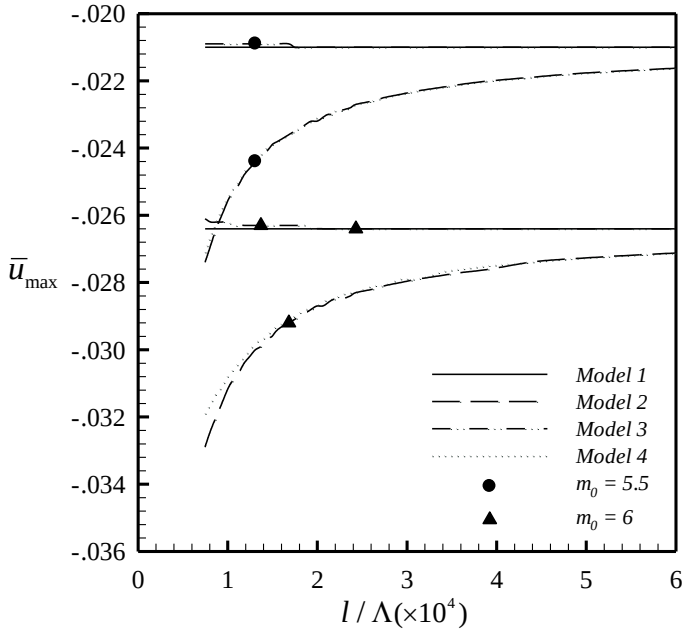

Figure 6.13 Relationship between normalized length and normalized maximum longitudinal displacement of fixed-rollered nano-beam under normalized end moment $\bar{m}_0 \in \{5.5, 6\}$

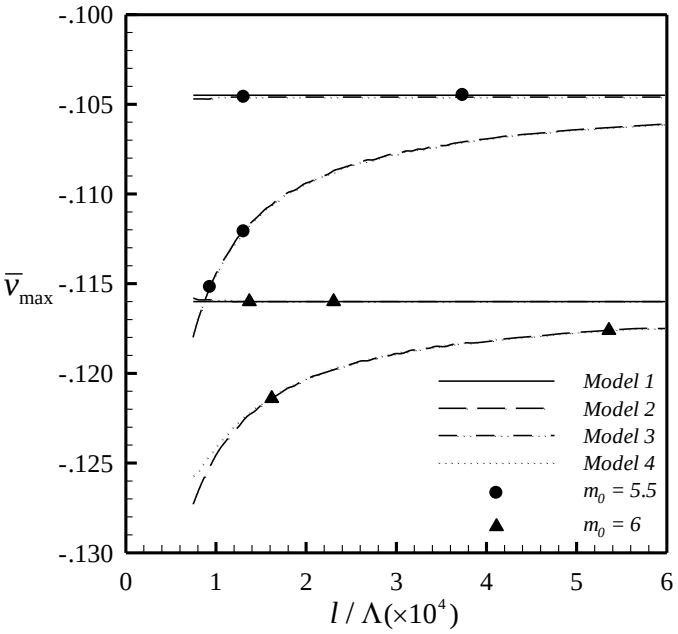

Figure 6.14 Relationship between normalized length and normalized maximum transverse displacement of fixed-rollered nano-beam under normalized end moment $\bar{m}_0 \in \{5.5, 6\}$

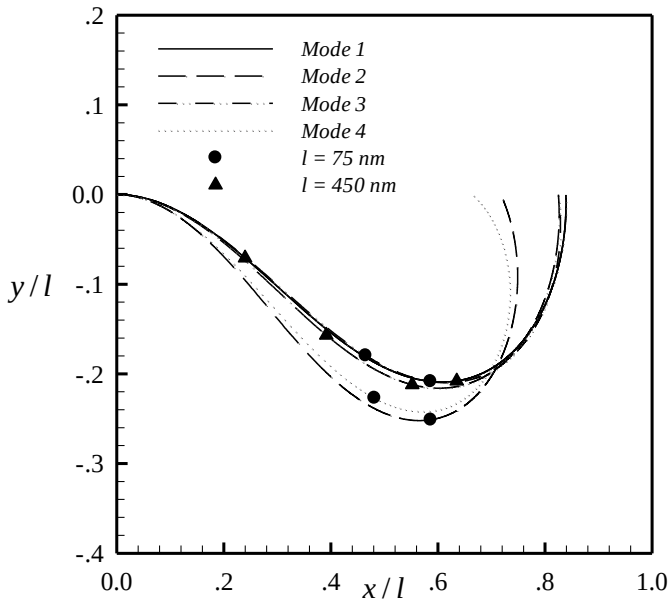

Figure 6.15 Deflected shape of fixed-rollered nano-beam under normalized end moment $\bar{m}_0 = 5.5$ for l = 75 nm, 450 nm

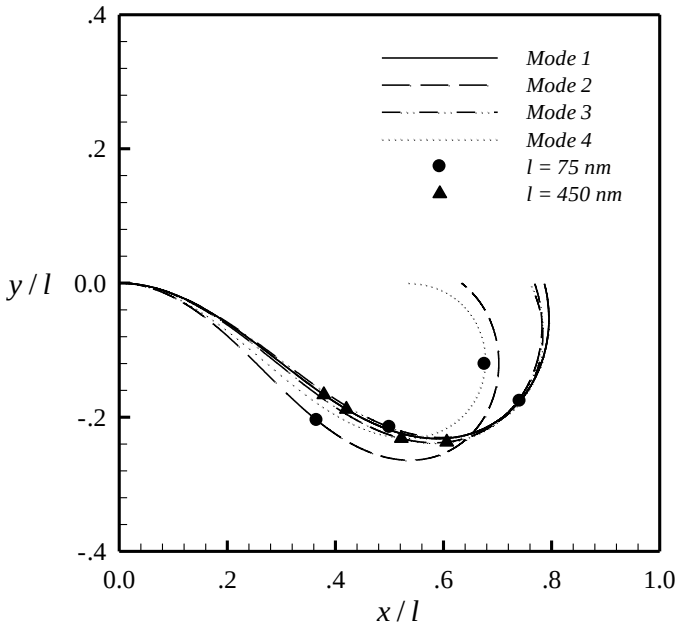

Figure 6.16 Deflected shape of fixed-rollered nano-beam under normalized end moment $\bar{m}_0 = 6$ for l = 75 nm, 450 nm

For the fixed-rollered nano-beam, the influence of the surface modulus of elasticity and the residual surface tension are also investigated. In numerical experiments, the length of the beam l = 500 nm, the cross sectional aspect ratio $b/h = 1$, three slenderness ratios $l/h \in \{5,10,15\}$, the nonlocal parameter $(e_0 a)^2 = 10^{-16}\,\mathrm{m}^2$, and the normalized end moment $\bar{m}_0 = 6$ are chosen. The tip rotation (θ_2), the normalized maximum longitudinal displacement ($\bar{u}_{\max} = u_{\max}/l$), and the normalized maximum transverse displacement ($\bar{v}_{\max} = v_{\max}/l$) versus E^s and τ^s are reported in Figures 6.23-6.25 and Figures 6.26-6.28, respectively. Similar to the fixed-free case, the surface stresses inclines to enhance the bending stiffness whereas the reverse effect can be observed when the positive τ^s is present. It is also apparent from results for both fixed-rollered and fixed-free elements that when the slenderness ratio of the member becomes larger, the effect of the surface stresses is clearly more prominent.

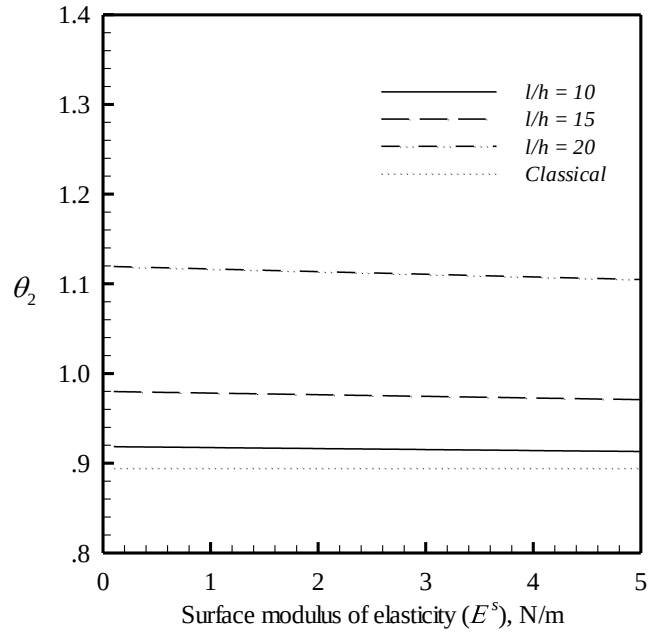

Figure 6.17 Relationship between surface modulus of elasticity and tip rotation of fixed-free nano-beam for three values of slenderness ratio

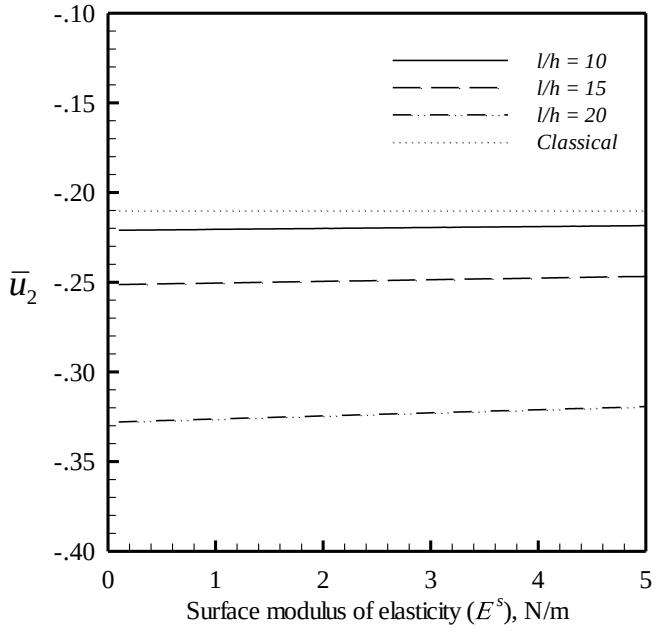

Figure 6.18 Relationship between surface modulus of elasticity and normalized longitudinal tip displacement of fixed-free nano-beam for three values of slenderness ratio

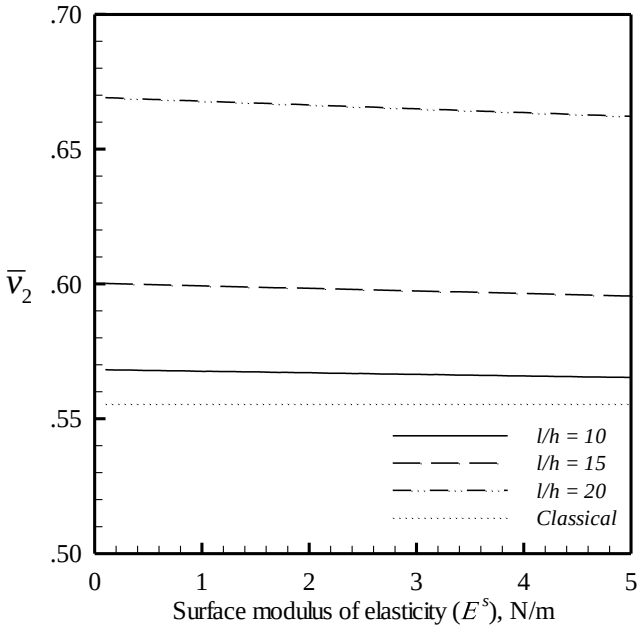

Figure 6.19 Relationship between surface modulus of elasticity and normalized transverse tip displacement of fixed-free nano-beam for three values of slenderness ratio

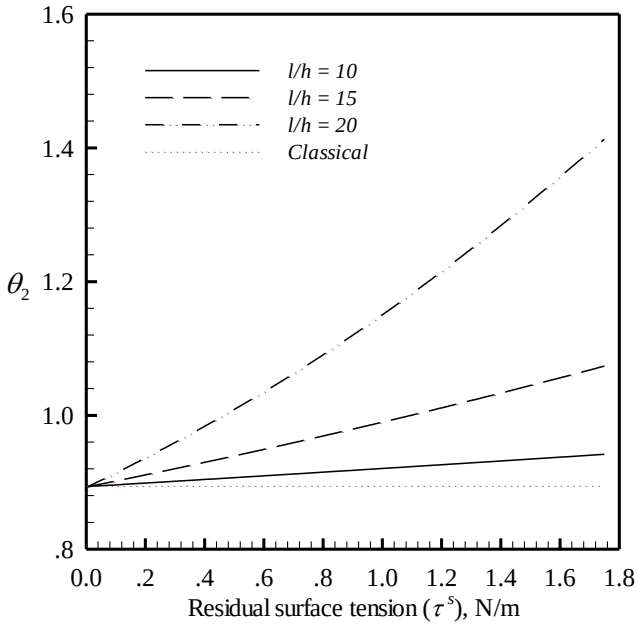

Figure 6.20 Relationship between residual surface tension and tip rotation of fixed-free nano-beam for three values of slenderness ratio

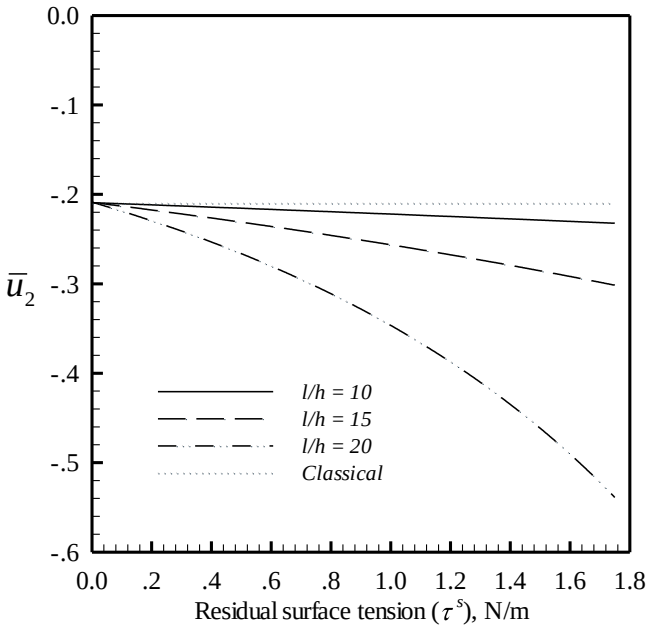

Figure 6.21 Relationship between residual surface tension and normalized longitudinal tip displacement of fixed-free nano-beam for three values of slenderness ratio

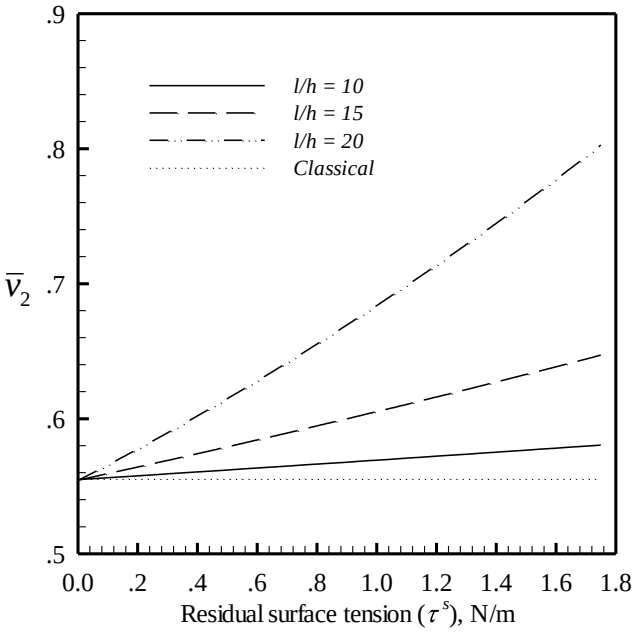

Figure 6.22 Relationship between residual surface tension and normalized transverse tip displacement of fixed-free nano-beam for three values of slenderness ratio

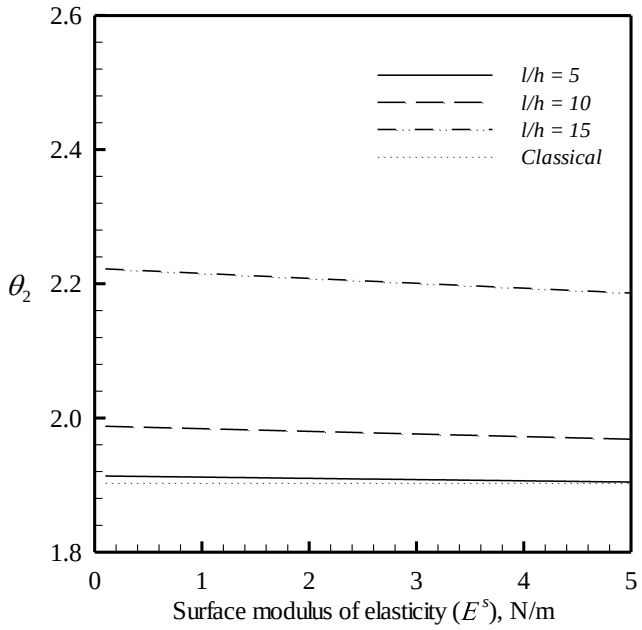

Figure 6.23 Relationship between surface modulus of elasticity and tip rotation of fixed-rollered nano-beam for three values of slenderness ratio

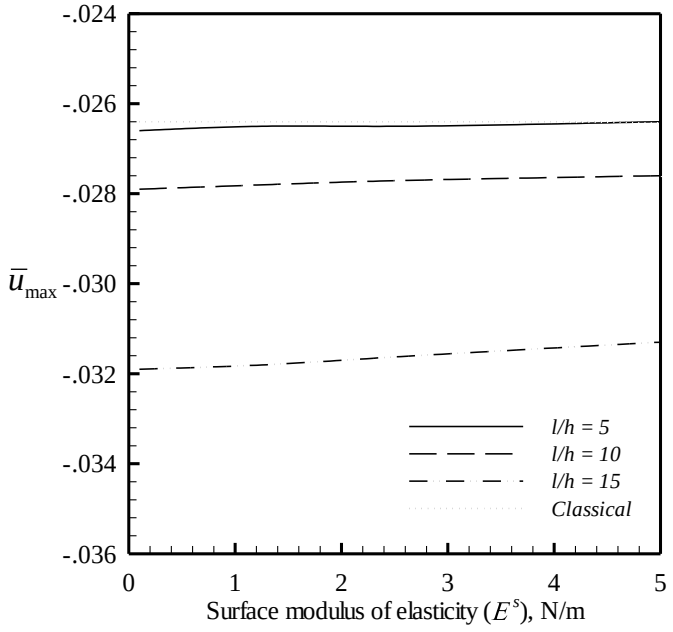

Figure 6.24 Relationship between surface modulus of elasticity and normalized maximum longitudinal displacement of fixed-rollered nano-beam for three values of slenderness ratio

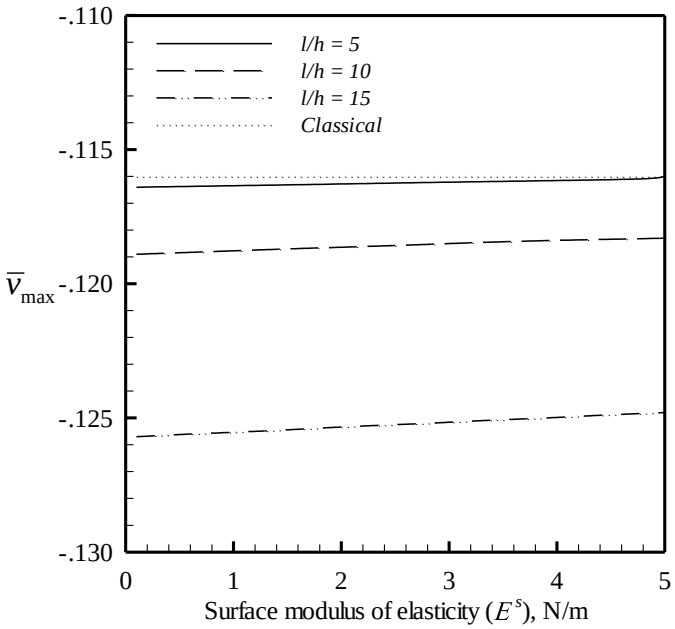

Figure 6.25 Relationship between surface modulus of elasticity and normalized maximum transverse displacement of fixed-rollered nano-beam for three values of slenderness ratio

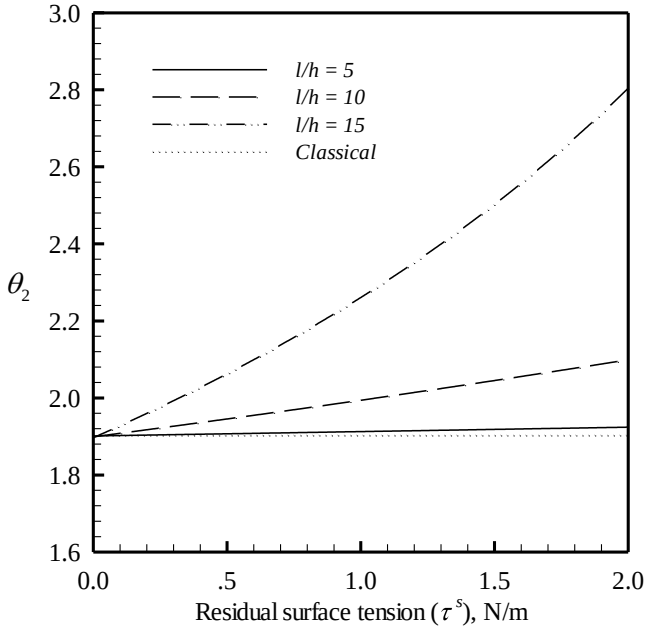

Figure 6.26 Relationship between residual surface tension and tip rotation of fixed-rollered nano-beam for three values of slenderness ratio

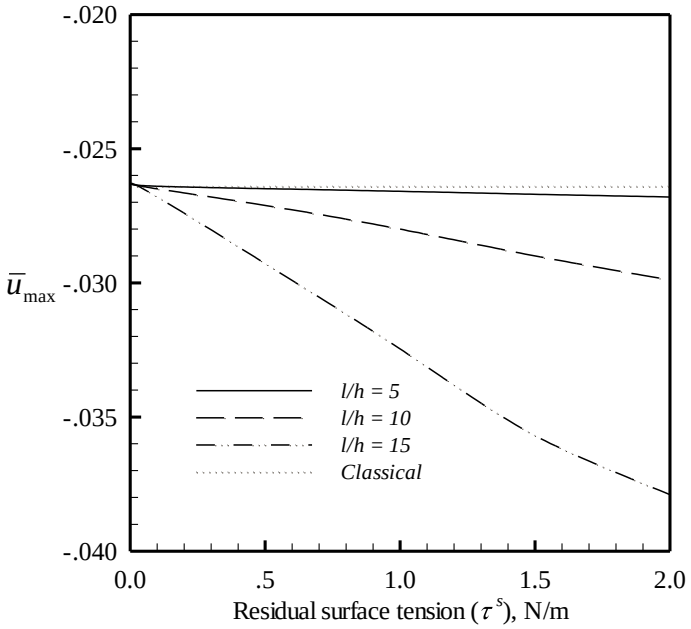

Figure 6.27 Relationship between residual surface tension and normalized maximum longitudinal displacement of fixed-rollered nano-beam for three values of slenderness ratio

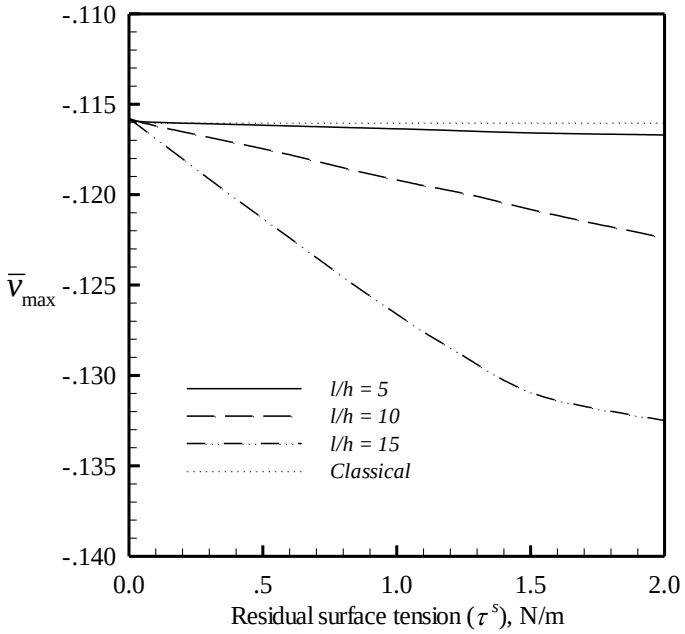

Figure 6.28 Relationship between residual surface tension and normalized maximum transverse displacement of fixed-rollered nano-beam for three values of slenderness ratio

To further investigate the influence of the nonlocal parameter (μ) on the bending responses of nano-elements, results are obtained for various values of μ while E^s and τ^s remain fixed (i.e., E^s = 1.22 N/m and τ^s = 0.89 N/m). In the numerical study, the cross-section aspect ratio, the length, and the slenderness ratio of the fixed-free and fixed-rollered beams are taken as $b/h=1$, $l=500$, $l/h \in \{10,15,20\}$ and $b/h=1$, $l=1500$, $l/h \in \{5,10,15\}$, respectively. Results for the tip rotation, the normalized longitudinal tip displacement, and the normalized transverse tip displacement of the fixed-free case and those for the tip rotation, the normalized maximum longitudinal and transverse displacements of the fixed-rollered case are reported as a function of the nonlocal parameter in Figures 6.29-6.31 and Figures 6.32-6.34, respectively. As become evident from these results, the bending response of both nano beams exhibits strong dependence on the nonlocal parameter, and this influence is more significant when the slenderness ratio of an element increases.

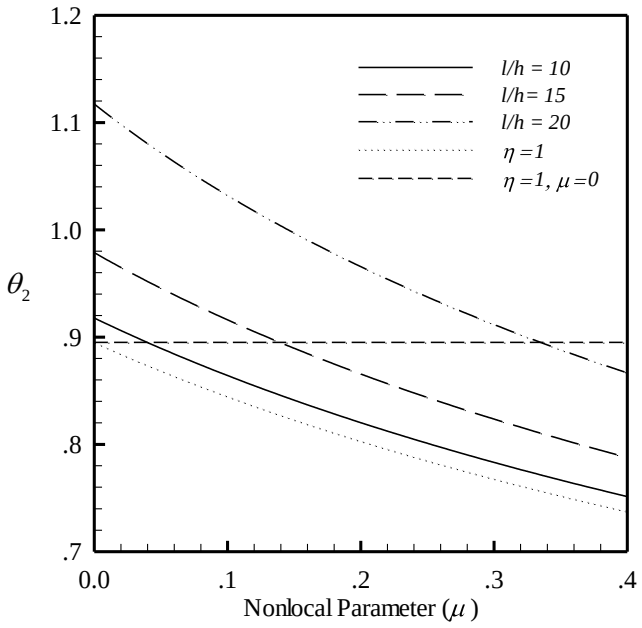

Figure 6.29 Relationship between nonlocal parameter and tip rotation of fixed-free nano-beam for three values of slenderness ratio

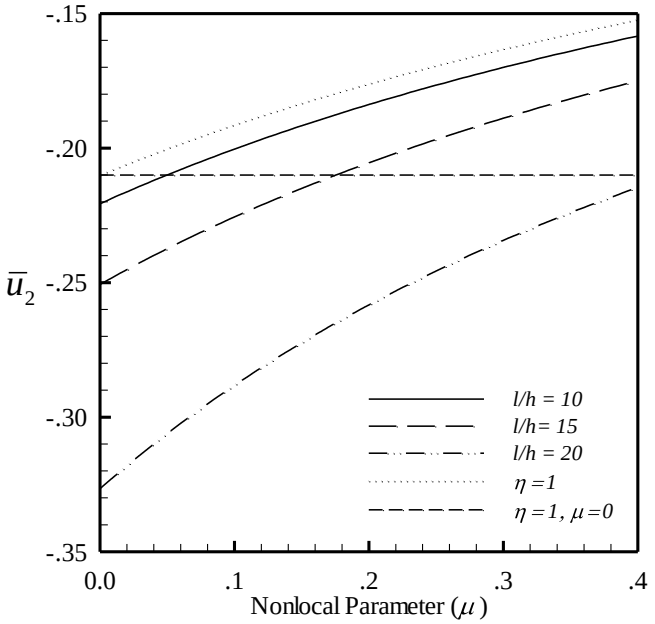

Figure 6.30 Relationship between nonlocal parameter and normalized longitudinal tip displacement of fixed-free nano-beam for three values of slenderness ratio

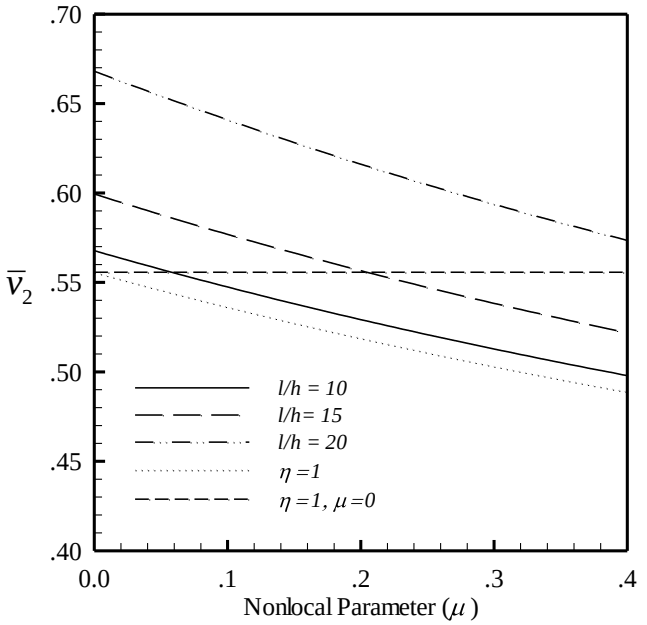

Figure 6.31 Relationship between nonlocal parameter and normalized transverse tip displacement of fixed-free nano-beam for three values of slenderness ratio

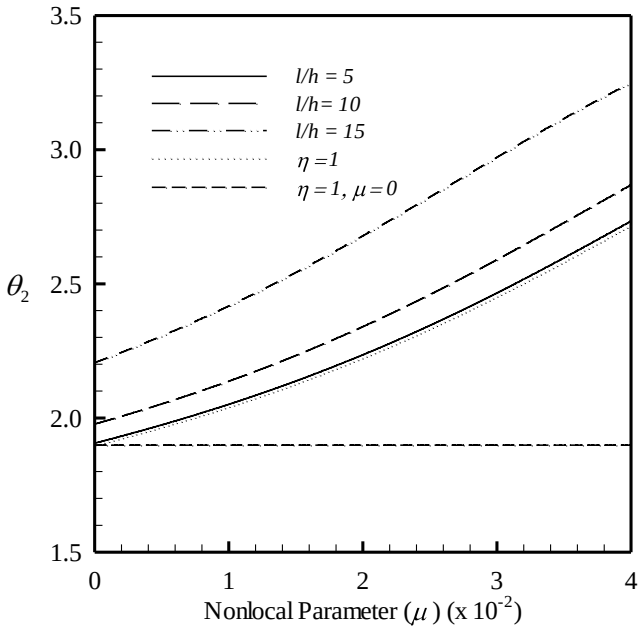

Figure 6.32 Relationship between nonlocal parameter and tip rotation of fixed-rollered nano-beam for three values of slenderness ratio

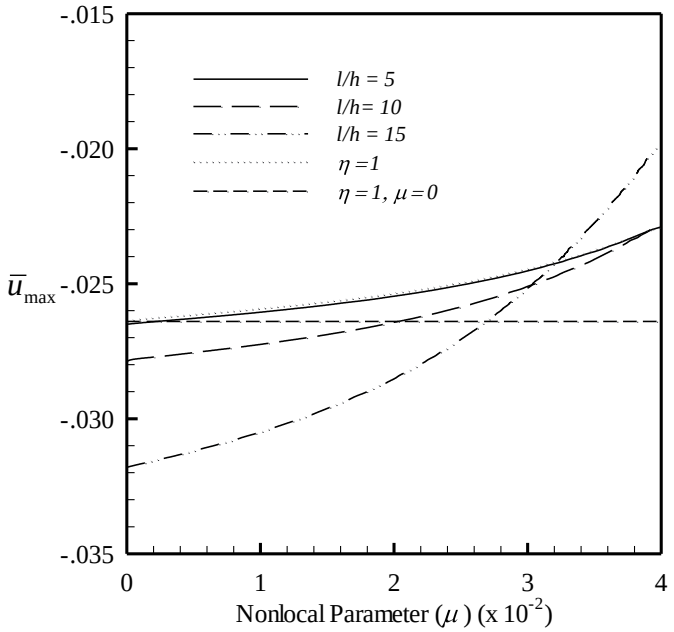

Figure 6.33 Relationship between nonlocal parameter and normalized maximum longitudinal displacement of fixed-rollered nano-beam for three values of slenderness ratio

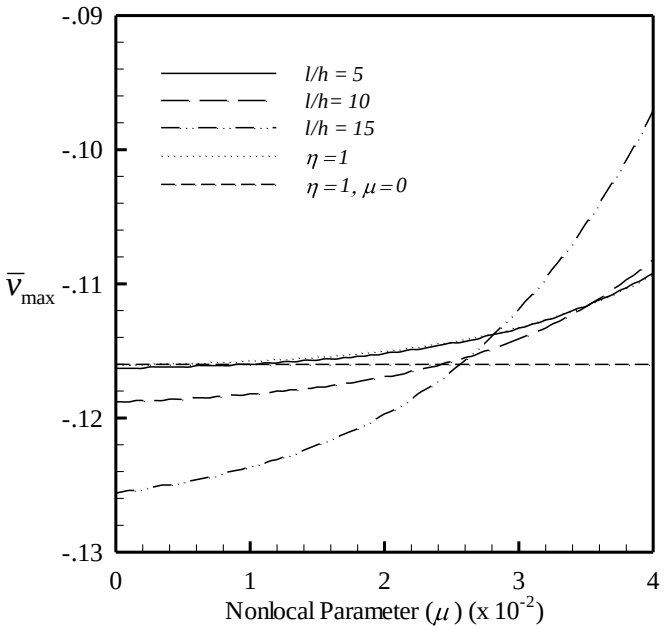

Figure 6.34 Relationship between nonlocal parameter and normalized maximum transverse displacement of fixed-rollered nano-beam for three values of slenderness ratio

6.2 Buckling Load of Nano-beam

In this section, results for buckling loads of both fixed-free and fixed-rollered nano-beams are presented. To verify the proposed technique, results for a classical case are obtained and compared with existing reference solutions. Once the formulation and implementation are extensively verified, the technique is then applied to investigate the effect of the surface stresses and nonlocal elasticity on values of buckling loads of both fixed-free and fixed-rollered nano-beams**.**

6.2.1 Verification

For nano-beams without the surface stresses and nonlocal linear elasticity (i.e., $\eta = 1$ and $\mu = 0$), the buckling load obtained from the current technique is reported and compared with results generated by classical Euler-Bernoulli beam theory as a function of the beam length in Figure 6.35 for the fixed-free beam and in Figure 6.36 for the fixed-rollered beam. It is apparent that the proposed technique yields results identical to the existing reference solutions. This additionally ensures the validity of the derived buckling load formula.

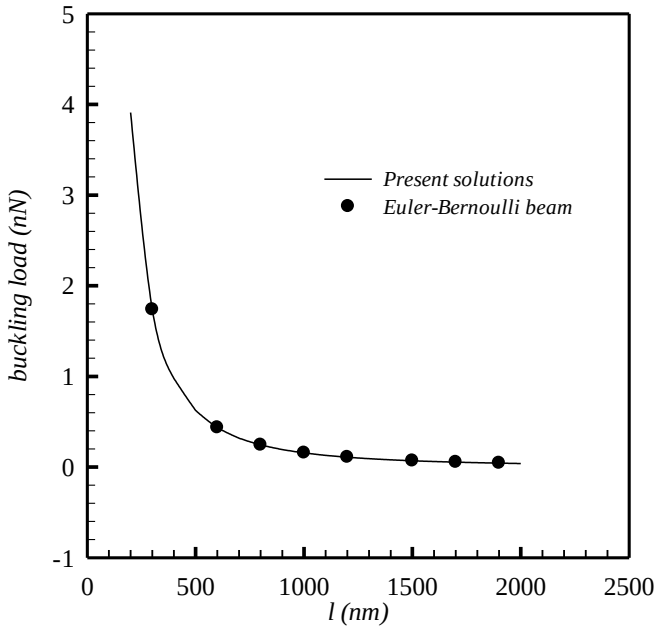

Figure 6.35 Comparison of buckling load generated by present technique and Euler-Bernoulli beam theory for fixed-free beam

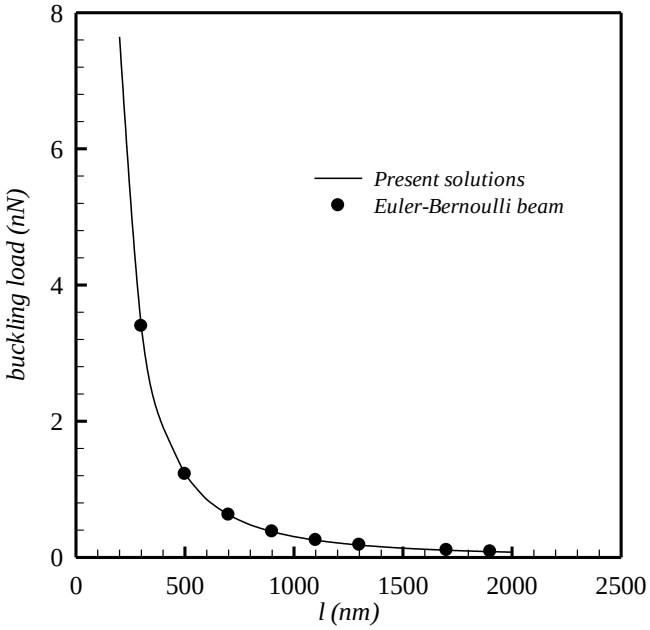

Figure 6.36 Comparison of buckling load generated by present technique and Euler-Bernoulli beam theory for fixed-rollered beam

6.2.2 Size Dependence Behavior

To consider the size dependency of predicted solution, the width b, the depth h and the length l of the nano-element are scaled by a proportional ratio β such that $l = \beta l_0$, $b = \beta b_0$ and $h = \beta h_0$ where l_0, b_0, h_0 denote the reference dimensions. In addition, the aspect ratio $h_0 / b_0 = 1$ with $h_0 = 10$ nm and $e_0 a = 100$ nm are chosen in the numerical study. The normalized buckling loads for both fixed-free and fixed-rollered nano-beams are reported in Figure 6.37 and Figure 6.38, respectively, for four slenderness ratios $l_0 / h_0 \in \{10, 20, 30, 40\}$ and for three models associated with the classical case, one with only the surface effect, and the other with both surface and nonlocal effects. It is seen from these results that the predicted normalized buckling loads with the integration of the surface stresses or both the surface and nonlocal effects exhibit strongly size dependent and, in particular, the discrepancy from the classical solution is very significant when the element size is within the range of nano-scale. In addition, the model with only the surface effect and that with both the surface and nonlocal effects predict lower buckling loads for both fixed-free and fixed-rollered nano-beams. Such finding is quite significant and different from the conclusion of the earlier work of Juntarasaid et al. (2012). This is owing mainly to that the presence of the positive residual surface tension generates the compressive residual stress in the bulk material and this, as a result, reduces the flexural rigidity of the beam.

6.2.3 Influence of Material Parameters

In this particular section, the effect of surface modulus of elasticity, the residual surface tension and the nonlocal parameter is investigated. In the numerical experiment, the length of the beam *l*, the slenderness ratio l/h, the cross-section aspect ratio b/h, and the nonlocal parameter $(e_0 a)^2$ are taken as *l* = 500 nm, $l/h \in \{10, 15, 20\}$, $b/h = 1$, and $(e_0 a)^2 = 10^{-14}$ m^2. The normalized buckling load P_{cr} / P_{cr}^c of the fixed-free and fixed-rollered nano-elements as a function of E^s is indicated in Figures 6.39 and 6.40, respectively, for τ^s = 0.89 N/m.

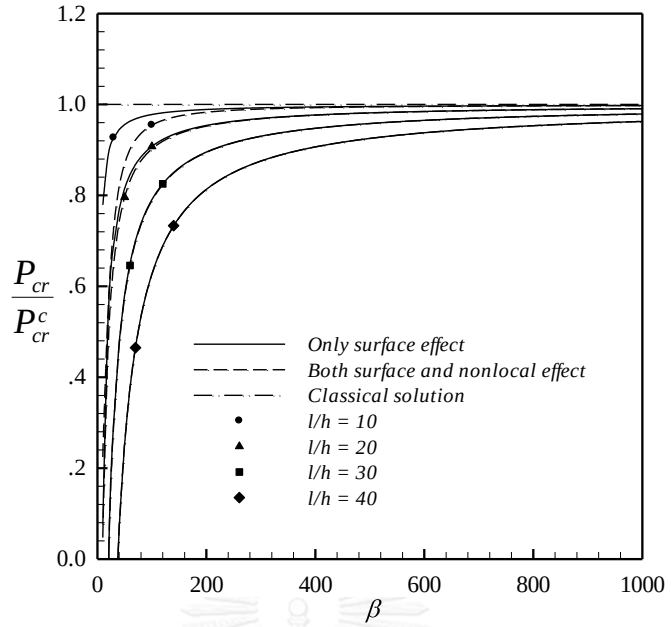

Figure 6.37 Normalized buckling load P_{cr} / P_{cr}^{c} of fixed-free nano-beam with a square cross section and different proportional ratio β.

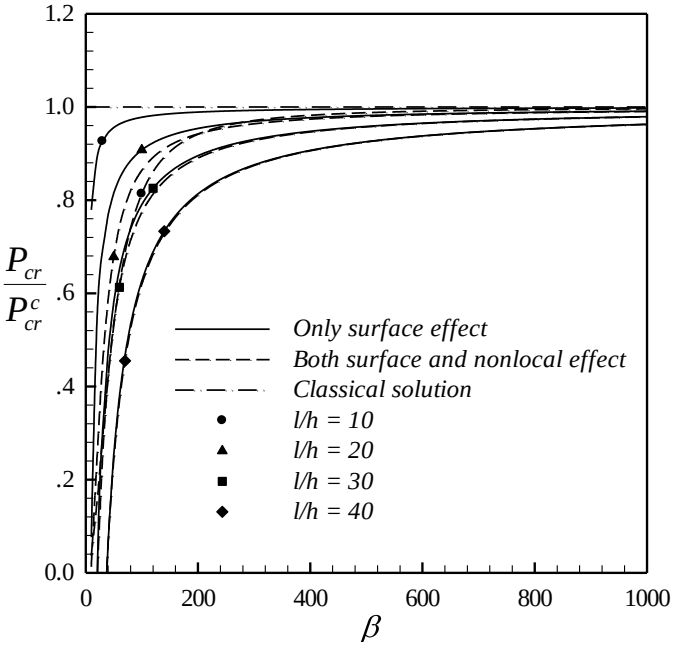

Figure 6.38 Normalized buckling load P_{cr} / P_{cr}^{c} of fixed-free nano-beam with a square cross section and different proportional ratio β

It can be deduced from these results that the enlargement of surface modulus of elasticity tends to stiffer the nano-beams. Additionally, the relation between the normalized buckling load P_{cr} / P_{cr}^{c} and the residual surface tension are presented in Figure 6.41 and Figure 6.42 for the fixed-free and fixed-rollered cases, respectively, and E^s = 1.22 N/m. Unlike the influence of E^s, the increment of τ^s tends to soften the nano-beams. Finally, the normalized buckling load P_{cr} / P_{cr}^{c} of both fixed-rollered and fixed-free nano-elements as a function of the nonlocal parameter μ is reported in Figures 6.43 and 6.44 for E^s = 1.22 N/m and τ^s = 0.89 N/m. It can be concluded that as μ increases, the normalized buckling load clearly reduces.

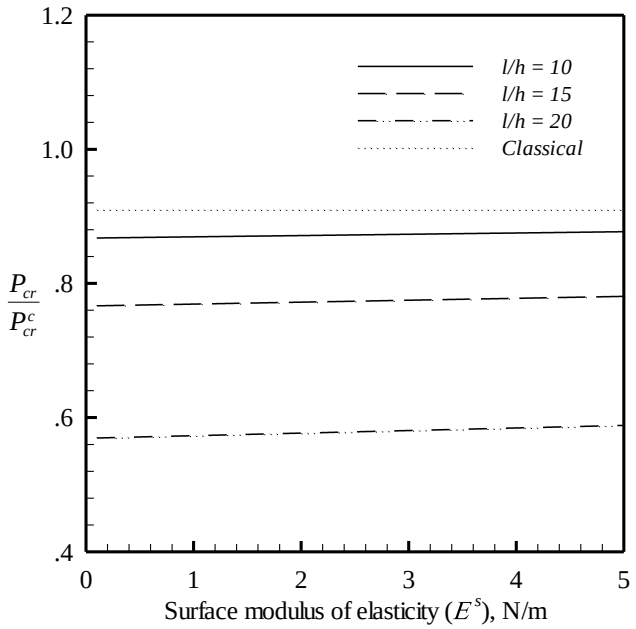

Figure 6.39 Normalized buckling load versus surface modulus of elasticity for fixed-free nano-beam

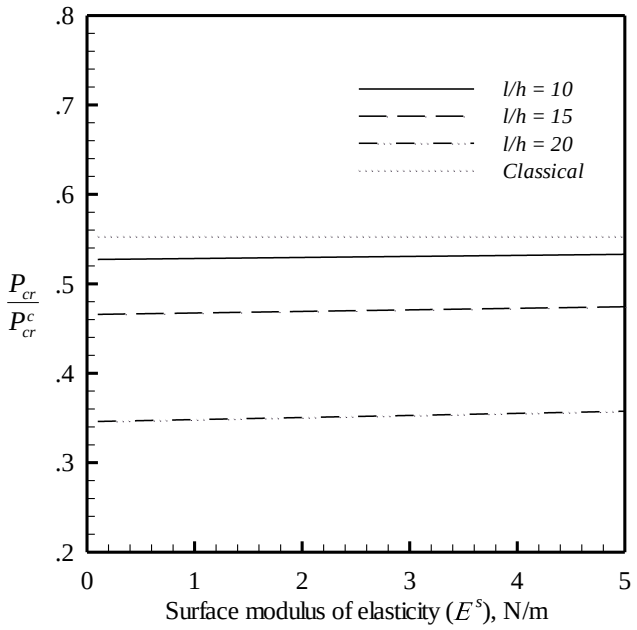

Figure 6.40 Normalized buckling load versus surface modulus of elasticity for fixed-rollered nano-beam

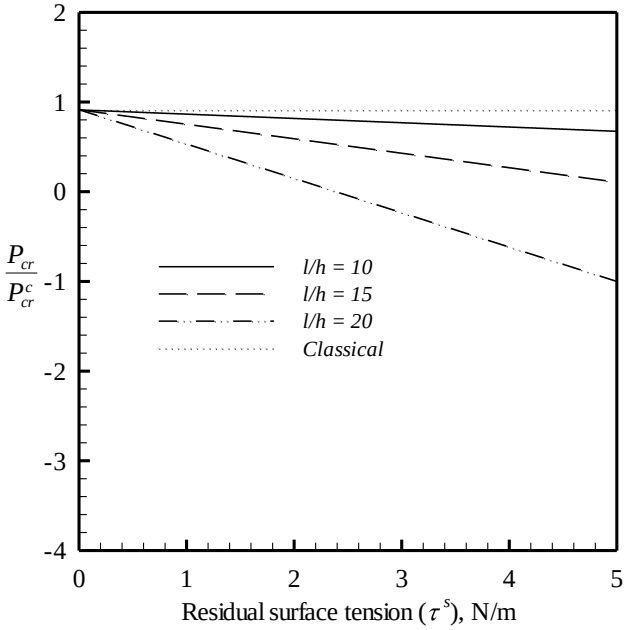

Figure 6.41 Normalized buckling load versus residual surface tension for fixed-free nano-beam

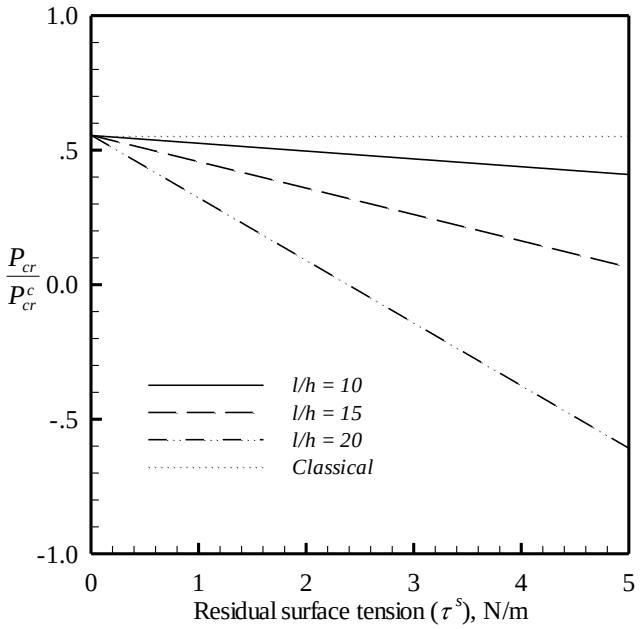

Figure 6.42 Normalized buckling load versus residual surface tension for fixed-rollered nano-beam

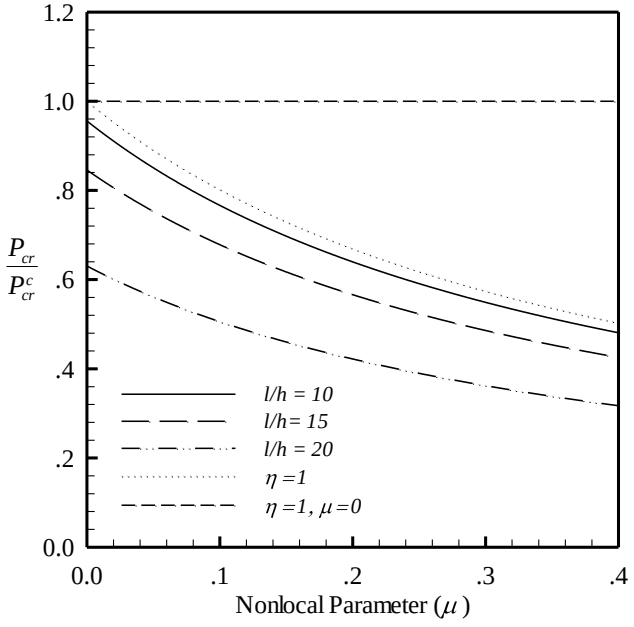

Figure 6.43 Normalized buckling load versus nonlocal parameter for fixed-free nano-beam

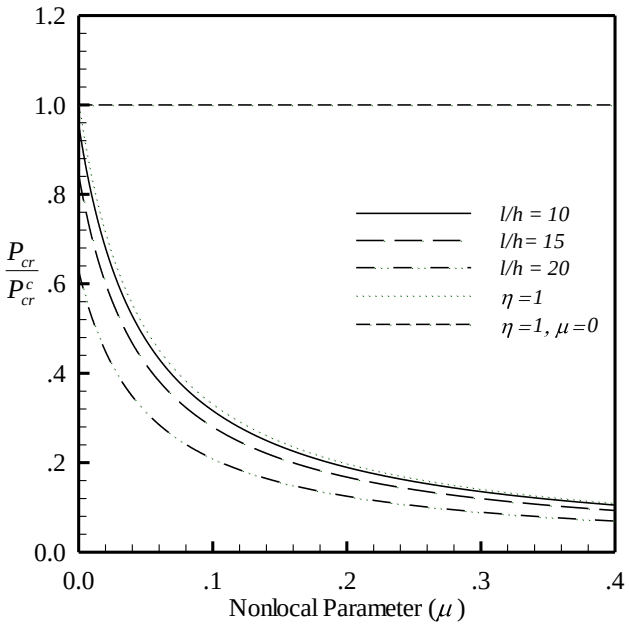

Figure 6.44 Normalized buckling load versus nonlocal parameter for fixed-rollered nano-beam

6.3 Post-buckling Responses of Nano-beams

In this section, results of post-buckling of nano-beams generated by the present technique are presented. To verify the current formulation and solution procedure and demonstrate the accuracy of the current technique, results from the classical model (i.e., model without surface stresses and nonlocal effect) are obtained first and compared with existing reference solutions. Then, the technique is employed to examine the effect of the surface stresses and nonlocal elasticity on the post-buckling response of both fixed-free and fixed-rollered nano-beams. Material parameters such as the modulus of elasticity and Poisson ratio of the bulk material, the residual surface tension, the surface modulus of elasticity, and nonlocal parameters employed by Juntarasaid et al. (2012) are chosen in the numerical study.

6.3.1 Verification

Let us consider first the post-buckling of a fixed-free nano-element without the consideration of the surface stresses and nonlocal linear elasticity (i.e., $\eta = 1$ and $\mu = 0$). Results of the normalized longitudinal and normalized transverse tip displacements ($\bar{u}_2$ and $\bar{v}_2$) and the tip rotation (θ_2) for various normalized tip load k

are reported and compared with those presented by Timoshenko and Gere (1961) in Figures 6.45-6.47. It is apparent that the developed technique offers very accurate numerical solutions for the classical case. In particular, as the normalized tip load k increases, both the tip rotation and the longitudinal tip displacement monotonically increase throughout the load history whereas the transverse tip displacement initially increases, then reaches the maximum value, and finally decays.

Next, the post-buckling of a fixed-rollered nano-beam is investigated using the classical model (i.e., $\eta = 1$ and $\mu = 0$). Results of the longitudinal tip displacement ($\bar{u}_2$), the tip rotation (θ_2), and the rotation at the interior inflection point (θ_z) are computed and then compared with those obtained by the semi-analytical technique similar to that proposed by Rungamornrat and Tangnovarad (2011) as shown in Figures 6.48-6.50. Similar to the previous case, numerical results generated by the present technique and the reference solutions are almost indistinguishable for all values of the normalized load k treated.

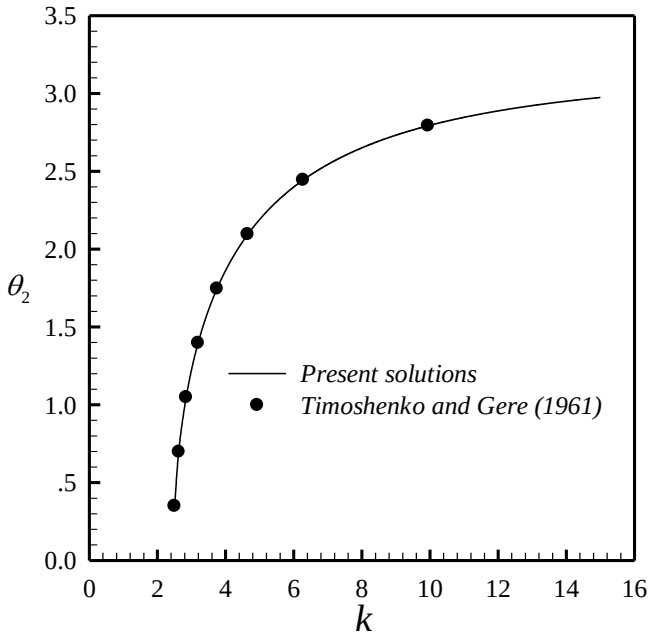

Figure 6.45 Relationship between normalized tip load and tip rotation of fixed-free nano-beam. Results are compared with those from Timoshenko and Gere (1961)

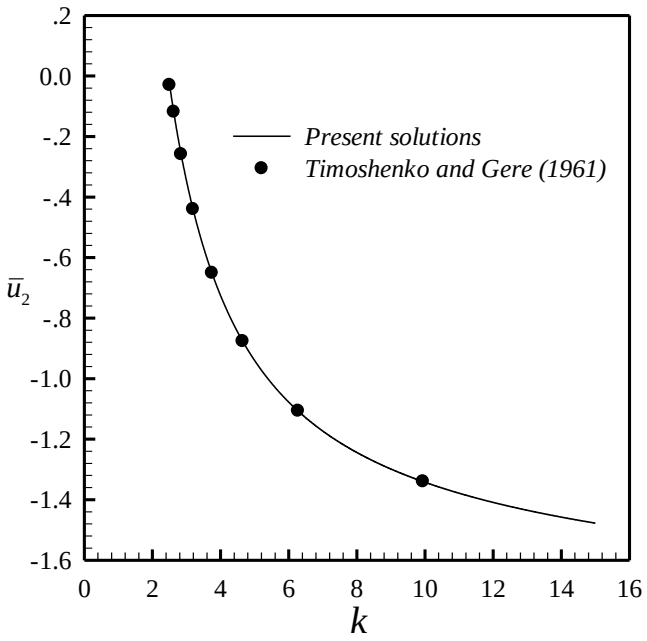

Figure 6.46 Relationship between normalized tip load and normalized longitudinal tip displacement of fixed-free nano-beam. Results are compared with those from Timoshenko and Gere (1961)

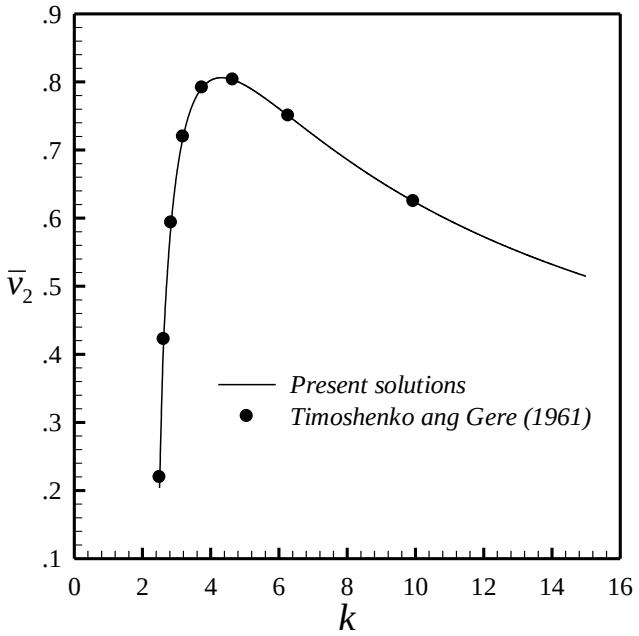

Figure 6.47 Relationship between normalized tip load and normalized transverse tip displacements of fixed-free nano-beam. Results are compared with those from Timoshenko and Gere (1961)

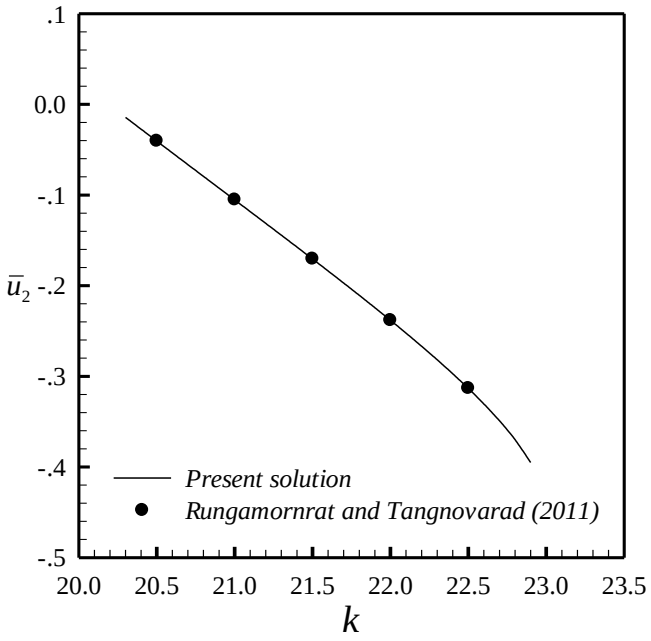

Figure 6.48 Relationship between normalized tip load and normalized tip displacement of fixed-rollered nano-beam. Results are compared with a technique proposed by Rungamornrat and Tangnovarad (2011)

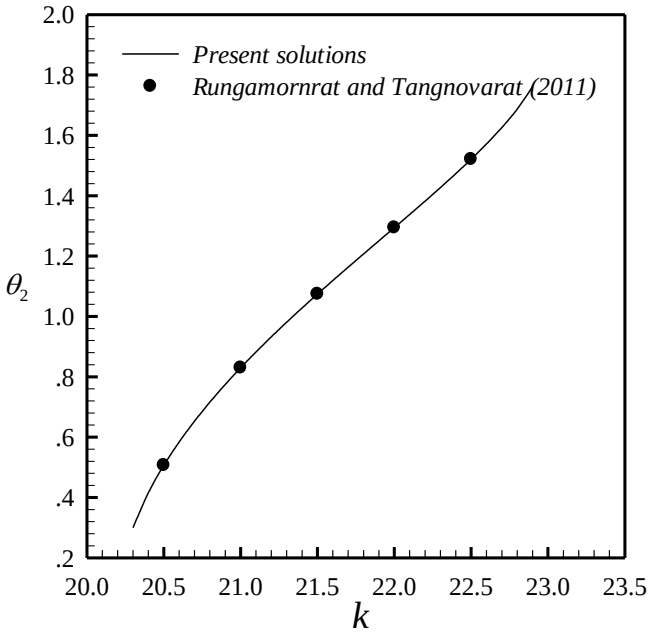

Figure 6.49 Relationship between normalized tip load and tip rotation of fixed-rollered nano-beam. Results are compared with a technique proposed by Rungamornrat and Tangnovarad (2011)

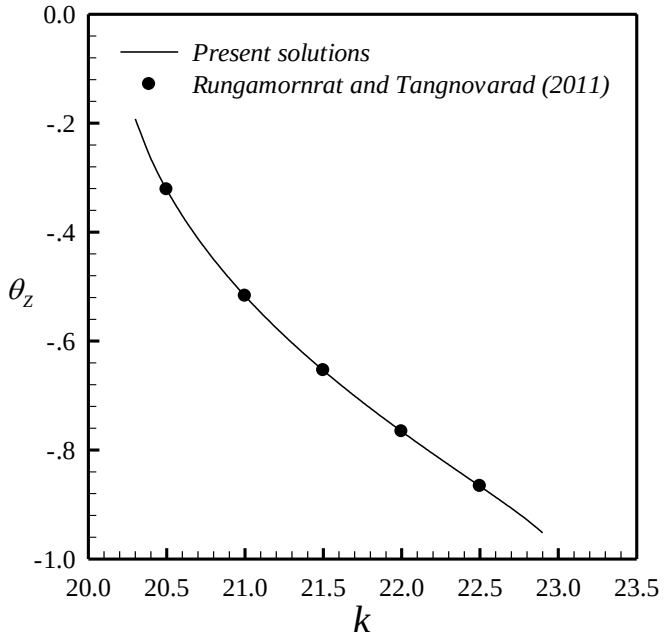

Figure 6.50 Relationship between normalized tip load and rotation at interior inflection point of fixed-rollered nano-beam. Results are compared with a technique proposed by Rungamornrat and Tangnovarad (2011)

6.3.2 Size Dependence Behavior

In order to explore the influence of both surface stresses and nonlocal elasticity on the post-buckling behavior of nano-beams, results are obtained by using four different models as follows: Model-1 for the classical case ($\eta = 1, \mu = 0$), Model-2 with only the surface effect ($\mu = 0$), Model-3 with only the nonlocal effect ($\eta = 1$), and Model-4 with both surface and nonlocal effects. To illustrate the size-dependent characteristic of numerical solutions, results are obtained as a function of the normalized length $\bar{l} = l / \Lambda$ while maintaining the slenderness ratio of the element $l / h = 10$ and the cross-section aspect ratio $b / h = 1$.

The tip rotation (θ_2), the normalized longitudinal tip displacement ($\bar{u}_2$), and the normalized transverse tip displacement ($\bar{v}_2$) for the fixed-free nano-beam are reported in Figures 6.51-6.53, respectively, for all four models and two values of the normalized load $k \in \{2.5,5\}$. The post-buckling shapes of the fixed-free nano-beam for *l* = 50 nm

and l = 1000 nm are also shown in Figures 6.54 and 6.55 for $k = 2.5$ and $k = 5$, respectively. It is deduced from those results that presence of the surface stresses with and without nonlocal effects (Model-2 and Model-4) tends to soften the nano-element (i.e., reduce the apparent bending stiffness) and the obtained solutions significantly deviate from results of the classical case (i.e., Model-1). It should also be evident by comparing results generated by the Model-2 and the Model-3 that the effect of surface stresses is more substantial than the local effect. This, as a direct consequence, renders the solutions obtained by the Model-2 and Model-4 only slightly different.

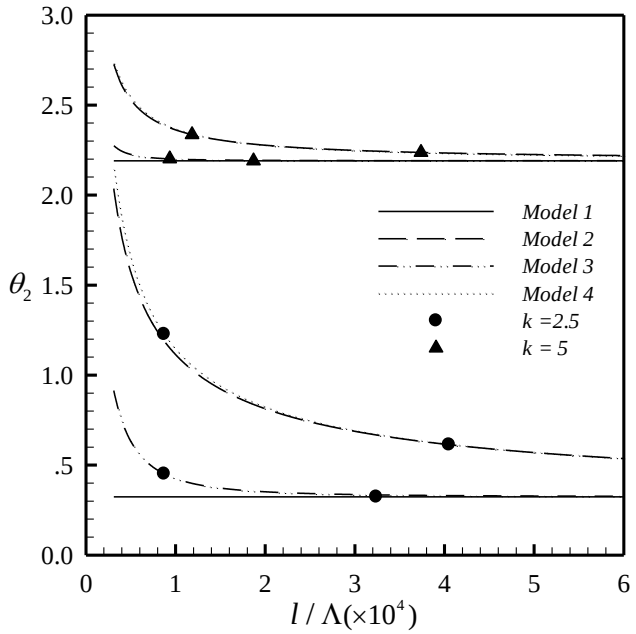

Figure 6.51 Relationship between normalized length and tip rotation of fixed-free nano-beam under normalized compression force $k \in \{2.5,5\}$

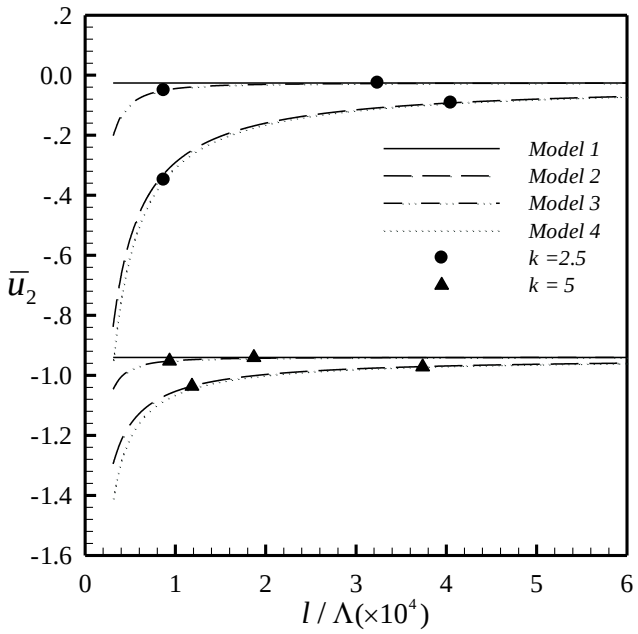

Figure 6.52 Relationship between normalized length and normalized longitudinal tip displacement of fixed-free nano-beam under normalized compression force $k \in \{2.5,5\}$

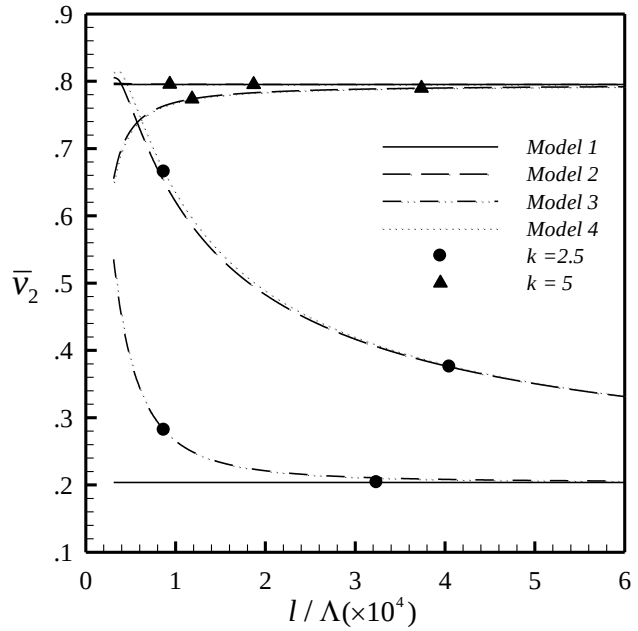

Figure 6.53 Relationship between normalized length and normalized transverse tip displacement of fixed-free nano-beam under normalized compression force $k \in \{2.5,5\}$

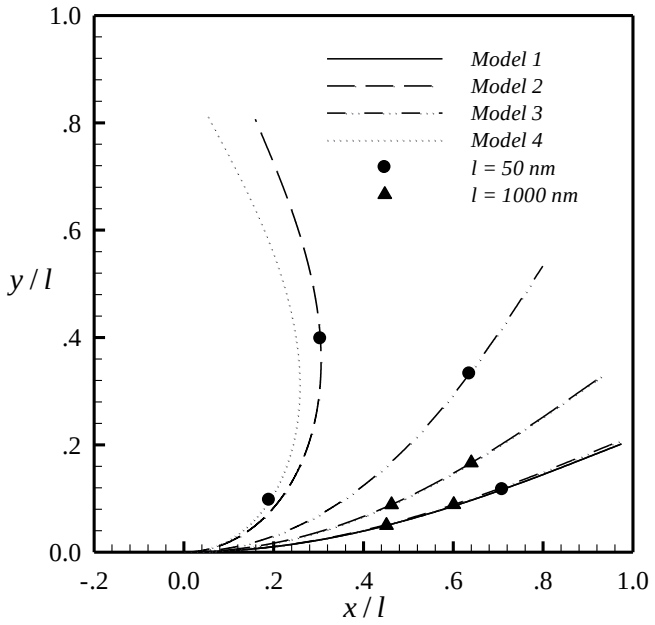

Figure 6.54 Post-buckling shape of fixed-free nano-beam under normalized compression force $k = 2.5$ for l = 50 nm and 1000 nm

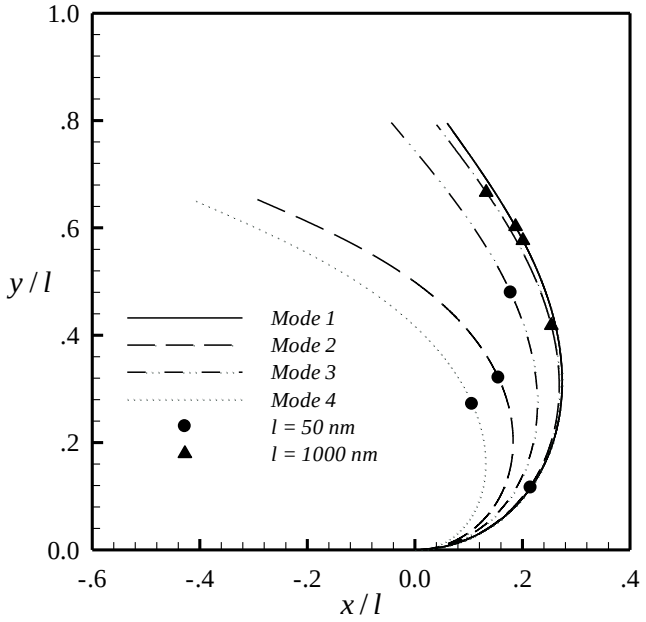

Figure 6.55 Post-buckling shape of fixed-free nano-beam under normalized compression force $k = 5$ for l = 50 nm and 1000 nm

A similar set of numerical experiments has also been conducted to examine the effect of the surface stresses and nonlocal effects on the post-buckling responses of a nano-beam with the fixed-rollered boundary condition. Results are obtained as a function of the normalized length $\bar{l} = l/\Lambda$ while maintaining the slenderness ratio $l/h = 10$ and the cross-section aspect ratio $b/h = 1$ similar to the previous case to illustrate the size-dependent behavior of the numerical solutions. The tip rotation (θ_2), the rotation at the interior inflection point (θ_z), and the normalized maximum longitudinal and transverse displacements as a function of the normalized length l/Λ are reported in Figures 6.56-6.59 for all four models and two values of the normalized end load $k \in \{20.5, 21.5\}$. The corresponding post-buckling shapes for $l = 500$ nm and $l = 1500$ nm are also presented in Figures 6.60 and 6.61 for $k = 20.5$ and $k = 21.5$, respectively. Similar to the fixed-free case, results obtained by the model considering the surface stresses significantly deviate from those of the classical case and presence of surface stress effect considerably reduces the apparent bending stiffness of the beam if its length l is close to the intrinsic length scale of the surface $\Lambda = E^s / E$. Likewise, the role of the nonlocal elasticity depends mainly on the characteristic length scale of the problem relative to the parameter μ; in particular, if the element length decreases to a nano level, the effect in reducing the member stiffness is prominent. It is also apparent from those results that the discrepancy between responses generated by the model incorporating only surface stresses (Model-2) and the classical solution is much larger than that obtained by the model including only the nonlocal effect (Model-3). In addition, the Model-4 (incorporating both the surface stresses and nonlocal effects) yields results nearly identical to those obtained from the Model-2. Similar to the fixed-free case, all models incorporating the nano-scale influence (i.e., Model-2, Model-3 and Model-4) exhibit strong size-dependent behavior. In particular, as the element size reduces to that comparable to the intrinsic length scale of material surface, the influence of both surface stresses and nonlocal elasticity are substantial and they must be properly taken into account in the modeling to reasonably capture the nano-scale phenomena.

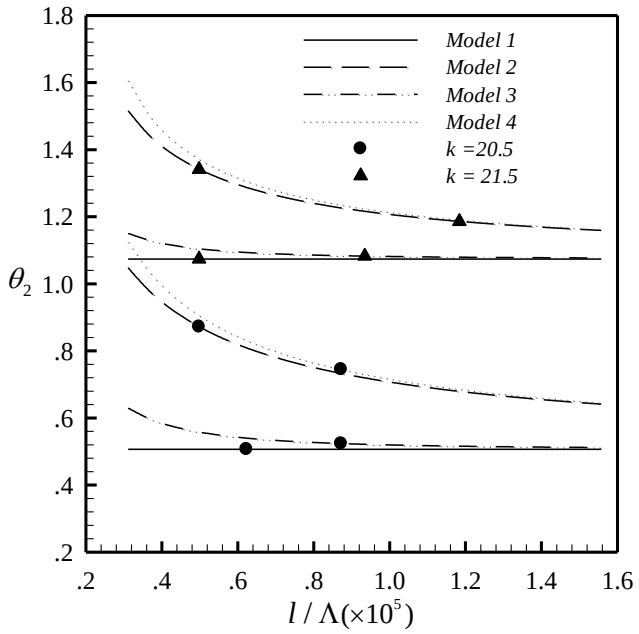

Figure 6.56 Relationship between normalized length and tip rotation of fixed-rollered nano-beam under normalized compression force $k \in \{20.5, 21.5\}$

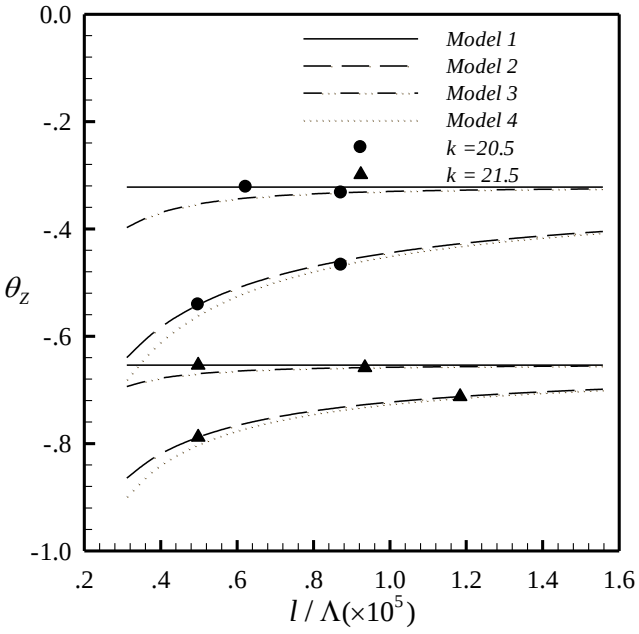

Figure 6.57 Relationship between normalized length and the rotation at interior inflection point of fixed-rollered nano-beam under normalized compression force $k \in \{20.5, 21.5\}$

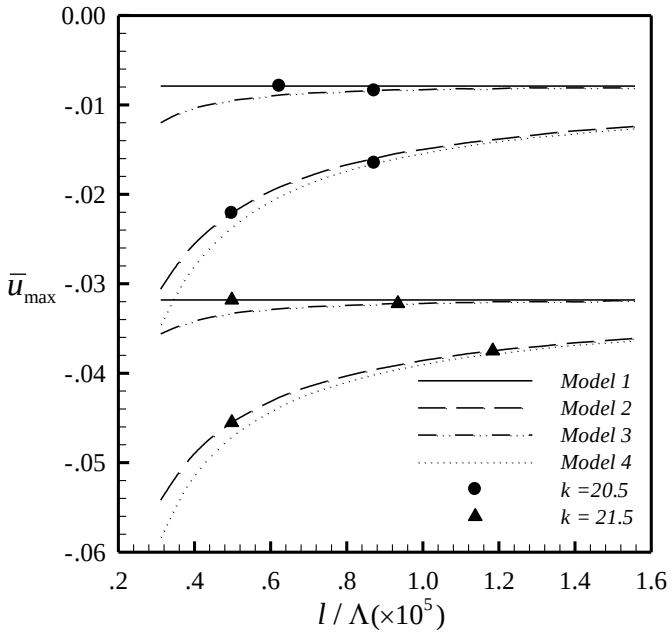

Figure 6.58 Relationship between normalized length and normalized maximum longitudinal displacement of fixed-rollered nano-beam under normalized compression force $k \in \{20.5, 21.5\}$

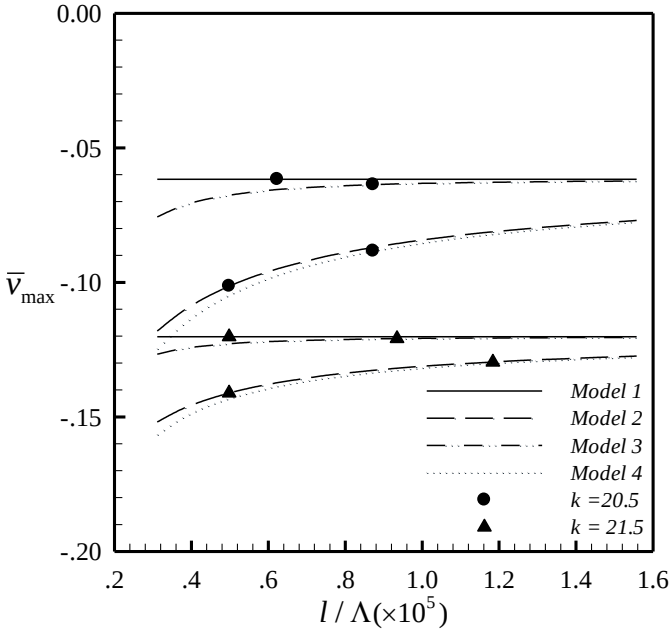

Figure 6.59 Relationship between normalized length and normalized maximum transverse displacement of fixed-rollered nano-beam under normalized compression force $k \in \{20.5, 21.5\}$

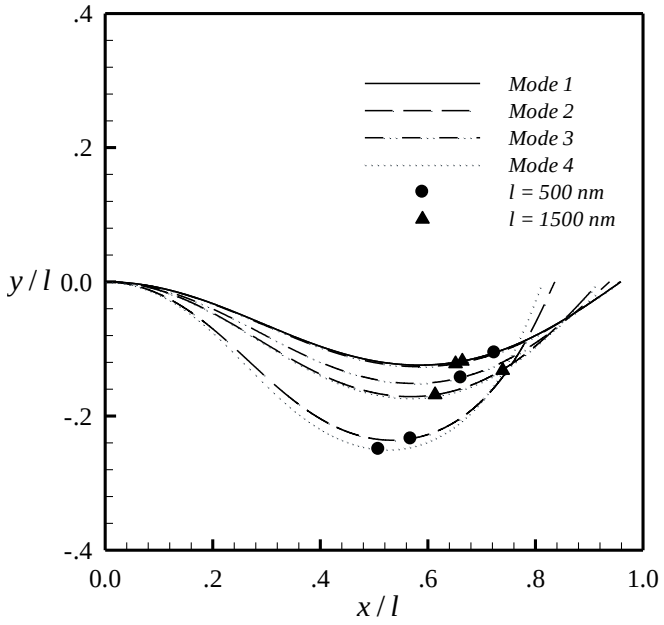

Figure 6.60 Post-buckling shape of fixed-rollered nano-beam under normalized compression force $k = 20.5$ for l = 500 nm and 1500 nm

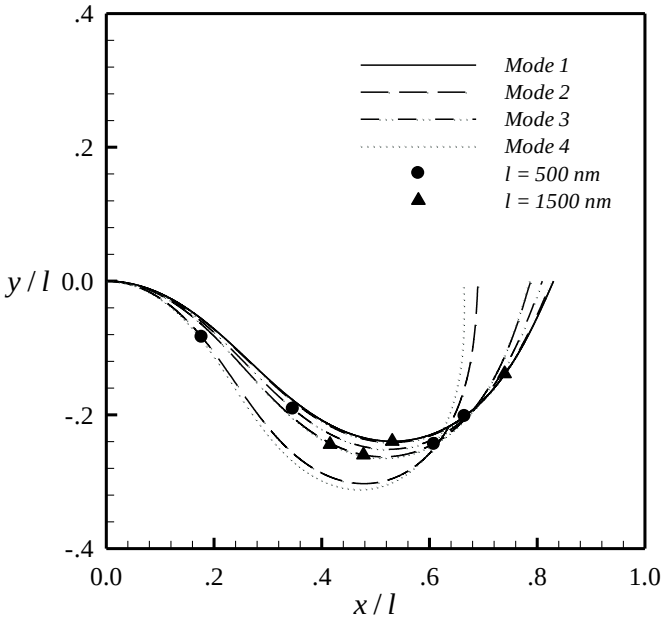

Figure 6.61 Post-buckling shape of fixed-rollered nano-beam under normalized compression force $k = 21.5$ for l = 500 nm and 1500 nm

6.3.3 Influence of Material Parameters

Every type of material has its own surface properties indicated by two surface material parameters which are the surface modulus of elasticity (E^s) and the residual surface tension (τ^s). Value of the effective flexural rigidity normalized by the classical flexural rigidity *EI* (i.e., η) which directly affects the mechanical behaviors of nano-beams depends mainly on those two surface material parameters as shown in equation (2.14). In order to demonstrate the effect of those surface parameters on the post-buckling behavior of fixed-free nano-element, the tip rotation θ_2, the normalized tip displacements $\bar{u}_2$ and $\bar{v}_2$ of the beam are obtained for various values of the surface modulus of elasticity parameter and the residual surface tension parameter while maintaining the nonlocal parameters.

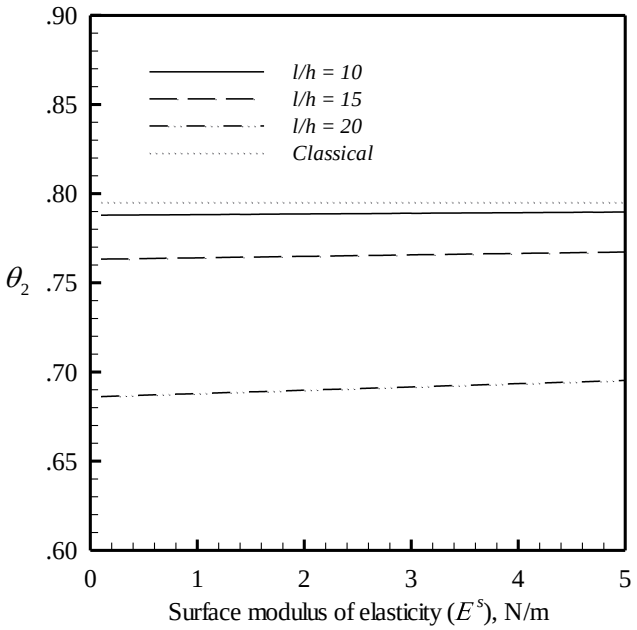

Figure 6.62 Relationship between surface modulus of elasticity and tip rotation of fixed-free nano-beam with three different values of slenderness ratio

In this numerical experiment, the beam length l = 500 nm, three slenderness ratios $l/h \in \{10,15,20\}$, the aspect ratio of the cross section $b/h = 1$, the normalized end load k = 5, and $(e_0 a)^2 = 10^{-16}\,\mathrm{m}^2$ are employed. The tip rotation and the normalized tip displacements of the element as a function of E^s and τ^s are reported in Figures 6.62-6.64 for τ^s = 0.89 N/m and in Figures 6.65-6.67 for E^s = 1.22 N/m, respectively. It can be deduced from these results that the increase of the surface modulus of elasticity tends to stiffen the nano-beams whereas increase of the residual surface tension tends to reverse such effect.

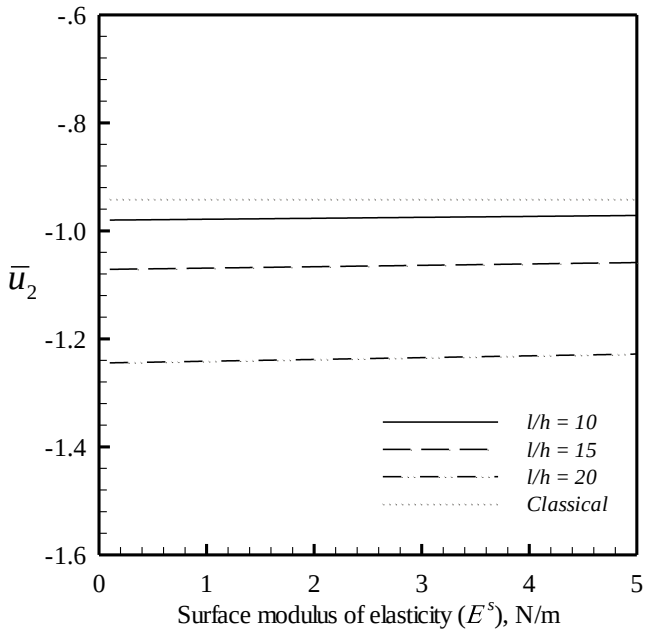

Figure 6.63 Relationship between surface modulus of elasticity and normalized longitudinal tip displacement of fixed-free nano-beam with three different values of slenderness ratio

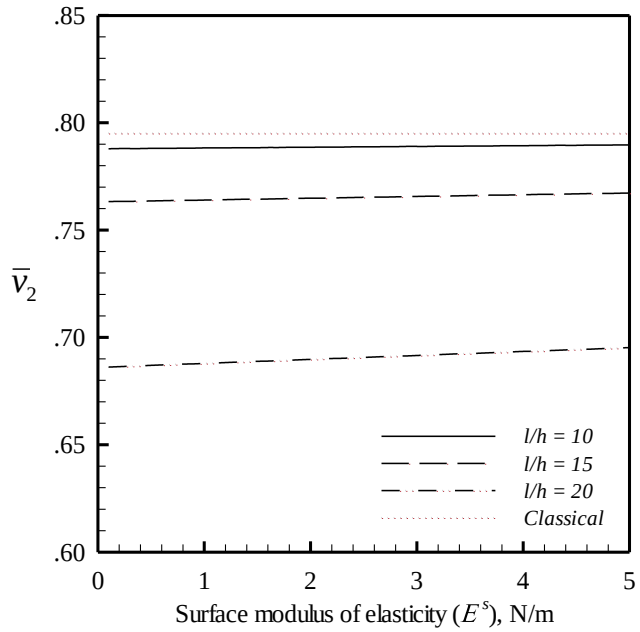

Figure 6.64 Relationship between surface modulus of elasticity and normalized transverse tip displacement of fixed-free nano-beam with three different values of slenderness ratio

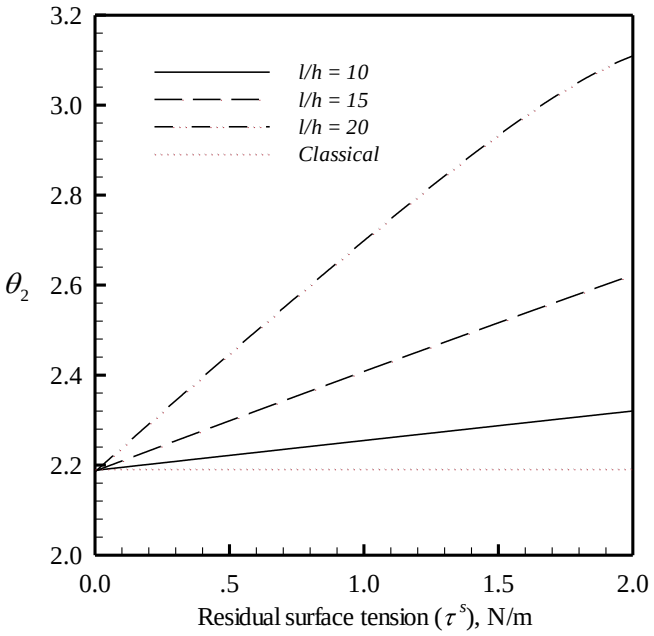

Figure 6.65 Relationship between residual surface tension and tip rotation of fixed-free nano-beam with three different values of slenderness ratio

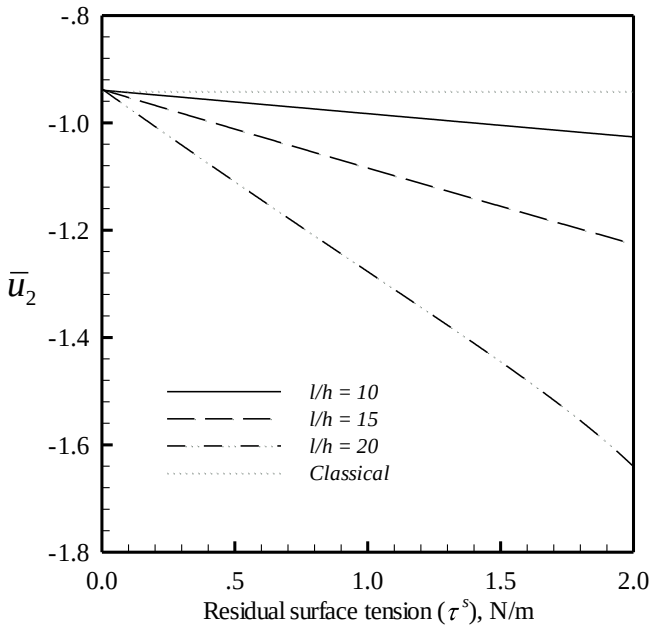

Figure 6.66 Relationship between residual surface tension and normalized longitudinal tip displacement of fixed-free nano-beam with three different values of slenderness ratio

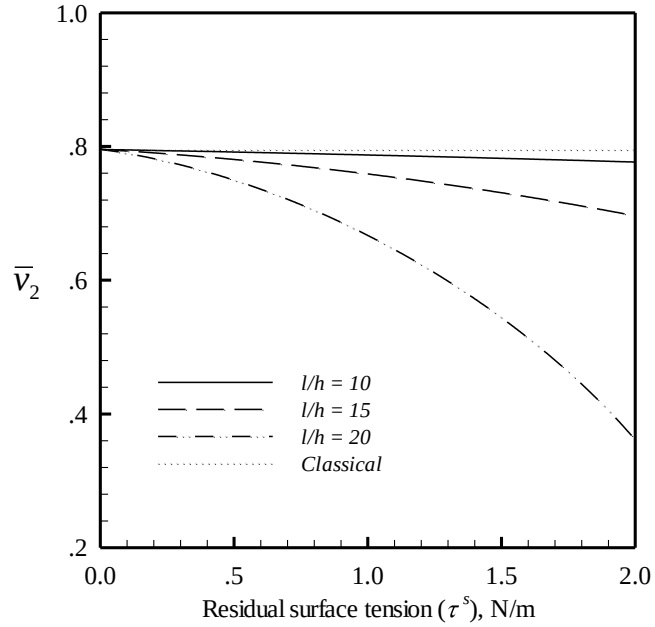

Figure 6.67 Relationship between residual surface tension and normalized transverse tip displacement of fixed-free nano-beam with three different values of slenderness ratio

For the case of a fixed-rollered nano-beam, the beam length l = 1500 nm, three slenderness ratios $l/h \in \{5,10,15\}$, the cross sectional aspect ratio $b/h = 1$, the normalized end load k = 20.5, and the nonlocal parameter $(e_0 a)^2 = 10^{-16}\,\mathrm{m}^2$ are chosen in the simulation. The tip rotation and the normalized maximum longitudinal and transverse displacements of the beam versus the surface modulus of elasticity parameter are reported in Figures 6.68-6.70 for τ^s = 0.89 N/m. Similarly, results as a function of τ^s are also depicted in Figures 6.71-6.73 for E^s = 1.22 N/m. Like the fixed-free case, the surface modulus of elasticity tends to enhance the member stiffness whereas presence of the residual surface tension clearly lowers the apparent bending stiffness. It is also apparent from results of both fixed-rollered and fixed-free nano-elements that the contribution of surface stresses is prominent when the slenderness ratio is relatively small and close to the intrinsic length scale of the material surface.

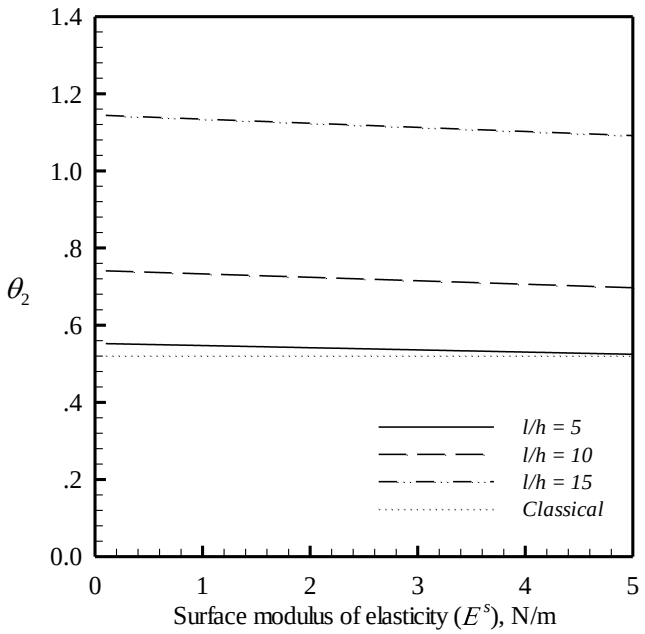

Figure 6.68 Relationship between surface modulus of elasticity and tip rotation of fixed-rollered nano-beam with three values of slenderness ratio

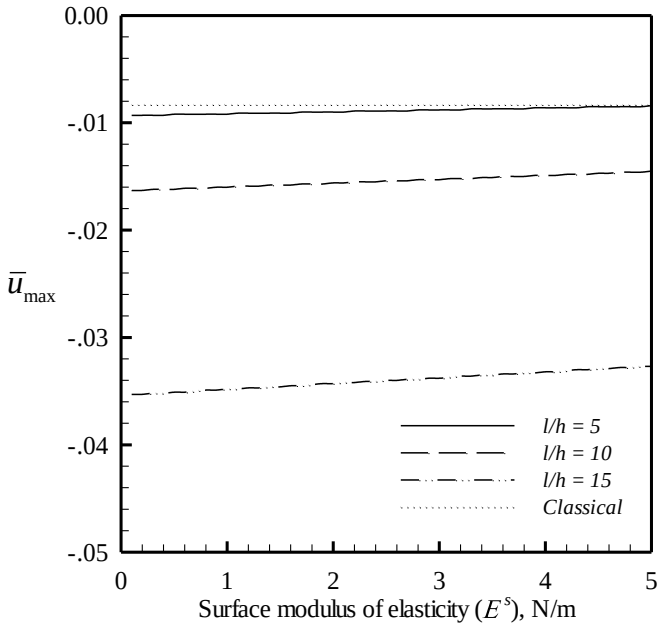

Figure 6.69 Relationship between surface modulus of elasticity and normalized maximum longitudinal displacement of fixed-rollered nano-beam with three values of slenderness ratio

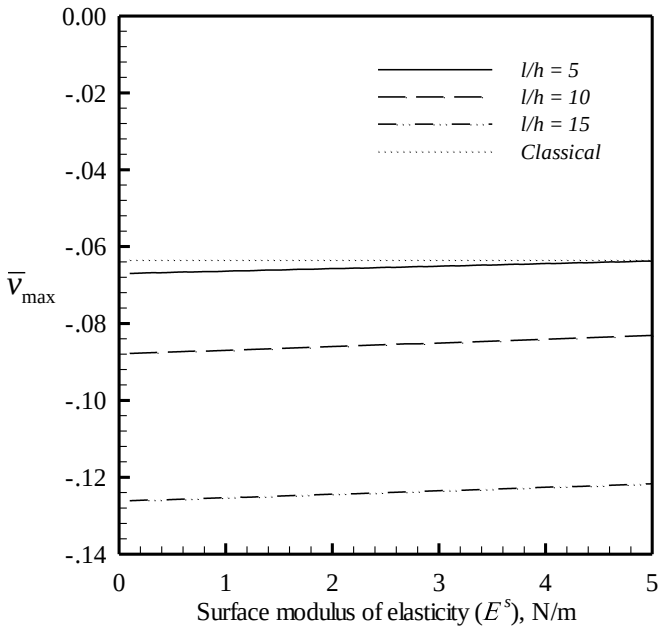

Figure 6.70 Relationship between surface modulus of elasticity and normalized maximum transverse displacement of fixed-rollered nano-beam with three values of slenderness ratio

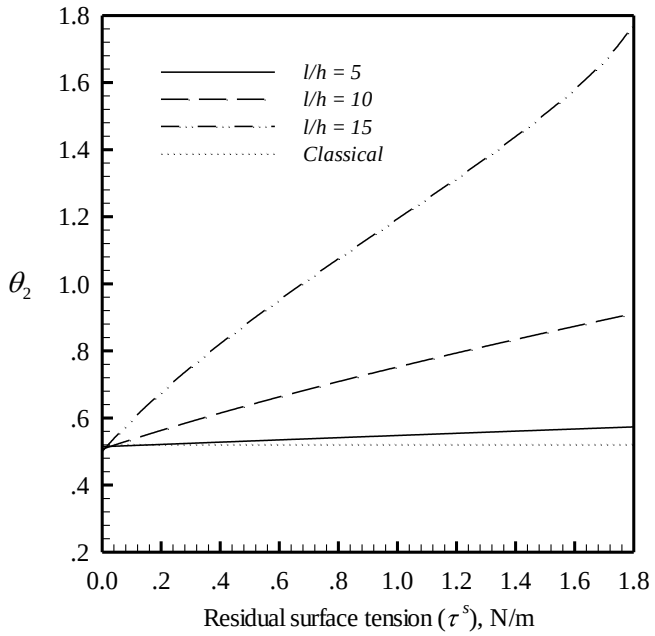

Figure 6.71 Relationship between residual surface tension and tip rotation of fixed-rollered nano-beam with three values of slenderness ratio

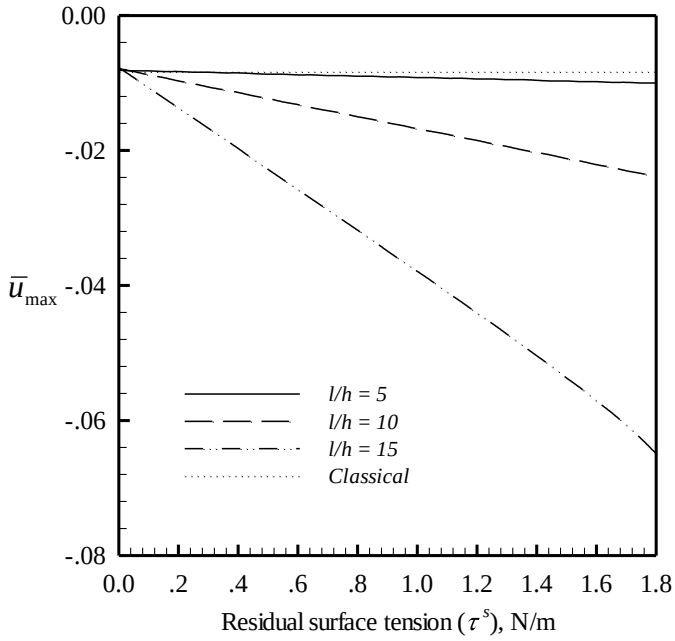

Figure 6.72 Relationship between residual surface tension and normalized maximum longitudinal displacement of fixed-rollered nano-beam with three values of slenderness ratio

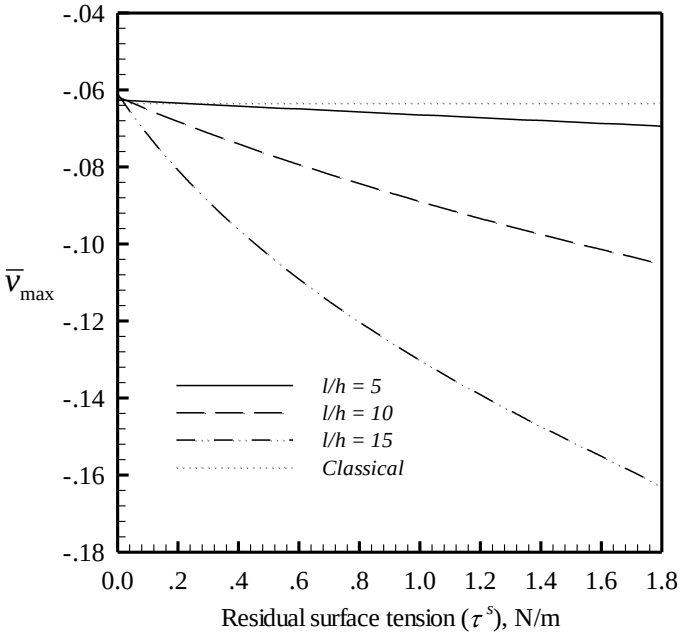

Figure 6.73 Relationship between residual surface tension and normalized maximum transverse displacement of fixed-rollered nano-beam with three values of slenderness ratio

To further explore the effect of the nonlocal parameter (μ) on the post-buckling of nano-beams, result are generated for various values of μ while maintaining the value of E^s = 1.22 N/m and τ^s = 0.89 N/m. In addition, the aspect ratio of the cross section, the beam length, the slenderness ratio, and the normalized end load are taken, in the numerical study, as $b/h = 1$, $l = 500$, $l/h \in \{10, 15, 20\}$, k = 5 for the fixed-free case and $b/h = 1$, $l = 500$, $l/h \in \{10, 15, 20\}$, k = 20.5 for the fixed-rollered case. Result for the tip rotation and the normalized longitudinal and transverse tip displacements for the fixed-free beam and the tip rotation and the normalized maximum longitudinal and transverse displacements for the fixed-rollered beam are reported in Figures 6.74-6.76 and Figures 6.77-6.79, respectively, as a function of μ. As apparent from this set of results, the post-buckling response of the nano beams are strongly dependent on the nonlocal parameter and such depedence becomes more prominent when the slenderness ratio of the element increases.

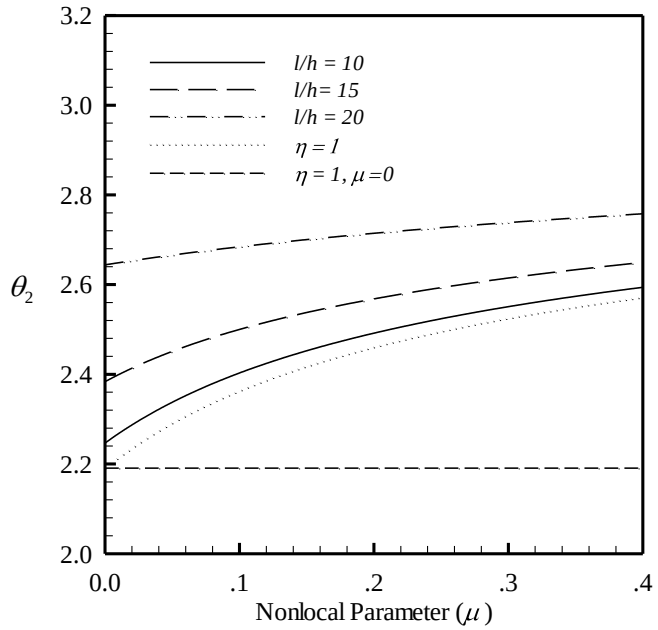

Figure 6.74 Relationship between the nonlocal parameter (μ) and tip rotation of fixed-free nano-beam with three values of slenderness ratio

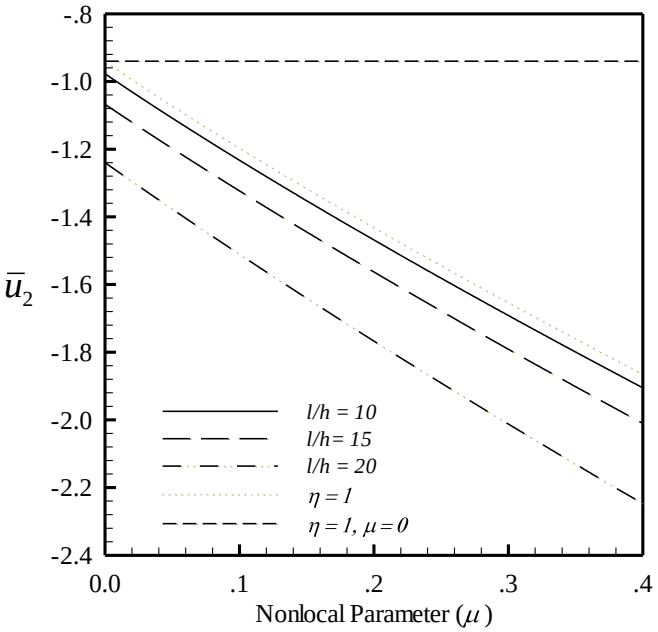

Figure 6.75 Relationship between the nonlocal parameter (μ) and normalized longitudinal tip displacement of fixed-free nano-beam with three values of slenderness ratio

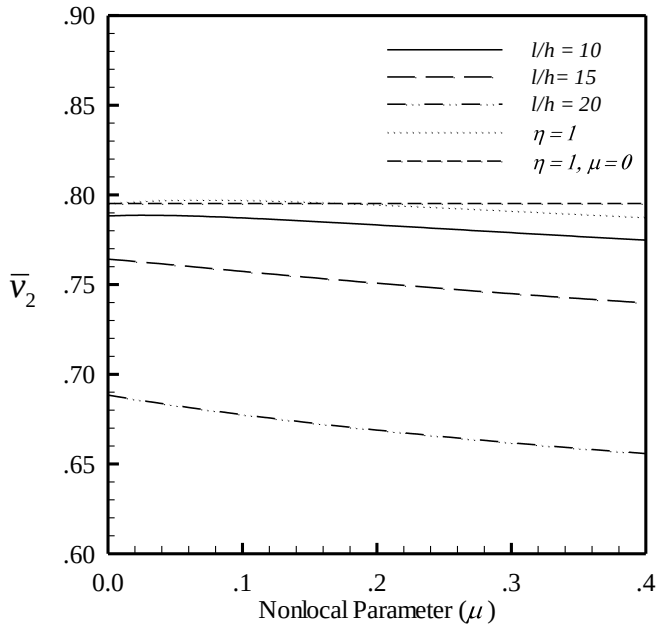

Figure 6.76 Relationship between the nonlocal parameter (μ) and normalized transverse tip displacement of fixed-free nano-beam with three values of slenderness ratio

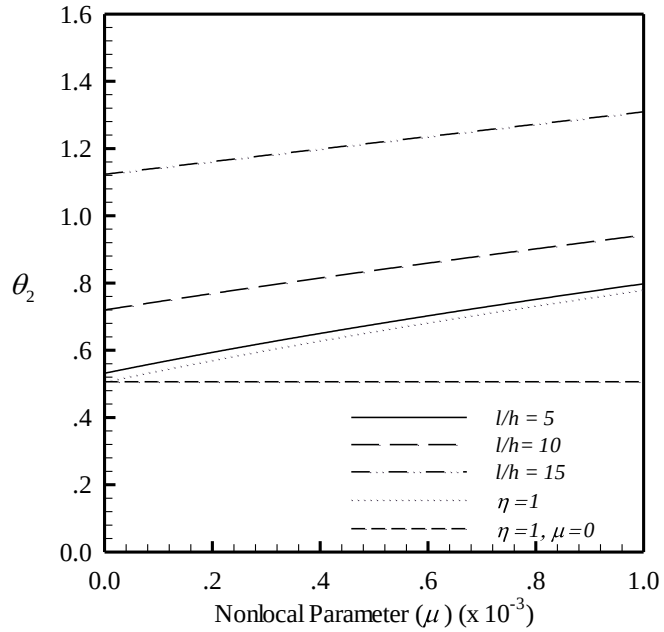

Figure 6.77 Relationship between the nonlocal parameter (μ) and tip rotation of fixed-rollered nano-beam with three values of slenderness ratio

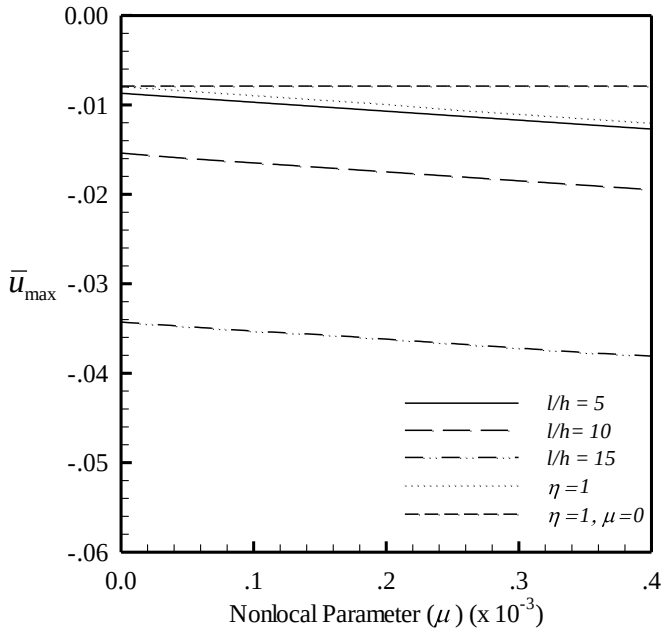

Figure 6.78 Relationship between the nonlocal parameter (μ) and normalized maximum longitudinal displacement of fixed-rollered nano-beam with three values of slenderness ratio

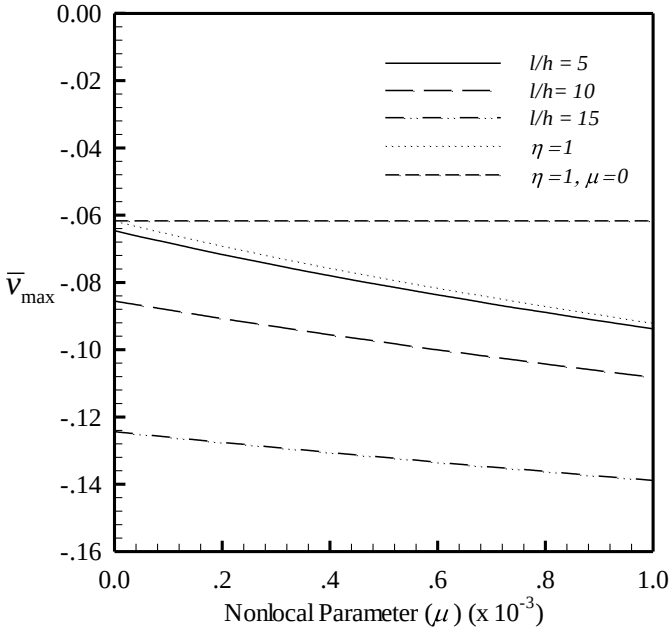

Figure 6.79 Relationship between the nonlocal parameter (μ) and normalized maximum transverse displacement of fixed-rollered nano-beam with three values of slenderness ratio.

CHAPTER VII

CONCLUSIONS

The theoretical model and efficient and accurate solution procedure for performing the analysis of bending, buckling, and post-buckling of nano-beams influenced by surface stresses and nonlocal elasticity have been established. The prismatic nano-beam with the fixed-free and fixed-rollered end conditions has been treated in the current investigation. Basic governing differential equations for a nano-beam undergoing large displacements and rotations have been formulated based on the nonlinear kinematics, equilibrium in the deformed state, and the enhanced moment-curvature relationship integrating both surface stresses and nonlocal effects. Gurtin-Murdoch surface elasticity theory has been used along with the presence of residual stress within the bulk to describe the influence of the surface stresses and finally derive the apparent flexural rigidity of the nano-beam. The nonlocal effect perceived in the nano-scale has been treated by utilizing the nonlocal theory of linear elasticity and this leads to the different form of moment-curvature relationship from the classical beam theory. A set of basic nonlinear differential equations has been employed along with the elliptic integral technique to derive a general set of nonlinear algebraic equations in terms of end displacements and end rotations for a nano-element under general boundary conditions.

A particular set of nonlinear algebraic equations governing the bending, buckling, and post-buckling responses of fixed-free and fixed-rollered nano-beams has been established by properly enforcing the natural and essential boundary conditions. This set of equations has been solved numerically using Newton-Raphson iteration to obtain the unknown rotations and displacements at the ends of the nano-element and rotation at the interior inflection point. In numerical implementations, a technique of variable transformation has been utilized to regularize all involved weakly singular integrals to ensure that the final integrals can be integrated in an efficient manner by standard low-order Gaussian quadrature. Once the end quantities and those associated with the interior inflection point have been determined, the displacement and rotation at interior points, the internal forces, and support reactions can be readily computed using post-processing equations.

To validate the problem formulation and numerical implementation, numerical experiments have been conducted for a classical model (neglecting the influence of both surface stresses and nonlocal linear elasticity) and the obtained solutions are compared with existing benchmark cases. It has been pointed out from an extensive numerical study that the proposed technique is robust and offers very accurate numerical solutions. Once the developed numerical technique has been fully verified, extensive numerical experiments have been carried out to explore the contribution of surface stresses and nonlocal linear elasticity. From obtained results, it has been pointed out that the mathematical model incorporating the surface stresses and nonlocal constitutive relation tends to lower the bending stiffness of the member. In the current study, the influence of surface stresses has been found in contrast with those presented by various investigators due to the integration of the residual compressive stress introduced within the bulk to maintain equilibrium at the initial state. The decrease in bending stiffness due to the the residual compressive stress in the bulk material is more significant than the enhancement of the stiffness due to in-plane stiffness of the surface and the residual surface tension. It can be also remarked that as the element size is close to the length scale of the material surface, solutions predicted by the current model are significantly different from those predicted by a classical model. This implies the necessity to properly incorporate both the surface stresses and nonlocal effect in the modeling of nano-scale problems. In addition, the predicted post-buckling responses of nano-beams also exhibit highly size-dependent. From the investigation of the influence of material parameters on the response of nano-beams, it has been deduced that the enlargement of surface modulus of elasticity tends to stiffen the nano-beams while the increment of the residual surface tension tends to soften the nano-beams. In addition, the response of nano beams is strongly dependent on the nonlocal parameter and such dependence becomes more prominent when the slenderness ratio increases. As a final remark, certain assumptions pertained in the present study are still impractical and can be potentially generalized to treat more realistic cases, e.g., nano-beams with initial imperfections and non-prismatic section, treatment of more realistic boundary conditions and applied loads, etc.

REFERENCES

Altenbach, H., Altenbach, J. W., and Kissing, W. (2004). "Mechanics of composite structural elements," Springer Science & Business Media.

Ansari, R., Mohammadi, V., Faghih Shojaei, M., Gholami, R., and Sahmani, S. (2013). Postbuckling characteristics of nanobeams based on the surface elasticity theory. *Composites Part B: Engineering* **55**, 240-246.

Ansari, R., Mohammadi, V., Faghih Shojaei, M., Gholami, R., and Sahmani, S. (2014). Postbuckling analysis of Timoshenko nanobeams including surface stress effect. *International Journal of Engineering Science* **75**, 1-10.

Ansari, R., and Sahmani, S. (2011). Bending behavior and buckling of nanobeams including surface stress effects corresponding to different beam theories. *International Journal of Engineering Science* **49**, 1244-1255.

Aydogdu, M. (2009a). A general nonlocal beam theory: Its application to nanobeam bending, buckling and vibration. *Physica E: Low-dimensional Systems and Nanostructures* **41**, 1651-1655.

Aydogdu, M. (2009b). A new shear deformation theory for laminated composite plates. *Composite Structures* **89**, 94-101.

Chiu, M.-S., and Chen, T. (2011a). Effects of high-order surface stress on static bending behavior of nanowires. *Physica E: Low-dimensional Systems and Nanostructures* **44**, 714-718.

Chiu, M.-S., and Chen, T. (2011b). Higher-order surface stress effects on buckling of nanowires under uniaxial compression. *Procedia Engineering* **10**, 397-402.

Chiu, M.-S., and Chen, T. (2013). Bending and resonance behavior of nanowires based on Timoshenko beam theory with high-order surface stress effects. *Physica E: Low-dimensional Systems and Nanostructures* **54**, 149-156.

Eltaher, M. A., Emam, S. A., and Mahmoud, F. F. (2013). Static and stability analysis of nonlocal functionally graded nanobeams. *Composite Structures* **96**, 82-88.

Eltaher, M. A., Hamed, M. A., Sadoun, A. M., and Mansour, A. (2014a). Mechanical analysis of higher order gradient nanobeams. *Applied Mathematics and Computation* **229**, 260-272.

Eltaher, M. A., Khairy, A., Sadoun, A. M., and Omar, F.-A. (2014b). Static and buckling analysis of functionally graded Timoshenko nanobeams. *Applied Mathematics and Computation* **229**, 283-295.

Emam, S. A. (2013). A general nonlocal nonlinear model for buckling of nanobeams. *Applied Mathematical Modelling* **37**, 6929-6939.

Eringen, A. C. (1976). "Continuum Physics," Academic Press, New York.

Eringen, A. C. (1983). On differential equations of nonlocal elasticity and solutions of screw dislocation and surface waves. *Journal of Applied Physics* **54**, 4703-4711.

Eringen, A. C. (2002). "Nonlocal continuum field theories," Springer-Verlag.

Fu, Y., Zhang, J., and Jiang, Y. (2010). Influences of the surface energies on the nonlinear static and dynamic behaviors of nanobeams. *Physica E: Low-dimensional Systems and Nanostructures* **42**, 2268-2273.

Ghannadpour, S. A. M., Mohammadi, B., and Fazilati, J. (2013). Bending, buckling and vibration problems of nonlocal Euler beams using Ritz method. *Composite Structures* **96**, 584-589.

Guo, J.-G., and Zhao, Y.-P. (2007). The size-dependent bending elastic properties of nanobeams with surface effects. *Nanotechnology* **18**, 295701.

Gurtin, M., and Ian Murdoch, A. (1975). A continuum theory of elastic material surfaces. *Archive for Rational Mechanics and Analysis* **57**.

Gurtin, M. E., and Murdoch, A. I. (1978). Surface stress in solid. *International Journal of Solids and Structures* **14**, 431-440.

Gurtin, M. E., Weissmüller, J., and Larché, F. (1998). A general theory of curved deformable interfaces in solids at equilibrium. *Philosophical Magazine A* **78**, 1093-1109.

He, J., and Lilley, C. M. (2008). Surface effect on the elastic behavior of static bending nanowires. *Nano Letters* **8**, 1798-1802.

Hsin, C.-L., Mai, W., Gu, Y., Gao, Y., Huang, C.-T., Liu, Y., Chen, L.-J., and Wang, Z.-L. (2008). Elastic Properties and Buckling of Silicon Nanowires. *Advanced Materials* **20**, 3919-3923.

Hu, K.-M., Zhang, W.-M., Zhong, Z.-Y., Peng, Z.-K., and Meng, G. (2014). Effect of surface layer thickness on buckling and vibration of nonlocal nanowires. *Physics Letters A* **378**, 650-654.

Husain, A., Hone, J., Postma, H. W. C., Huang, X. M. H., Drake, T., Barbic, M., Scherer, A., and Roukes, M. L. (2003). Nanowire-based very-high-frequency electromechanical resonator. *Applied Physics Letters* **83**, 1240.

Jahed, Z., Jin, S., Burek, M. J., and Tsui, T. Y. (2012). Fabrication and buckling behavior of polycrystalline palladium, cobalt, and rhodium nanostructures. *Materials Science and Engineering: A* **542**, 40-48.

Janghorban, M. (2012). Static analysis of tapered nanowires based on nonlocal Euler-Bernoulli beam theory via differential quadrature method. *Latin American Journal of Solids and Structures* **9**, 299-307.

Jiang, L. Y., and Yan, Z. (2010). Timoshenko beam model for static bending of nanowires with surface effects. *Physica E: Low-dimensional Systems and Nanostructures* **42**, 2274-2279.

Jing, G. Y., Duan, H. L., Sun, X. M., Zhang, Z. S., Xu, J., Li, Y. D., Wang, J. X., and Yu, D. P. (2006). Surface effects on elastic properties of silver nanowires: Contact atomic-force microscopy. *Physical Review B* **73**.

Jing, Y., Meng, Q., and Gao, Y. (2009). Molecular dynamics simulation on the buckling behavior of silicon nanowires under uniaxial compression. *Computational Materials Science* **45**, 321-326.

Juntarasaid, C., Pulngern, T., and Chucheepsakul, S. (2012). Bending and buckling of nanowires including the effects of surface stress and nonlocal elasticity. *Physica E: Low-dimensional Systems and Nanostructures* **46**, 68-76.

Koo, S.-M., Edelstein, M. D., Li, Q., Richter, C. A., and Vogel, E. M. (2005). Silicon nanowires as enhancement-mode Schottky barrier field-effect transistors. *Nanotechnology* **16**, 1482-1485.

Levinson, M. (1981). A new rectangular beam theory. *Journal of Sound and Vibration* **74**, 81-87.

Li, X.-F., Wang, B.-L., Tang, G.-J., and Lee, K. Y. (2011). Size effect in transverse mechanical behavior of one-dimensional nanostructures. *Physica E: Low-dimensional Systems and Nanostructures* **44**, 207-214.

Li, X.-F., and Zhang, H. (2013). Buckling load and critical length of nanowires on an elastic substrate. *Comptes Rendus Mécanique* **341**, 636-645.

Li, X.-F., Zhang, H., and Lee, K. Y. (2014). Dependence of Young′s modulus of nanowires on surface effect. *International Journal of Mechanical Sciences* **81**, 120-125.

Liu, J. L., Mei, Y., Xia, R., and Zhu, W. L. (2012). Large displacement of a static bending nanowire with surface effects. *Physica E: Low-dimensional Systems and Nanostructures* **44**, 2050-2055.

Lowe, P. G. (1971). "Classical Theory of Structures: Based on the Differential Equation," Cambridge University Press

Mahmoud, F. F., Eltaher, M. A., Alshorbagy, A. E., and Meletis, E. I. (2013). Static analysis of nanobeams including surface effects by nonlocal finite element. *Journal of Mechanical Science and Technology* **26**, 3555-3563.

Olsson, P. A. T., and Park, H. S. (2011). Atomistic study of the buckling of gold nanowires. *Acta Materialia* **59**, 3883-3894.

Peddieson, J., Buchanan, G. R., and McNitt, R. P. (2003). Application of nonlocal continuum models to nanotechnology. *International Journal of Engineering Science* **40**, 305-312.

Pradhan, S. C., and Phadikar, J. K. (2009). Bending, buckling and vibration analyses of nonhomogeneous nanotubes using GDQ and nonlocal elasticity theory. *Structural Engineering and Mechanics* **33**, 193-213.

Reddy, J. N. (1984). A Simple Higher-Order Theory for Laminated Composite Plates. *Journal of Applied Mechanics* **51**, 745-752.

Reddy, J. N. (2007). Nonlocal theories for bending, buckling and vibration of beams. *International Journal of Engineering Science* **45**, 288-307.

Riaz, M., Fulati, A., Yang, L. L., Nur, O., Willander, M., and Klason, P. (2008). Bending flexibility, kinking, and buckling characterization of ZnO nanorods/nanowires grown on different substrates by high and low temperature methods. *Journal of Applied Physics* **104**, 104306.

Roque, C. M. C., Ferreira, A. J. M., and Reddy, J. N. (2011). Analysis of Timoshenko nanobeams with a nonlocal formulation and meshless method. *International Journal of Engineering Science* **49**, 976-984.

Rungamornrat, J., and Tangnovarad, P. (2011). Analysis of Linearly Elastic Inextensible Frames Undergoing Large Displacement and Rotation. *Mathematical Problems in Engineering* **2011**, 1-37.

Ryu, S. Y., Xiao, J., Park, W. I., Son, K. S., Huang, Y. Y., Paik, U., and Rogers, J. A. (2009). Lateral buckling mechanics in silicon nanowires on elastomeric substrates. *Nano Lett* **9**, 3214-9.

Samaei, A. T., Bakhtiari, M., and Wang, G. F. (2012). Timoshenko beam model for buckling of piezoelectric nanowires with surface effects. *Nanoscale Res Lett* **7**, 201.

Şimşek, M., and Yurtcu, H. H. (2013). Analytical solutions for bending and buckling of functionally graded nanobeams based on the nonlocal Timoshenko beam theory. *Composite Structures* **97**, 378-386.

Song, F., and Huang, G. L. (2009). Modeling of surface stress effects on bending behavior of nanowires: Incremental deformation theory. *Physics Letters A* **373**, 3969-3973.

Thai, H.-T. (2012). A nonlocal beam theory for bending, buckling, and vibration of nanobeams. *International Journal of Engineering Science* **52**, 56-64.

Thai, H.-T., and Vo, T. P. (2012). A nonlocal sinusoidal shear deformation beam theory with application to bending, buckling, and vibration of nanobeams. *International Journal of Engineering Science* **54**, 58-66.

Timoshenko, S. P., and Gere, J. M. (1961). "Theory of elastic stability," McGraw-Hill, Singapore.

Wang, C. M., Kitipornchai, S., Lim, C. W., and Eisenberger, M. (2008a). Beam Bending Solutions Based on Nonlocal Timoshenko

Beam Theory. *Journal of Engineering Mechanics* **134**, 475-481.

Wang, C. M., Zhang, Y. Y., Ramesh, S. S., and Kitipornchai, S. (2006). Buckling analysis of micro- and nano-rods/tubes based on nonlocal Timoshenko beam theory. *Journal of Physics D: Applied Physics* **39**, 3904-3909.

Wang, G.-F., and Feng, X.-Q. (2009). Surface effects on buckling of nanowires under uniaxial compression. *Applied Physics Letters* **94**, 141913.

Wang, G.-F., and Yang, F. (2011). Postbuckling analysis of nanowires with surface effects. *Journal of Applied Physics* **109**, 063535.

Wang, Q., and Liew, K. M. (2007). Application of nonlocal continuum mechanics to static analysis of micro- and nano-structures. *Physics Letters A* **363**, 236-242.

Wang, Z.-Q., Zhao, Y.-P., and Huang, Z.-P. (2010). The effects of surface tension on the elastic properties of nano structures. *International Journal of Engineering Science* **48**, 140-150.

Wang, Z., Zu, X., Yang, L., Gao, F., and Weber, W. J. (2008b). Buckling of GaN nanotubes under uniaxial compression. *Solid State Communications* **146**, 293-297.

Wang, Z., Zu, X., Yang, L., Gao, F., and Weber, W. J. (2008c). Molecular dynamics simulation on the buckling behavior of GaN nanowires under uniaxial compression. *Physica E: Low-dimensional Systems and Nanostructures* **40**, 561-566.

Wen, Y.-H., Wang, Q., Liew, K. M., and Zhu, Z.-Z. (2010). Compressive mechanical behavior of Au nanowires. *Physics Letters A* **374**, 2949-2952.

Wu, Q., Volinsky, A. A., Qiao, L., and Su, Y. (2015). Surface effects on static bending of nanowires based on non-local elasticity theory. *Progress in Natural Science: Materials International* **25**, 520-524.

Xu, S. P., Wang, C. M., and Xu, M. R. (2012). Buckling analysis of shear deformable nanorods within the framework of nonlocal elasticity theory. *Physica E: Low-dimensional Systems and Nanostructures* **44**, 1380-1385.

Yang, Y., and Lim, C. W. (2011). A Variational Principle Approach for Buckling of Carbon Nanotubes Based on Nonlocal Timoshenko Beam Models. *Nano* **06**, 363-377.

Yao, H., and Yun, G. (2012). The effect of nonuniform surface elasticity on buckling of ZnO nanowires. *Physica E: Low-dimensional Systems and Nanostructures* **44**, 1916-1919.

Zeng, D., and Zheng, Q. (2010). Large deflection theory of nanobeams. *Acta Mechanica Solida Sinica* **23**, 394-399.

VITA

The author, Miss. Jintara Lawonglerd graduated her Bachelor of Engineering degree in Civil Engineering from Thammasat University in 2011. She then worked as a Structure Engineer in Bangkok, Thailand for Two years. As she would like to obtain the advanced knowledge of structure engineering, she continued her Master's degree in structure civil engineering at Chulalongkorn University in 2013 under the supervision of Associate Professor Dr. Jaroon Rungamornrat